Real-Time, Non-Additionally Invasive Metrics of Cardiovascular Performance in Critical Care: A Model-Based Framework

Shaun Davidson

A thesis submitted for the degree of

Doctor of Philosophy in Mechanical Engineering

at the

University of Canterbury,

Christchurch, New Zealand

August 2017

Acknowledgements

There are a number of people I would like to thank, without whom this thesis either would not have been written, or have turned out quite differently.

Special thanks to my primary supervisor, Geoff Chase, for his guidance, tireless work ethic, which puts my own to shame, and for being always available and happy to discuss, provide suggestions on, and read through my work. It's easy to feel lost on this journey, and having something of a giant pointing the way is invaluable.

To my secondary supervisors, Chris Pretty, Thomas Desaive, and Geoff Shaw. Chris, for both his broad knowledge base, and the work he put into guiding, troubleshooting and providing valuable feedback on my work. Thomas, for taking care of me while in Liège, providing useful feedback, and providing opportunities to interact directly with the experimental side of this work. And Geoff Shaw, for his invaluable physiological and clinical expertise.

To the other cardiovascular PhD students, Shun Kamoi, Antoine Pironet and Joel Balmer. Shun, for providing his method for estimating stroke volume, Antoine, for his physiological insights, and Joel, for being an excellent person to discuss ideas with.

To Nathalie Janssen at the CHU de Liège, for all the work that goes into running the experiments that this research was validated across.

To Paul Docherty, for helping start me on this career path, stoking my enthusiasm for research, and influencing my thought process and approach to various aspects of it.

To Elizabeth, for your unconditional enthusiasm for my work and moral support, and to my parents, for your faith, guidance and support being the foundation this was built upon.

Table of Contents

List of Figures

List of Tables

List of Nomenclature

Physiological Waveforms:

P_{lv}	Left-ventricular pressure
V_{lv}	Left-ventricular volume
P_{ao}	Aortic pressure
P_{fe}	Femoral pressure
P_{vc}	Central venous pressure

Physiological Values:

V_{es}	End-systolic volume
V_{ed}	End-diastolic volume
P_{sys}	Mean-systolic pressure
P_{dia}	Mean-diastolic pressure
MAP	Mean arterial pressure
MVP	Mean venous pressure
P_{es}	End-systolic pressure
E_{es}	End-systolic elastance
V_d	Unstressed or ‘dead space’ ventricular volume
V_0	Ventricular volume at zero pressure
HR	Heart rate
CO	Cardiac output
SV	Stroke Volume
SW	Stroke work
PRSW	Preload Recruitable Stroke Work
LVEF	Left-Ventricular Ejection Fraction

Physiological Relationships

ESPVR	End-systolic pressure-volume relation
EDPVR	End-diastolic pressure-volume relation
TVE	Time varying elastance
P-V loop	Pressure-volume loop

Clinical Terminology:

CVS	Cardiovascular system
CVD	Cardiovascular disease and dysfunction
ICU	Intensive care unit
ECG	Electrocardiogram
PEEP	Positive end-expiratory pressure
RM	Recruitment Manoeuvre

Mathematical Symbols and Terminology:

Δ	Difference in magnitude
δ	Difference in timing
R	Pearson's correlation coefficient
IQR	Inter-quartile range
GMD	Geometric mean deviation
AIC	Akaike information criterion

Abstract

Cardiovascular disease and dysfunction (CVD) are leading causes of Intensive Care Unit (ICU) admission, costs, and mortality worldwide. Aging populations demand increasingly personalised and optimised cardiovascular care in the ICU to meet demand for more care at lower costs. However, inadequate or incorrect diagnosis of cardiac disturbances resulting in increased length of stay, cost and mortality is an ongoing issue.

Cardiac management in the ICU is informed by measurements taken from a variety of instruments, such as catheters placed near the heart. However, despite the rich information available from such instruments, their use is not necessarily associated with improved clinical outcomes. This discrepancy may be due to the clinical simplification of instrument outputs into lumped metrics that can be easily and rapidly parsed, but fail to preserve much of the initially gathered, patient-specific information. Thus, patient-specific information is lost and care is titrated based on population driven metrics, reducing the potential quality of care. Hence, improvement in the extraction of patient-specific cardiac information from these instruments has the potential to yield significant patient-centred, social, and economic value from clinically available data that has potentially been under-utilised to date.

This thesis develops a patient-specific modelling framework for the non-additionally invasive clinical estimation of a number of key, interlinked, and patient-specific cardiovascular metrics, including the end-systolic pressure-volume relation (ESPVR), pressure-volume (P-V) loop, unstressed or 'dead space' ventricular volume (V_d), time-varying elastance (TVE), and end-systolic elastance (E_{es}). These metrics are already accepted parts of clinically standard frameworks of understanding the underlying physiological behaviour of the circulatory system. However, they are not currently available in the ICU, forcing clinicians to make links between simple, observed

parameters and these metrics using their own mental models of understanding, experience, and intuition. Hence the provision of these particular patient-specific metrics from clinically available measurements in the ICU has the potential to provide significant benefits in clinical decision making, and personalisation of care, at little additional cost by leveraging models and computation.

This thesis further explores directly extracting information about the condition of the systemic circulation from various commonly measured pressure waveforms. In particular, relationships between the aortic, femoral and central venous pressures are explored through the medium of both transfer functions and a simple waveform energetics framework. The goal of this additional research is to provide further simple, intuitive and clinically sensitive metrics of systemic circulation condition from commonly available clinical data.

Each area of study is validated across two experimental animal trial data sets. These data sets encompass several popular clinical interventions in cardiac and circulatory management, such as fluid resuscitation, the administration of inotropic drugs, and recruitment manoeuvres. They also include an animal model of septic shock, which is a leading cause of acute circulatory and/or cardiac failure. In each case, a wide variety of information was invasively measured, allowing direct validation of model generated outputs against direct, invasively measured equivalents. Additionally, the interventions and conditions selected were designed to provide a diverse and challenging range of cardiovascular states, ensuring an overall robust and rigorous validation of each metric, model and method developed.

Overall, this thesis provides a coherent, interlinked framework for the non-additionally invasive model-based estimation of patient-specific and time-specific cardiovascular metrics central to titrating clinical care. The provision of these metrics in the ICU has the potential to optimise patient monitoring, aid real-time clinical decision making at

the patient bedside, and provide personalised care, closing the gap between the conceptual models of understanding a clinician relies on, and the surface level measured and summarised metrics clinically available. In essence, using available data, models and computation to create a much clearer physiological and patient-specific picture for clinicians to use in care and management.

1

Introduction

This first chapter provides a broad overview of the current state of the medical industry, the significance of cardiovascular disease, both within this industry and in general, and the state of current research surrounding diagnosis and treatment of cardiovascular disease. This overview is used to place the research goals, laid out in the second half of the chapter, in context.

1.1 General Background

1.1.1 Cardiovascular Disease and the Intensive Care Unit

Cardiovascular disease and dysfunction (CVD) are leading causes of illness, mortality and healthcare associated costs worldwide. CVD was responsible for 31% of global deaths in 2013, and the estimated worldwide cost associated with CVD in 2010 was $863 billion USD, accounting for approximately 1.39% of gross world product in the same year [1]. Further, cardiac events are estimated to account for over 50% of postoperative deaths [2, 3]. CVD can occur in many areas of the cardiovascular system (CVS) due to a wide variety of causes including age, congenital defects and illness.

Because of its prevalence, CVD is a leading cause of intensive care unit (ICU) admission [2, 4-8], including both patients who require cardiac and circulatory monitoring for disease or dysfunction [9-11] and intraoperative complications [3, 11, 12]. The estimated medical cost associated with CVD in the US is approximately $273 billion per annum, which is expected to triple to $818 billion per annum by 2030 [13].

This rapid escalation in costs, driven by rising obesity, sedentary lifestyles, and, predominantly, aging populations, means management and treatment of CVD patients in the ICU will continue to be a major clinical and economic burden for the foreseeable future.

1.1.2 Patient Monitoring in Intensive Care

Patients admitted to the ICU with CVD generally require intensive monitoring and support [14-16]. A number of instruments are typically attached to an ICU patient to assess their cardiac and haemodynamic condition in real time. These measurements include electrocardiograms (ECGs), which measure the electrical signals generated by heart muscle activation, in addition to various catheters that measure blood pressure and/or flow [17]. Current clinical decision making takes into account metrics derived from these instruments such as cardiac output, mean or peak arterial or venous pressures, heart rate and blood oxygenation to assess patient condition and titrate dose [16, 18]. The goals of using haemodynamic monitoring to inform decision making are [15]:

- Haemodynamic monitoring can be used to identify disease or cause of dysfunction, even if the link between the monitored variable and dysfunction are unclear.
- Haemodynamic parameters can be used to define cardiovascular state, thus restoration of these parameters to their normal values should improve tissue perfusion and patient outcomes.
- Haemodynamic parameters can be used to drive goal-directed therapy in a clear, consistent manner.

However, despite the rich information available from many of the instruments employed, such as arterial catheters, their use is not necessarily associated with

improved clinical outcomes [19, 20]. This perhaps unexpected result occurs because the information gained from these measurements is not always recorded or used effectively [21]. For example, while continuous measurement of the entire arterial pressure waveform is common, treatment is typically titrated based on discrete, intermittently used measures derived from this waveform, such as peak or average systolic and diastolic pressure. Thus, potentially clinically useful information in the shape of the arterial pressure waveform is lost [22]. Similarly, the monitoring of stroke volume and cardiac output have been shown to have little effect on clinical outcomes [15, 23], despite the clear importance of these metrics as indicators of cardiovascular health and function.

There are a number of potential causes for this outcome. One major cause is the limits of human ability to process multiple sources of information simultaneously. The human mind can simultaneously track only three to four variables effectively [24], and the volume of information presented to clinicians in an ICU environment is often far greater than this number, which is easily surpassed by data dense waveforms. This difficulty drives the simplification of information, such as catheter waveforms, into mean and peak pressures that clinicians can parse rapidly, and be fit easily to population based care guidelines.

The need for simplification of information from instrumentation will not change. Specifically, the human mind is simultaneously a superior decision making machine to a computer, but unable to parse as much information. The potential use of cardiovascular modelling to extract more meaningful, clinically relevant, yet still simple, metrics from the wealth of information available in an ICU is thus of great interest. The ability to transform, with models, waveform data into metrics providing a clear physiological picture, and to present these metrics to the clinician for decision

making, provides a means of mitigating this issue and best utilising the advantages of both.

However, for current clinical practice, the standard approach frequently relies on "one size fits all" protocols [25] for general populations, which titrate care based on single, localised metrics and generalised targets that often fail to provide a full picture of cardiovascular health [26-29]. These protocols, while sometimes beneficial across an entire population, can be excessively simple and actually harm individual patients [30]. The alternative is relying purely on rules-of-thumb, clinical surrogates of the desired treatment target, and ultimately clinical experience to select and dose therapies [31], which leads to variable care between ICUs and quality of care highly dependent on a clinician's experience and expertise [32].

Thus, inadequate or incorrect diagnosis of cardiac disturbances resulting in increased length of stay, cost and mortality is an ongoing issue [33, 34]. Simultaneously, there is sufficient individualised information available, but unused in the ICU, to titrate patient care within a standardised framework on a more patient specific basis [35-39]. As expressed in a recent overview of ICU Haemodynamic Monitoring, "*the quest for the holy grail of non-invasive cardiac output assessment methods continues*" [40].

1.1.3 Model Based Patient Care

The applicability and efficacy of a model based approach to assisting clinical decision making and patient care have already been demonstrated in the field of glycaemic control [35-39], among others [25, 41-43]. Ideal model based methods for haemodynamic monitoring should avoid requiring additional invasive instrumentation of the patient and increasing the workload of clinicians, while simultaneously providing real-time, clinically relevant and easily interpretable metrics at the patient bedside. In

such a case, improved, patient specific understanding of a patient's disease state and response to care could be provided at little extra cost or effort.

Thus, there is significant potential, and a definite need, for new model-based approaches to help ICU clinicians optimise and customise treatments for each individual patient, based on their specific state and response to treatment and without requiring any additional, invasive measurements [25, 44, 45]. This non-additionally-invasive model-based approach would combine information from various, commonly measured ICU metrics and synthesize this data into meaningful information pertaining to the normally obscured internal dynamics of the heart and circulation. Such a model-based approach would help create a clear physiological and patient-specific picture that would improve clinical decision making. The end outcome would provide improved, personalised care and thus help ease the significant economic and human cost associated with ICU care of patients with CVD [8].

1.2 Goals of this Thesis

The aim of this thesis is to develop a simple, patient-specific modelling framework for the CVS to improve information extraction and synthesis in critical care. Rather than modelling the entire circulatory system, which, while having a lot of promise, can create issues with over-parameterization, parameter trade-off and identifiability, this research takes a different approach. Specifically, the research in this thesis seeks to combine a number of open loop estimation methods, which avoid simultaneous parameter identification, and a clinically standard framework of understanding the underlying behaviour of the circulatory system.

Thus, this thesis looks at direct estimation of the interlinked concepts of the end-systolic pressure-volume relation (ESPVR), pressure-volume (P-V) loop, unstressed or 'dead space' ventricular volume (V_d), time-varying elastance (TVE) and end-systolic

elastance (E_{es}). This set of physiological metrics are part of the physiological framework used to define the fundamental functioning of the heart, and frequently employed by clinicians as a way to understand and predict the underlying behaviour of the CVS [46]. However, due to direct measurement requiring invasive instrumentation not employed in the ICU, these metrics are not clinically available. Thus, clinicians must make the link between observed parameters, such as heart rate, and mean and peak arterial pressures, and these metrics reflecting underlying CVS behaviour using their own mental models of understanding, experience, and intuition.

As such, using simple, localised modelling to estimate these underlying metrics tied directly to heart function, rather than relying on direct clinical interpretation of observed metrics, has potential to provide significant benefits in clinical decision making. The approach presented in this thesis uses computer modelling to draw a wider base of relevant information from the large variety of metrics and full waveforms measured in the ICU, and uses this information to provide simple, clinically familiar, but far more physiologically relevant parameters, directly to clinicians. It thus seeks to maximise the utility of the information already available to clinicians to improve insight and decision making.

The focus of the thesis on the left heart was motivated by several reasons. First, the left heart is considerably larger than the right heart, and tends to dominate the coupled relationship between the two [46]. Thus, while it is possible to model the left heart as independent from the right heart, modelling the right heart must take left heart behaviour into account. Second, the left ventricle outputs blood into the systemic circulation, which interacts with every major organ in the body, while the right heart outputs blood into the pulmonary circulation, which interacts solely with the lungs [46]. Finally, instrumentation is more commonly clinically available in the larger and more easily accessible arteries and veins of the systemic circulation as opposed to the smaller

and more difficult to access arteries and veins of the pulmonary circulation [47-49]. Thus, the left heart is a relatively independent and extremely important component of the circulatory system, with a relative wealth of associated clinically available data.

Further work in this thesis explores the direct extraction of information from several commonly measured arterial and venous waveforms, and the relationships between them. Specifically, the relationships between aortic pressure, femoral pressure and central venous pressure, all of which reside in the systemic circulation, are explored. These relationships are used to provide several new metrics, derived from a simple wave energetics approximation, which provide indications of the behaviour and condition of the systemic circulation, rather than the heart. These metrics have the potential to aid in diagnosis of conditions such as distributive shock, which primarily effect the peripheral circulation.

The work in this thesis is validated over two experimental animal trial data sets encompassing a variety of common clinical interventions such as recruitment manoeuvres, fluid resuscitation, and the administration of inotropic drugs, as well as a model of septic shock. These data sets provide a wide variety of invasively measured information, allowing direct validation of derived metrics against invasively measured metrics where relevant. Further, these data sets include interventions and disease states specifically designed to challenge model assumptions and provide a diverse range of circulatory states, conditions and levels of health encountered in the ICU, ensuring a rigorous validation of the model work.

1.3 Overview

This thesis is broadly structured as follows:

Chapters 1 – 2 provide background and context for the content of this thesis. Specifically, Chapter 1 provides an overview of the relevant aspects of current clinical

practice and the problem of CVD, and places the thesis goals in context relative to these. Chapter 2 provides a summary of relevant cardiovascular physiology, and details the experimental protocols used to gather the data employed throughout this thesis

Chapters 3 – 6 develop a modelling framework for the estimation of the TVE curve and several related metrics. Specifically, Chapter 3 develops a simple model with a fixed shape for estimating TVE. Chapter 4 develops a means of non-additionally invasively estimating V_d. Chapter 5 develops a means of non-additionally invasively estimating end-systolic and end-diastolic volumes beat-by-beat. Finally, Chapter 6 combines the work of Chapter 4 and 5 to estimate the beat by beat left ventricular pressure and volume profiles, and use these to estimate TVE without assuming an underlying shape.

Chapters 7 – 8 look at alternate uses and applications for the modelling framework developed in Chapters 3 – 6. Specifically, Chapter 7 looks at using the modelling framework from Chapter 6 to estimate the P-V loop, rather than TVE. The P-V loop is more clinically applicable, but more challenging to estimate accurately than the TVE curve. Chapter 8 looks at the estimation of the ventricular volume at zero pressure (V_0) using an experimentally standard method, explores the linearity of the ESPVR under such conditions, and compares the results with those for V_d in Chapter 4.

Chapters 9 – 10 explore an alternative approach to providing clinical metrics for diagnostic aid. Here, arterial and venous waveforms are directly compared using a simple waveform energetics approach. Chapter 9 explores the use of transfer functions, which demonstrate physiologically expected relationships but provide spectra as outputs that are too difficult to rapidly and easily interpret. Chapter 10 explores using a simpler framework where each waveform is treated as a pulse subject to a phase shift, amplitude offset and scaling factor. Here, simple metrics which are shown to be consistently sensitive to changes due to septic shock are developed, but require further validation against current, clinically standard metrics.

Finally, Chapters 11 and 12 provide a summary of the contents of this thesis and their overall implications, as well as discussing several possible avenues to extend and complement the work presented within this thesis.

2

Physiology and Experimental Data

An important foundation for any research into modelling the cardiovascular system (CVS) is the vast amount of existing knowledge about the functioning of this complex and vital physiological system. The first half of this chapter provides an overview of the CVS along with various methods and metrics used to describe it. The second half of this chapter provides details on the experimental data sets and protocols that were used as the basis for the research in this thesis.

2.1 Physiology

The CVS serves the purpose of circulating blood throughout the tissues of the body. Blood is used to carry oxygen and other nutrients to, and to extract waste products from, these tissues. The CVS can, broadly, be broken into 3 components, as shown in Fig. 2.1. These first of these components is the pulmonary circulation, encompassing the lungs and blood vessels leading to and from the lungs where carbon dioxide in the blood is exchanged with oxygen. The second is the systemic circulation encompassing the vessels leading to and from the organs where oxygen is exchanged for carbon dioxide and other waste products. The third and final component is the heart, a pump which sits in between these two circulatory loops and provides all flow [46].

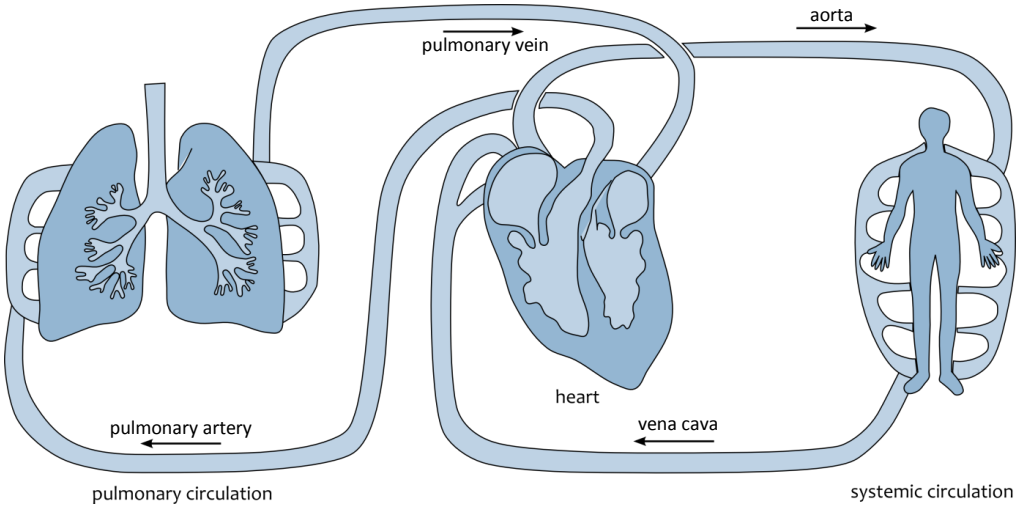

Fig. 2.1: Schematic of the three components of the CVS, and interconnecting arteries and veins [50].

2.2.1 The Heart

The heart serves as the pump that drives the entire circulatory system, and consists of four chambers constituting two parallel pumps. The right side of the heart, encompassing the right atrium and right ventricle, pumps deoxygenated blood returning from the systemic circulation into the pulmonary circulation for oxygenation. Similarly, the left side of the heart, encompassing the left atrium and ventricle, pumps oxygenated blood from the pulmonary circulation into the systemic circulation to supply the organs.

Each atrium serves as both an elastic reservoir which prevents the interruption of venous flow into the heart during, and a means of aiding in, ventricular contraction. The ventricles serve as the 'pump' itself, sealable chambers that alternately fill with and then forcibly eject blood. The inflow and outflow into each ventricle are controlled by a valve that allows flow in only one direction. Inflow into the right ventricle from the vena cava in the systemic circulation is controlled by the tricuspid valve (**1** in Fig. 2.2), and outflow into the pulmonary artery controlled by the pulmonary valve (**2** in Fig. 2.2). Similarly, inflow into the left ventricle from the pulmonary vein is controlled by the mitral valve (**3** in Fig. 2.2), and outflow into the aorta in the systemic circulation

controlled by the aortic valve (**4** in Fig. 2.2). The two ventricles share a common muscle wall called the septum, meaning the ventricles directly interact with one another.

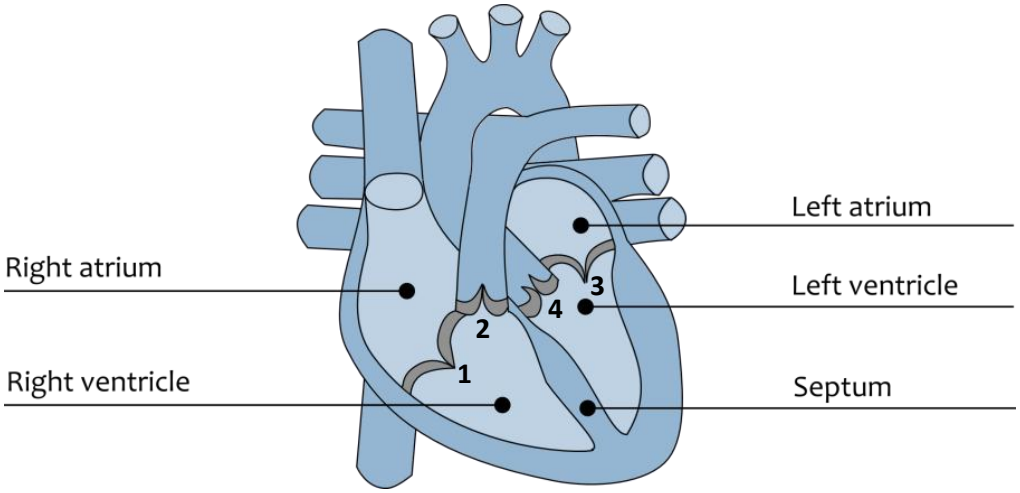

Fig. 2.2: The chambers and valves of the heart [50].

2.2.1.1 Electrical Activation of the Heart

The sequential relaxation and contraction of the chambers of the heart is driven by an electrical signal, detectable by an electrocardiogram (ECG) [51, 52]. This signal manifests as a distinct, rhythmic pattern of peaks and troughs in an ECG signal, corresponding to the electrical activation of different heart chambers, as shown in Fig. 2.3. The P wave represents the contraction of the atria, which increases preload on the ventricles and occurs prior to ejection of blood from the heart. The large peak, referred to as the QRS complex, corresponds to the contraction of the left and right ventricles, and thus ejection of the blood from the heart into circulation, during which the heart serves its primary output function. Relaxation of the atria occurs during the QRS complex, and is thus masked by the larger electrical signal associated with the ventricle contraction. Finally, the 'T' wave corresponds to relaxation of the ventricles after ejection.

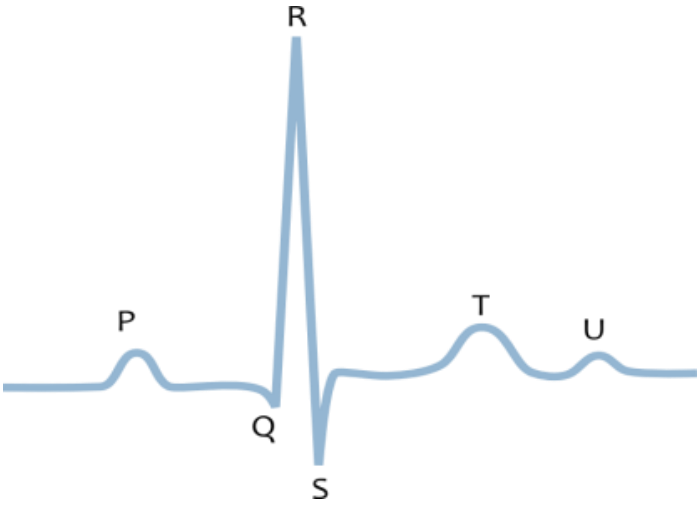

Fig. 2.3: An ideal ECG signal for a single heartbeat [50].

2.2.1.2 The Cardiac Cycle

The beat-by-beat cycle of the heart can be broken down into two regions and four segments. Systole encompasses the contraction of the ventricle and ejection of blood into the circulation, and diastole encompasses the relaxation and subsequent filling of the ventricle. The four segments of the cardiac cycle can be described with regards to the pressure and volume in a given ventricle, and form a close loop called the pressure-volume (P-V) loop as shown in Fig. 2.4. The four sides of the closed loop correspond to: filling (near-isobaric volume increase), contraction (near-isovolumetric pressure increase), ejection (near-isobaric volume decrease) and relaxation (near-isovolumetric pressure decrease). The P-V loop is a fundamental means of expressing information about cardiac dynamics and function [46].

The difference between the maximum (end-diastolic, V_{ed}) and minimum (end-systolic, V_{es}) ventricular volume for a given heartbeat is the stroke volume (*SV)*:

$$SV = V_{ed} - V_{es} \tag{2.1}$$

This value corresponds to the volume of blood ejected by the ventricle in a given heartbeat. When multiplied by the heart rate (*HR*) this becomes the cardiac output (*CO*):

$$CO = SV \times HR \tag{2.2}$$

where *CO* is a measure of the rate at which blood is being supplied to the circulation by the heart.

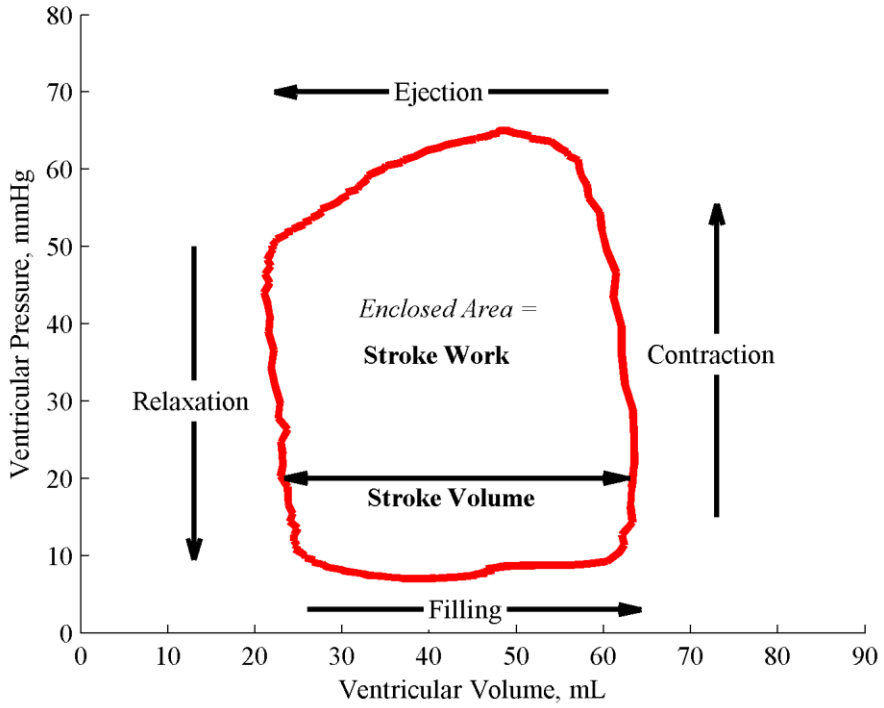

Fig. 2.4: The cardiac cycle, stroke work and stroke volume as described by a P-V loop.

The area enclosed by the P-V loop is the stroke work (*SW*), an important metric. It is sensitive to cardiac dysfunction and corresponds to work done by the ventricle ejecting blood into the aorta [53, 54]. It is thus a desirable, derived metric of heart function.

2.2.1.3 Cardiac Elastance

Ventricular elastance represents the ability of the heart to contract independent of loading conditions, and is thus representative of the intrinsic contractility of the heart tissue independent of the condition of the surrounding circulatory system. This elastance is frequently expressed as a pair of boundary relationships for the P-V loop, the end-systolic pressure-volume relation (ESPVR) and end-diastolic pressure-volume relation (EDPVR) [55, 56], which are shown in Fig. 2.5. The top left (end-systolic) and bottom right (end-diastolic) corners of the P-V loop are bound by the ESPVR and EDPVR lines, roughly defining a full set of possible P-V loops for the current contractile state, with shifts along the lines caused by changes in loading conditions, typically referred to as preload and afterload, which are discussed in Section 2.2.1.4.

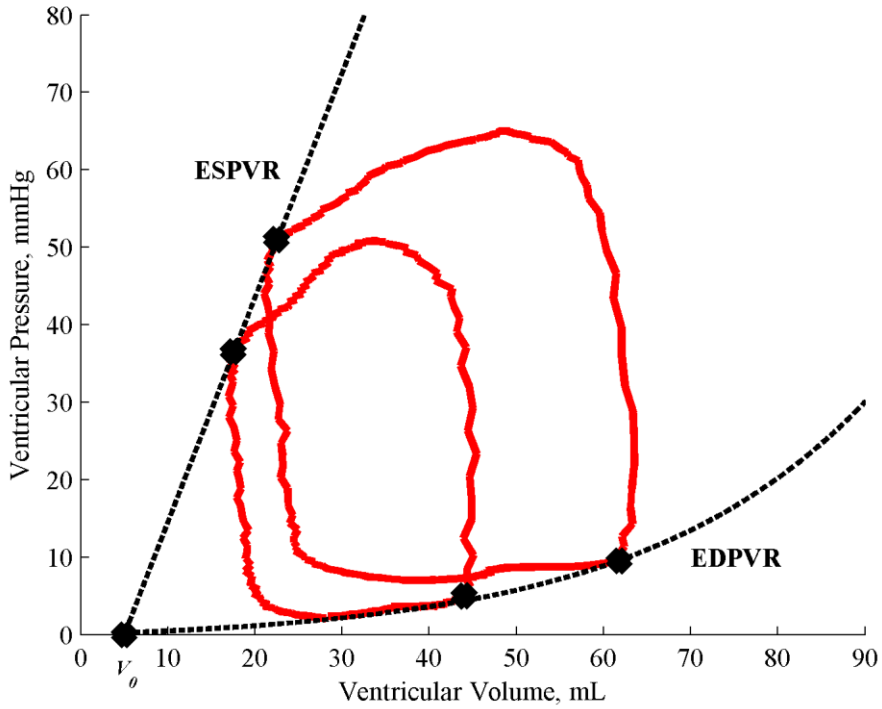

Fig. 2.5: The ESPVR and EDPVR, and their relation to P-V loops and V_0.

The gold standard measure of cardiac elastance is the slope of the linear ESPVR, called the end-systolic elastance (E_{es}) [55, 57, 58] and mathematically derived:

$$P_{es} = E_{es} \times (V_{es} - V_0) \quad (2.3)$$

where P_{es} is the end-systolic pressure and V_0 is the linear intercept of the ESPVR with the x-axis, the ventricular volume at zero pressure. This V_0 value is closely related to V_d, the unstressed or 'dead space' volume of the ventricle [59]. The ESPVR and E_{es} define the maximum pressure that can be produced by the ventricle wall for a given amount of volume, and is thus the pressure that can be exerted by the ventricle to eject blood, and a measure of how 'hard' the heart is able to 'beat'. Elastance can be clinically altered through the use of inotropic drugs [57, 60, 61], which either increase E_{es} to improve *SV* and *CO* or, in the opposite case, reduce E_{es} to reduce cardiac workload.

2.2.1.4 Preload and Afterload

As mentioned, changes in CVS behaviour for a given contractile state are driven by changes in loading conditions. These boundary conditions are commonly expressed in terms of preload and afterload. Succinctly, they are measures of cardiac pump priming, and the exiting resistance the heart must overcome, respectively.

Preload represents the loading conditions upstream from the heart, and is strictly defined as the maximum extension in a single cardiac cell prior to contraction. It thus assesses the circulation's ability to fill the heart chambers. However, due to the clinical unavailability of the cellular definition of the measure, it is more commonly defined by the surrogate measure V_{ed} [62]. Increased preload increases ventricular filling and thus *SV*, and vice versa via the Frank-Starling Law (Section 2.2.3.1). Preload is subject to various influences, including venous return, venous pressure, and respiration. Preload can be clinically regulated by fluid infusion, a common and core ICU therapy in circulatory management [30, 63-66], which increases total blood volume and thus venous return and pressure [67].

Afterload is the load downstream from the ventricle, against which the ventricle must act to eject blood. Technically, it is defined as the maximum stress developed in the ventricle wall during ejection. However, this measure is not available directly under clinical conditions, so downstream arterial pressure such as P_{ao} is a common surrogate [68]. Afterload can be clinically influenced by vasoactive drugs that either broaden vascular diameter, decreasing flow resistance and thus afterload, or narrow vascular diameter, increasing flow resistance and thus afterload. Again, these drugs are a common and core therapeutic approach [11, 66, 69-72].

Both afterload and preload change according to a variety of cardiovascular, regulatory, clinical and disease state influences. They are thus a function of patient response to disease, insult, or dysfunction, as well as a clinically managed variable. Overall, preload and afterload provide an indicator on the overall state of the CVS, but not necessarily a clear metric for specific diagnosis.

2.2.2 The Circulation

As previously mentioned, the circulation consists of two parallel loops separated by the heart, the systemic and pulmonary circulation. Each loop consists of an arterial system which carries blood away from the heart, a dense network of narrow capillaries where gas exchange occurs and a venous system that returns blood to the heart.

2.2.2.1 Pulmonary Circulation

The pulmonary circulation is, broadly, responsible for carrying deoxygenated blood to the lungs where gas exchange occurs, expelling carbon dioxide from the blood and introducing oxygen into the bloodstream. This oxygenated blood is then returned from the lungs to the heart. The artery carrying deoxygenated blood from the heart into the pulmonary circulation is the pulmonary artery, while the vein carrying oxygenated blood from the lungs to the heart is the pulmonary vein. While the pulmonary circuit is

important, a combination of relatively narrow vessel diameters and integration with fewer organ systems than the systemic circulation means instrumentation of the systemic circulation is favoured over the pulmonary circulation in clinical practice [47-49], thus the pulmonary circulation is less of a focus in this thesis.

2.2.2.2 Systemic Circulation

The systemic circulation is responsible for carrying oxygenated blood to the various organs and tissues of the body, and carrying waste products away from these organs and tissues. These waste products are expelled through several means including blood filtration in the kidneys, and removal of carbon dioxide from the bloodstream in the lungs. The artery responsible for supplying oxygenated blood from the heart to the systemic circulation is the aorta, and the vein responsible for returning deoxygenated blood from the systemic circulation to the heart is the vena cava. Relative to the pulmonary circulation, blood vessels are larger, all organs are integrated, and more blood volume resides in the systemic circulation. Clinically, instrumentation is more common in the systemic circulation, due to a combination of large vessels making instruments easier to insert and the systemic circulation's direct interaction with a large variety of organs making it more likely to contain broad diagnostic information [47-49].

The aorta, as previously mentioned, is the large artery situated directly downstream from the left ventricle, separated by the aortic valve. Due to the large diameter of the aorta and its direct proximity to the heart, measuring aortic pressure is relatively popular in clinical practice [47, 48]. A typical aortic pressure (P_{ao}) waveform, measured from a pig, is shown in Fig. 2.6. The P_{ao} waveform is pulsatile, with a steep increase in pressure between minimum aortic pressure (MN) and maximum aortic pressure (MX) as ventricular ejection occurs while the aortic valve is open and a less steep decrease in pressure between MX and MN as the aorta, which is highly elastic, relaxes and

continues to force blood downstream during ventricular filling while the aortic valve is closed. In this way, the aorta serves to lessen the pulsatile nature of blood flow, ensuring a more steady, continuous supply of blood to the systemic circulation. A topographical feature of note in the aortic pressure waveform is the Dicrotic notch (DN), which is a distinct dip in the aortic pressure waveform that occurs when the aortic valve closes as pressure in the left ventricle falls below pressure in the aorta during ventricular relaxation.

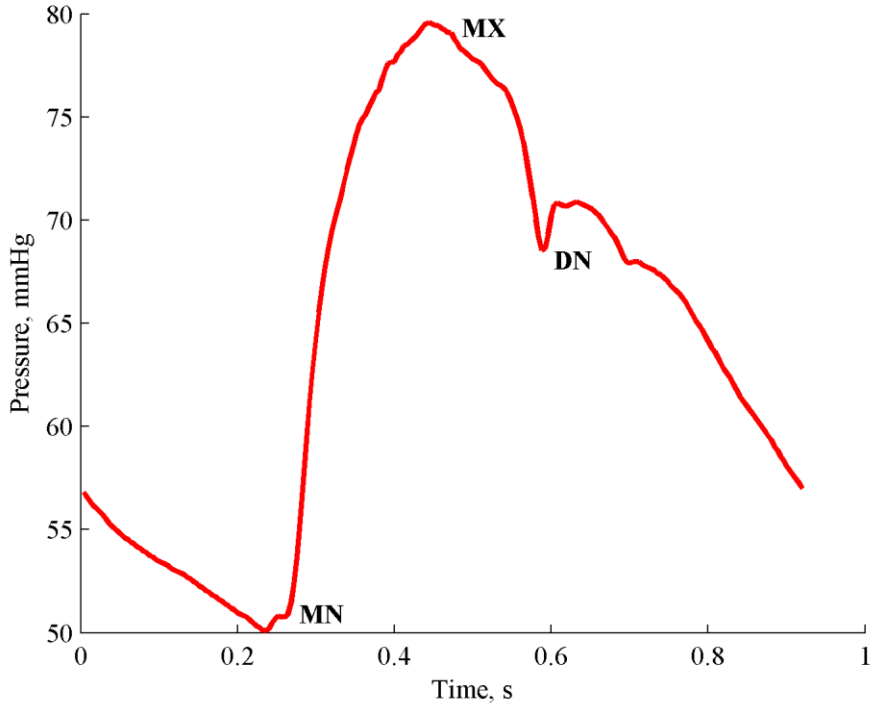

Fig. 2.6: A typical P_{ao} waveform, where MN represents the minimum aortic pressure, MX the maximum aortic pressure and DN the Dicrotic Notch.

The femoral artery sits downstream from the aorta, and is considerably narrower and less elastic [46]. Femoral pressure (P_{fe}) can be measured as an indicator of 'peripheral pressure', pressure near the organs, further away from the heart [73]. A typical P_{fe} waveform, measured from a pig, is shown in Fig. 2.7, with a P_{ao} waveform overlaid in black. As can be seen, a combination of the elastic action of the arteries and narrowing of vessels both smooths the waveform, eliminating the Dicrotic notch, and concentrates

it, resulting in typically slightly larger peaks and troughs. Also of note is the time lag between MX and MX* and MN and MN*, indicative of the pulse wave velocity in the arterial system. P_{fe} is not as commonly clinically measured as P_{ao}, as the artery is smaller and more difficult to locate, and does not necessarily provide additional information not available from P_{ao}.

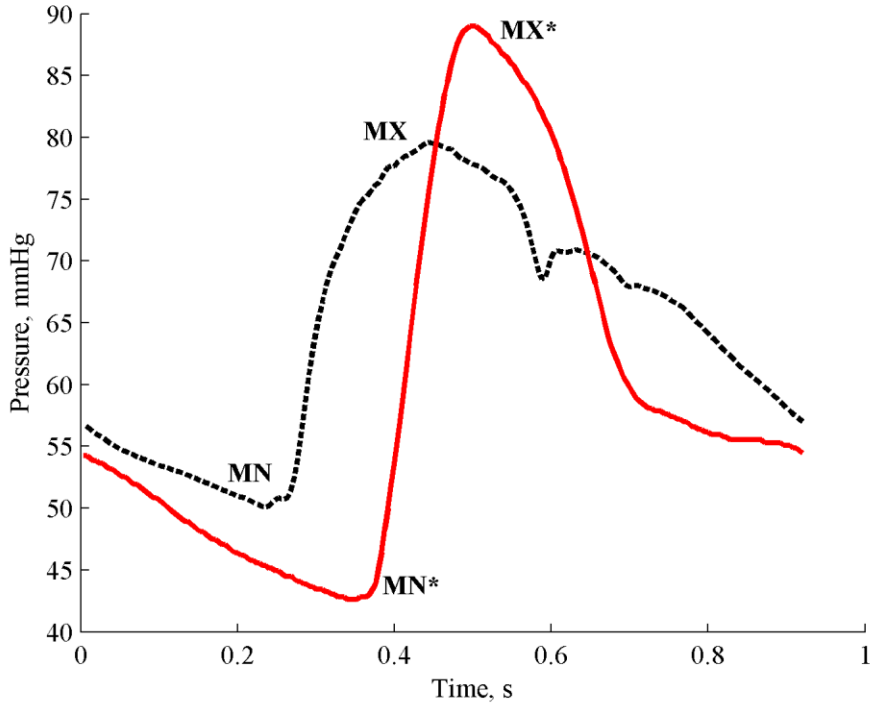

Fig. 2.7: A typical P_{fe} waveform, with a P_{ao} waveform overlaid in black, where MN represents the minimum aortic pressure, MN* the minimum femoral pressure, MX the maximum aortic pressure and MX* the maximum femoral pressure.

The vena cava is situated in the venous system, on the far side of the capillary beds from the aorta and femoral artery. A combination of the high flow resistance in these capillaries due to their narrow diameter, and the highly elastic walls of the subsequent veins results in a significant decrease in flow velocity and pressure in the venous system relative to the arterial system. As can be seen in Fig. 2.8, the pressure in the vena cava (P_{vc}) is an order of magnitude lower than that in the arterial system. It is sufficiently low, in fact, that a significant portion of the central venous pressure waveform is

influenced by downstream behaviour of the right ventricle, rather than upstream behaviour of the left ventricle.

In Fig. 2.8, the ‘A’ peak represents right atrial contraction, where the lack of a valve upstream from the right atria combined with the low pressure in the vena cava creates slight backflow. The ‘C’ peak is associated with the ventricle contracting and the tricuspid valve bulging outwards due to the increase in pressure. Thus, only the area in the latter half of the waveform, from the ‘X’ trough to the ‘V’ peak and back to the ‘Y’ trough, represents the flow of blood arriving from the left ventricle via the systemic circulation.

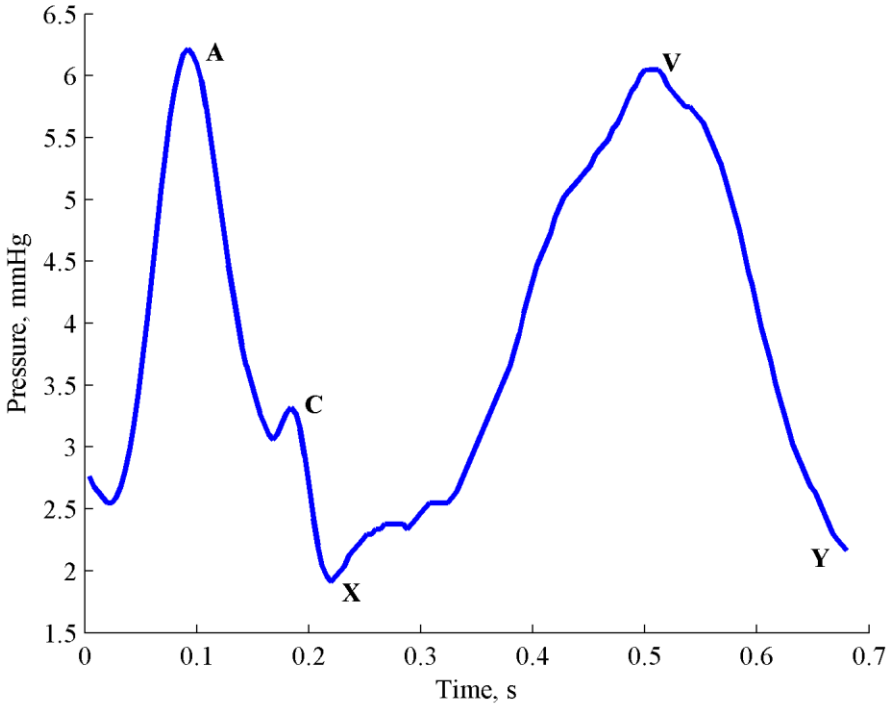

Fig. 2.8: A typical P_{vc} waveform, where the ‘A’ and ‘C’ peaks are the result of the downstream action of the right heart, while the ‘V’ peak is the result of the upstream flow of blood from the left heart.

These factors combine to make information extraction from P_{vc} somewhat difficult. On the one hand, it serves as an output to the systemic circulation. On the other hand, its low magnitude, influence by upstream, as well as downstream behaviour, and the fact

that the body seeks to maintain P_{vc} at all costs, because it is necessary for venous return, make its sensitivity to changes in condition a point of ongoing clinical and research discussion [30, 74, 75].

2.2.3 Cardiovascular Regulation and Interaction

2.2.3.1 Homeostasis

Homeostasis refers to the body's active regulation of various properties to a near constant value. The CVS contains a variety of homeostasis mechanisms to ensure continual distribution of blood and oxygen to where it is most needed [76]. These homeostasis mechanisms act to continually maintain an equilibrium state, perturbed by changes in condition or therapy.

Neural regulation is homeostasis controlled by the autonomous nervous system [46]. This regulation acts through two main pathways, the sympathetic nervous system, which drives a 'fight or flight' response, increasing *HR* and E_{es}, and diverting blood flow to muscles and lungs, and the parasympathetic nervous system, which drives a 'rest and digest' response, decreasing *HR* and E_{es}, and diverting blood to the gastro-intestinal tract. An example of neural regulation is the baroreflex, a negative feedback loop in which elevated blood pressure drives a fall in *HR*, and thus a fall in blood pressure, and vice versa. This process is controlled by baroreceptors, a system of pressure sensors throughout the CVS that interact with the sympathetic and parasympathetic nervous systems [46].

Auto regulatory mechanisms refer to local mechanisms that maintain homeostasis without neural oversight. Examples of this form of regulation include circulatory auto regulation, where the small arteries in an organ automatically dilate in response to decreased perfusion pressure and thus decreased blood flow. The amount of dilation is organ specific, with increased dilation in vital organs such as the brain, ensuring that

even in the absence of neural regulation blood is diverted to organs where it is most needed. Another example of auto regulatory mechanisms is the Frank-Starling law, where increased stretching of the ventricle walls due to increased filling causes the ventricles to contract more forcefully, ejecting more blood [46, 77-79]. Thus, the ventricles act as a 'demand pump', ejecting whatever blood is received and ensuring output and input into the heart is intrinsically synchronised.

Finally, humoral regulation refers to the regulation of circulatory behaviour through the release and absorption of hormones and ions throughout the body. These hormones are typically secreted by specialised glands, and can have either localised or circulatory system wide effects, including vasoconstriction and vasodilation. Thus, these hormones can be used to regulate both local and global flow resistance, and the relationship between pressure and flow throughout the body.

2.2.3.2 Cardiopulmonary Interaction

The cardiovascular and pulmonary systems interact in several significant ways. First, the pulmonary system is the sole organ system that the pulmonary circulation passes, thus changes in pulmonary conditions have a large influence on one of the two loops of the CVS. The inflation of the lungs causes the small capillaries in the lungs to stretch, increasing pulmonary vascular resistance and thus resistance in the pulmonary circulation. The subsequent deflation of the lung during exhalation causes the larger arteries and veins in the pulmonary circulation to compress, increasing the resistance in these arteries and veins.

Second, intrathoracic pressure, the common pressure in the thoracic cavity, is highly subject to the behaviour of the pulmonary system and acts as an external pressure on the heart, as well as proximal arteries and veins. Increased thoracic pressure increases pressure in the right atrium and decreases the relative peak ejection pressure of the left

ventricle [80-82]. This increase in the downstream, right atrial pressure and decrease in the upstream, peak ejection pressure of the left ventricle combine to reduce the pressure gradient for venous return, leading to decreased intrathoracic volume. This effect is often exacerbated in the ICU by positive pressure ventilation, where a sedated subject's inhalation is driven by an externally applied increase in end-expiratory pressure rather than a local, diaphragm driven, decrease in pressure. The outcome of this therapeutic choice is an increase in thoracic pressure above what would normally be seen in a healthy individual.

2.2 Experimental Data

This section details the experimental protocols for the two data sets that were used throughout this thesis [59, 83]. All experimental procedures and protocols were reviewed and approved by the Institutional Animal Care and Use Ethics Committee of the University of Liège, Belgium (Reference Number 14-1726). Their guidelines conform completely with the Guide for the Care and Use of Laboratory Animals published by the US National Institutes of Health (NIH Publication No. 85-23, revised 1996), as well as EU DIRECTIVE 2010/63/EU on the protection of animals used for scientific purposes.

2.2.1 Protocol D, Dobutamine

Seven male, pure Piétrain pigs were sedated and anesthetised by an initial intramuscular dose of Zoletil 100 (0.1 mL/kg) and Ketamine 1000 (0.1 mL/kg). Sedation and anaesthesia was maintained by a continuous infusion of Nimbex (1 mL/kg/h at 2 mg/mL), Sufenta (0.1 mL/kg/h at 0.005 mg/mL) and Thiobarbital (0.1 mL/kg/h) via a central venous catheter positioned within the superior vena cava. The pigs were mechanically ventilated (GE Engstrom CareStation) through a tracheotomy, with a baseline positive end-expiratory pressure (PEEP) of 5 cmH_2O and tidal volume of 270 mL. The heart was accessed via a median sternotomy, and a micromanometer-

tipped admittance pressure-volume catheter (Transonic, NY, USA) with a sampling rate of 250 Hz inserted into the left ventricle via an apical stab [84, 85]. Proximal aortic and femoral pressures were continually sampled using pressure catheters (Transonic, NY, USA) with sampling rates of 250 Hz. Euthanasia was performed via a bolus of Pentobarbital (30 mg/kg) and Sufentanil (5 µg/kg) causing respiratory arrest. The instrumentation set up is shown in Fig. 2.9.

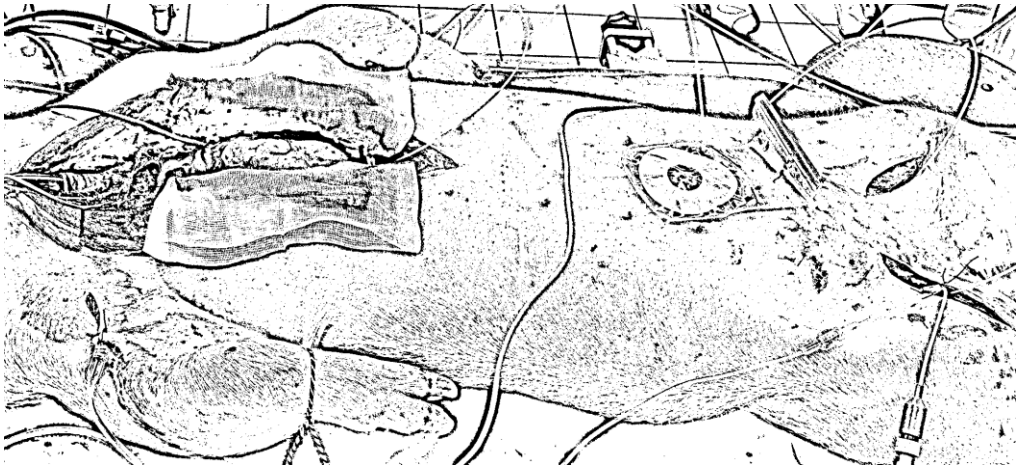

Fig. 2.9: Example experimental equipment set up.

The dobutamine protocol encompassed:

- An infusion of dobutamine over a period of 30 minutes. Dobutamine directly increases contractility in order to improve cardiac output, and is and is a core circulation management therapy [11, 66, 69-72].
- Several positive end-expiratory pressure (PEEP) driven recruitment manoeuvres (RMs), from 5 cmH_2O to 25 cmH_2O in steps of 5 cmH_2O, both pre- and post- dobutamine infusion. RMs drive a change in preload conditions and are typically associated with a decrease in mean blood pressure and cardiac output [86].
- Two vena cava occlusion manoeuvres, performed with a fluid filled balloon, at each PEEP level during a RM. Vena cava occlusion manoeuvres cause a

sharp decrease in cardiac preload, and can be used to provide a short term estimate of the ESPVR [87].

- 2-6 rapid 225mL saline solution boluses. Infusions were given before and after dobutamine infusions. Saline infusions change circulatory volume and simulate fluid resuscitation, important components of typical hemodynamic management [30, 63-66].

The experimentally available waveforms include:

- Continuous left-ventricular pressure (P_{lv}) from a pressure-volume catheter in the left ventricle
- Continuous left-ventricular volume (V_{lv}) from a pressure-volume catheter in the left ventricle
- Continuous aortic pressure (P_{ao}) from a pressure catheter in the aorta
- Continuous femoral pressure (P_{fe}) from a pressure catheter in the femoral artery

Issues with the admittance pressure-volume catheter being incorrectly situated in the ventricle led to one pig being excluded. A second pig, which was included, suffered sensor drift in the V_{lv} waveform which will be discussed in Chapters 5 and 7. As the shape of the V_{lv} waveform, and the shape and magnitude of all pressure waveforms were correct, it was decided to retain this data. Note that not all pigs completed the entire protocol, and as such the length of the monitoring period varies across the cohort. However, each included dataset consists of at least 5,000 heartbeats of data.

2.2.2 Protocol S, Sepsis

Eight male, pure Piétrain pigs weighing between 18.5 and 29 kg were sedated, anaesthetised and mechanically ventilated identically to the pigs described in Section 2.2.1. The heart was accessed via a median sternotomy, and an admittance pressure-volume catheter (Transonic, NY, USA) with a sampling rate of 250 Hz inserted into

the left ventricle via an apical stab [84, 85]. Proximal aortic, femoral and central venous pressures were continually sampled using pressure catheters (Transonic, NY, USA) with sampling rates of 250 Hz. Euthanasia was performed via a bolus of Pentobarbital (30 mg/kg) and Sufentanil (5 µg/kg) causing respiratory arrest.

The sepsis protocol included:

- An endotoxin infusion (lipopolysaccharide from E. Coli, 0.5 mg/kg) over 30 mins, an induced model of septic shock, which causes inflammatory responses and capillary leakage, decreasing afterload, leading to hypovolemia, global tissue hypoxia, and cardiac failure [88]. As such, this model of septic shock would be expected to cause dramatic changes in the behaviour of the systemic circulation.
- Several PEEP driven recruitment manoeuvres (both pre- and post- endotoxin infusion), which drive a change in preload conditions and are typically associated with a decrease in mean blood pressure and cardiac output [86].
- One to four infusions of 500 mL saline solution over 30 minute periods (both pre- and post- endotoxin infusion), simulating fluid resuscitation therapy, a key component of hemodynamic resuscitation in patients with severe sepsis, which results in a change in circulatory volume [30, 63-66].

The experimentally available waveforms include:

- Continuous P_{lv} from a pressure-volume catheter in the left ventricle
- Continuous V_{lv} from a pressure-volume catheter in the left ventricle
- Continuous P_{ao} from a pressure catheter in the aorta
- Continuous P_{fe} from a pressure catheter in the femoral artery
- Continuous P_{vc} from a pressure catheter in the superior vena cava

Three pigs from Protocol S were excluded due to equipment issues. In one case, the admittance catheter was incorrectly situated in the ventricle, in another equipment became disconnected and needed to be replaced during the experiment and in the final case there was a data acquisition issue. The data from the final case, where there was a data acquisition issue, was still usable, but consisted of an extremely large number of disjointed data segments with short gaps between them. As such, this data was extremely labour intensive to process and make use of, and was only used in Chapter 4, where the relatively simple, robust modelling required and the unusual and ambiguous nature of V_d made the effort involved with including this additional data worthwhile.

Once sepsis was sufficiently progressed and the various ventricular, arterial and venous waveforms became drastically different and largely incoherent, information was discarded. Due to the extremely advanced stage of circulatory failure at which this level of disturbance to the measurements occurred, this information is likely of no use for diagnostic ICU monitoring. Note that not all pigs completed the entire protocol due to varying reactions to the endotoxin infusion. As such, the length of the monitoring period varies. However, each dataset consists of at least 5,000 heartbeats.

A summary schematic of the two protocols is shown in Fig. 2.10.

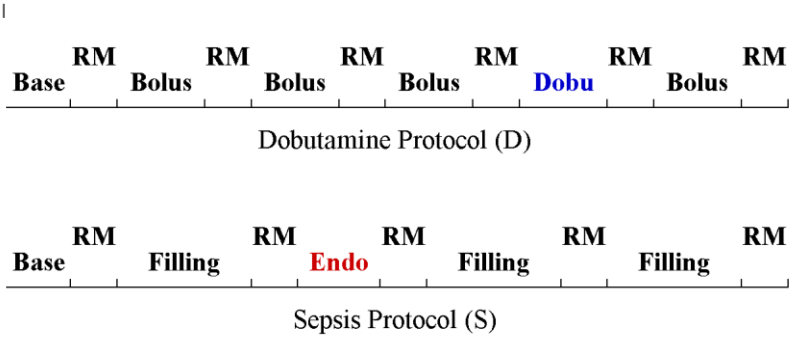

Fig. 2.10: A schematic of experimental protocols D (top) and S (bottom). 'Dobu' denotes a dobutamine infusion, 'Endo' denotes an endotoxin infusion and 'RM' denotes a recruitment manoeuvre.

2.3 Summary

This chapter provided a comprehensive overview of the aspects of cardiovascular physiology and clinical models of understanding that will be relevant throughout this thesis. These include the concepts of the P-V loop, elastance and pressure wave profiles. Further, this chapter provided a detailed explanation of the two experimental protocols used to generate the data sets on which this thesis is validated, as well as any complications that led to individual subjects being partially or entirely excluded.

3

Time Varying Elastance

An existing model for the time varying elastance (TVE) developed by Stevenson et al. [89, 90] was used as the basis for this chapter. The approach had previously shown promise, but been validated only across a small data set of 80 heartbeats. With a considerably larger amount of data now available, the intent of this chapter was to perform a large-scale validation of the approach's performance and sensitivity, and to modify the approach based on the results.

3.1 Background

TVE is an important means of expressing internal cardiac dynamics and function [55]. The TVE curve represents the active elastance changes in the ventricles that drive heart contraction, thus providing valuable intra-beat information about cardiac behaviour and energetics [55, 91, 92]. The TVE curve has a wide range of potential applications. It is often employed as an input in large cardiovascular models that seek to model the entire circulatory system [93-97], and also frequently used in the determining of important cardiac metrics, such as the End-Systolic Pressure-Volume Relation (ESPVR) [91]. TVE is defined [98]:

$$e(t) = \frac{P_{lv}(t)}{V_{lv}(t) - V_d} \tag{3.1}$$

where P_{lv} is the left-ventricular pressure, V_{lv} is the left-ventricular volume, and V_d the unstressed or 'dead space' ventricular volume, which is frequently assumed to be

equivalent to V_0, the intercept of the ESPVR with the volume axis [57]. In this chapter, V_d is set to 0, as in [89, 90], due to the highly invasive and specialised experimental procedures typically needed to establish this subject specific value [55, 57, 98]. The maximum magnitude of the TVE curve is usually normalised to a value of 1.0 for modelling, serving as an intra-beat indicator of relative, dynamic ventricular elastance, and coupled with a separate estimate of End-Systolic Elastance (E_{es}) [98].

There has been more limited investigation into the utility of the TVE curve in isolation. The area under the TVE curve is analogous to work done by the ventricle. It is thus a potentially significant indicator of patient condition. However, the typical normalisation of the TVE curve means only relative changes in work for a given inotropic state can be compared.

The TVE curve relies on a combination of ventricular pressure and volume waveforms similar to pressure-volume (P-V) loops. It thus contains information concerning cardiac work [53, 54] and contractility [55, 56], both of which change in response to cardiac dysfunction. As such, it has been suggested that the shape of the ventricular elastance curve itself may have diagnostic use [44, 89, 90, 99].

Unfortunately, the TVE curve can only be directly measured by placing catheters into the heart chambers, which is, understandably, not common practice. As such, the traditional approach to non-invasively generate a TVE curve is to fix it as a population based waveform [91, 95, 96]. Most existing work surrounding TVE curves is focused on using the TVE curve to estimate a clinical parameter, such as ejection fraction [100], and, most commonly, end-systolic elastance [91, 101, 102]. However, these studies are validated on correlations with the derived parameter, rather than on the shape and change in shape of the TVE curve itself. Thus, these approaches are not validated for use as part of a larger model of cardiac dynamics, or for direct use as a diagnostic aid.

Previous work specifically focused on experimentally generating a TVE curve and validating it based on its correlation with the analytically derived function showed promise, and noted changes in the TVE curves during pulmonary embolism and septic shock [89]. This previous work, which forms the basis for this chapter, was limited by the availability of data for validation [89, 90], a limitation this chapter seeks to alleviate. Work has also been undertaken in modelling time varying ventricular elastance, split into active and passive components, in humans [99]. Active elastance was shown to compare well with other metrics of contractility, and the properties of these elastance curves were shown to change for different disease states. However, this method required highly invasive ventricular catheterisation and thus is not broadly implementable in a clinical environment. Hence, there is a significant gap created by the current clinical inability to directly measure or estimate the TVE curve every beat.

This chapter presents a validation and concordant modification of a previously described approach for estimating the TVE curve [89, 90], taking advantage of a large amount of experimental data across multiple porcine subjects, a volume of data unavailable in the original study. The approach uses population values to determine the majority of the TVE curve, but selects the activation and deactivation timing of the TVE curve using strong correlations ($R > 0.97$) with readily measurable and clinically available aortic pressure waveform features. The use of population values in this chapter is distinct from the approach presented in [89, 90], which avoids their use. This modification of the methodology was driven by a combination of low correlation coefficients and low model sensitivity for certain parameters, as established in this chapter using the relative wealth of relevant data now available. The modified approach presented in this chapter captures the general form of the TVE curve on a beat-to-beat basis for minimal computational effort, using extremely robust, physiologically grounded correlations.

3.2 Methods

3.2.1 Experimental Data

This chapter makes use of the Protocol D data from all 6 pigs. The waveforms employed include continuously sampled aortic pressure (P_{ao}) as a method input, and continuously sampled P_{lv} and V_{lv} to provide the invasively measured TVE curve for direct comparison and validation.

3.2.2 Time Varying Elastance Model

The general form of the TVE curve was modelled using a phenomenological three-part piecewise equation featuring a Gaussian rise followed by a shoulder and subsequent Gaussian decay as shown in Fig. 3.1. This phenomenological piecewise waveform, as originally described in [89, 90], is uniquely defined using 7 parameters derived from desired TVE curve: the time (t_1), height (x_1) and value ($\dot{x}_1$) of the maximum positive gradient, the height (x_2) at the beginning of the shoulder section and the time (t_3), height (x_3) and value ($\dot{x}_3$) of the maximum negative gradient.

Using these 7 parameters, the following terms are defined:

$$a_{\propto} = x_2 \tag{3.2a}$$

$$b_{\propto} = -\frac{\log\left(\frac{x_1}{x_2}\right)}{\exp\left(2\log\left(\frac{-2x_1}{\dot{x}_1}\log\left(\frac{x_1}{x_2}\right)\right)\right)} \tag{3.2b}$$

$$c_{\propto} = -\frac{2\log\left(\frac{x_1}{x_2}\right)x_1 - \dot{x}_1 t_1}{\dot{x}_1} \tag{3.2c}$$

$$a_{\beta} = 1 \tag{3.3a}$$

$$b_\beta = -\frac{\log(x_3)}{\exp\left(2\log\left(\frac{-2x_3}{\dot{x}_3}\log(x_3)\right)\right)} \tag{3.3b}$$

$$c_\beta = -\frac{2\log(x_3)x_3 - \dot{x}_3 t_3}{\dot{x}_3} \tag{3.3c}$$

The piecewise waveform is then defined:

$$e(t) = \begin{cases} f_\propto(t) & 0 < t < c_\propto \\ \dfrac{(1-x_2)(t-c_\propto)}{c_\beta - c_\alpha} & c_\propto < t < c_\beta \\ f_\beta(t) & c_\beta < t < period \end{cases} \tag{3.4}$$

where:

$$f_i = a_i \cdot e^{-b_i(t-c_i)^2} \tag{3.5}$$

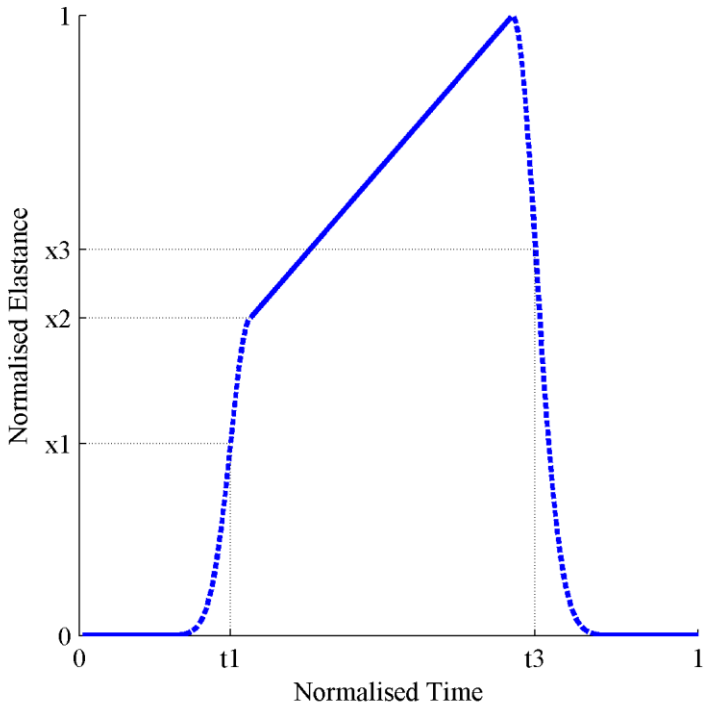

Fig. 3.1: An example TVE curve generated using Eq. 3.4.

For consistency and ease of comparison between heartbeats, and as in [98], the period t of each heartbeat was normalised to 1, and any comparisons with measured data involved a concordant normalisation of the measured heartbeats' period to 1.

3.2.3 TVE Curve Correlations

Fig. 3.2 shows an illustrative plot of several experimentally measured TVE curves for every 100th heartbeat over a 50-minute period, a total of 45 TVE curves. This plot serves to demonstrate the resemblance between the measured TVE curve and Fig. 3.1 generated by Eq. 3.4. Additionally, as illustrated in Fig. 3.2, t_3 appears to vary more significantly than the other parameters and, as will be shown later, has a large influence on area under the curve error. Parameter x_2, the 'shoulder height', also exhibits notable variation in measured waveforms.

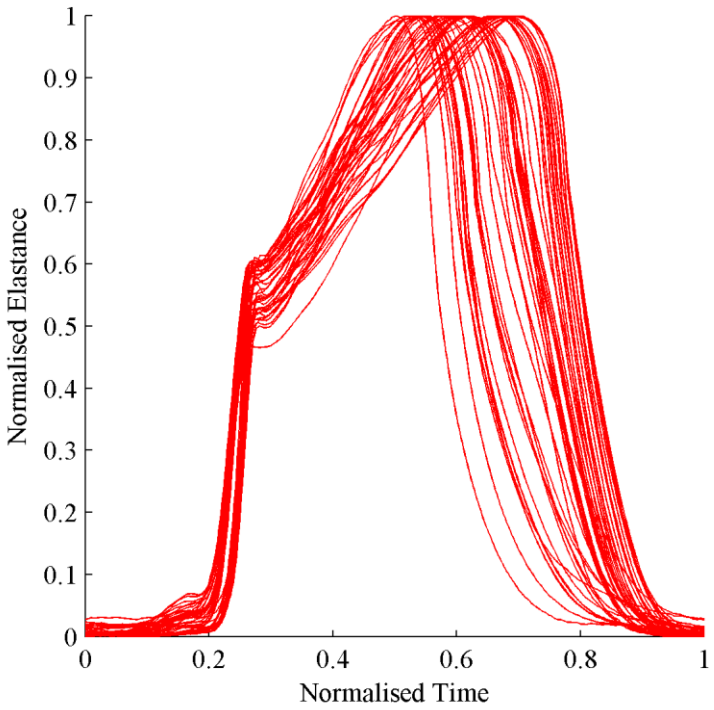

Fig. 3.2: Experimentally measured TVE curves over a 50-minute period.

Distinct from the methodology presented in [89, 90], the decision was made to explore fixing several parameters based on population values, taking advantage of the relative

wealth of data available in this study and seeking to address relatively poor correlation coefficients and ambiguous physiological relationships in the correlations originally used to derive some parameters, which sometimes performed poorly on the broader data set employed here. To determine which parameters should be fixed and which should be derived from correlations to other measurements to provide the greatest approach accuracy for least complexity, a parameter sensitivity analysis was conducted. This was performed by using nonlinear least squares (Levenberg-Marquardt as implemented by MATLAB's lsqnonlin function, R2014a, 64-bit, The Mathworks, Natwick, MA, USA) to find the ideal value for each parameter, and then varying these ideal values by 10% while holding all other parameters constant. Error was calculated by taking the absolute value of the difference between the estimated and measured TVE curves at each point, and normalising based on the area under the measured TVE curve, providing a lumped, normalised indication of the difference in shape between the measured and estimated curves. An example of the error area (shaded) between an estimated and measured TVE curve is shown in Fig. 3.3. In this example the error is 8%.

Using the results from the sensitivity analysis, the parameters t_1 and t_3 were identified as having significant influence on error, thus selected for beat-by-beat correlation. These parameters were assessed over a development cohort of 2 pigs (38,106 heartbeats), and strong correlations with aortic pressure waveform features were evaluated for both. To provide a point of comparison, fixed median values for t_1 and t_3 were generated across the same development cohort of 2 pigs. These median values were calculated for normalised heartbeat lengths and then scaled on a beat-to-beat basis by the length of the specific heartbeat when generating a TVE curve.

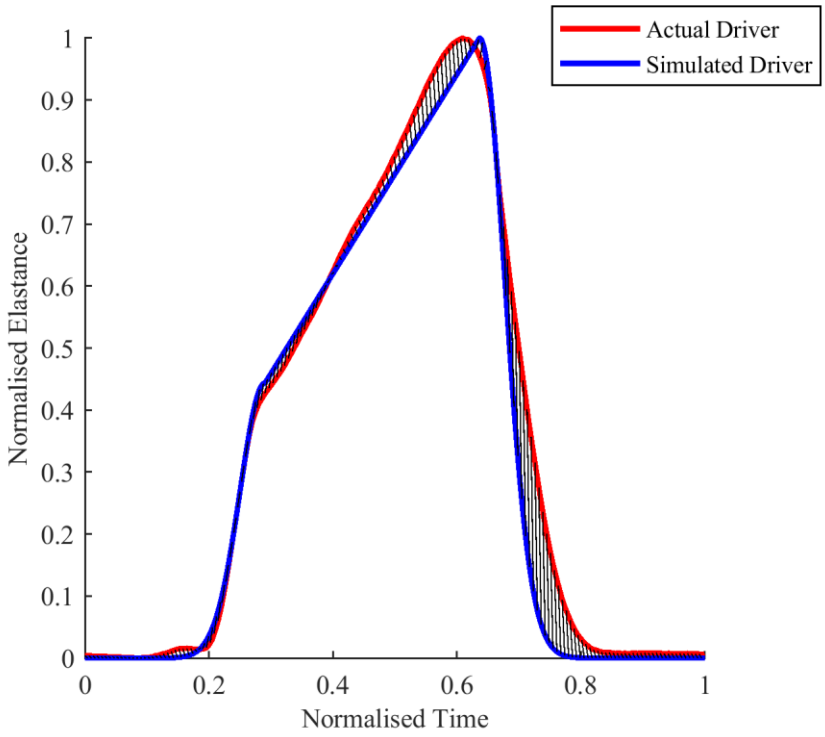

Fig. 3.3: Example of error (shaded area) between measured and estimated TVE curves.

3.2.4 Evaluation of Results

Error was calculated, as in Section 3.2.3, by taking the absolute value of the difference between the estimated and actual TVE curves at each point, and normalising based on the area under the curve of the estimated driver. The errors were evaluated over a test cohort of 4 pigs (54,410 heartbeats), entirely independent from the 2 pigs used in the development cohort, although subject to the same protocol. The errors associated with TVE curves generated using the dynamic, correlated values for t_1 and t_3, and those associated with the fixed median values for t_1 and t_3 were calculated for each heartbeat and compared to determine whether the dynamic timing resulted in a significant reduction in error.

3.3 Results

3.3.1 Sensitivity Analysis

The results of the sensitivity analysis of TVE curve error to changing parameters are shown in Fig. 3.4, where the box represents the 25th and 75th percentile values, and the 'whiskers' the 5th and 95th percentile values. It is clear that the activation and deactivation timings of the TVE curve (t_1 and t_3) are large contributors to area under the curve error. Thus, accurate identification of these timings is important to deriving an accurate TVE curve. It is also worth noting that a modest 8% median error remains even when all parameters are fitted using nonlinear least squares due to model data mismatch.

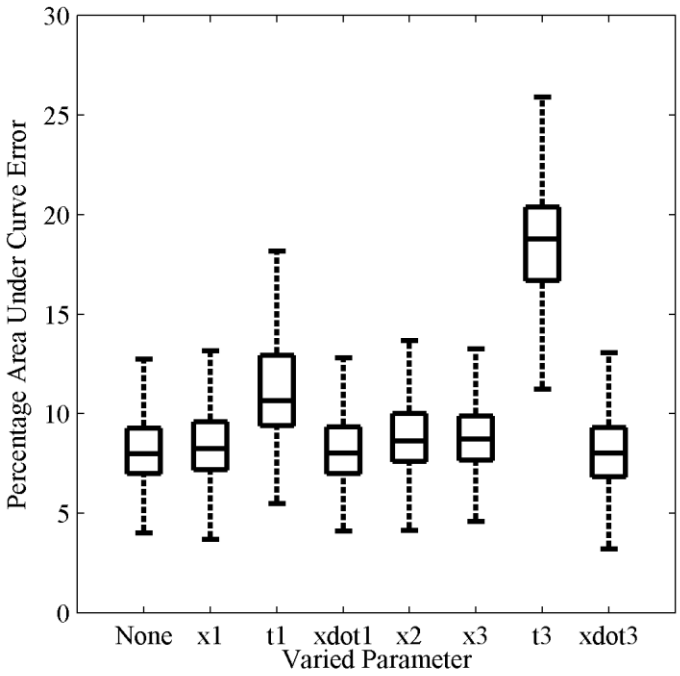

Fig. 3.4: Error sensitivity to different parameter changes for a 10% change from optimal values. 'None' denotes no parameter variation and thus minimal model error. The 5th percentile error for non-ideal cases occasionally being lower than for the ideal case is due to the broader error distribution in non-ideal cases resulting in fewer extreme data points being classified as outliers and thus discarded.

3.3.2 TVE Curve Correlations

Using 38,106 heartbeats across the 2 pig development cohort, t_1 was confirmed to have a strong, 1:1 correlation with the timing of the minimum aortic pressure (R = 0.972) and t_3 a strong, 1:1 correlation with the timing of the Dicrotic notch (R = 0.997) as seen in Fig. 3.5. These strong, physiologically expected 1:1 correlations were used in the approach:

$$t_1 = t_{min(P_{ao})} \tag{6a}$$

$$t_3 = t_{DN} \tag{6b}$$

As the minimum aortic pressure occurs directly before the aortic valve opens and blood is ejected from the left ventricle, the correlation between this point and t_1, which represents contraction of the left ventricle, is unsurprising. Similarly, the correlation of t_3 to the Dicrotic notch is unsurprising given the Dicrotic notch corresponds to aortic valve closure and thus the relaxation of the left ventricle, which is where the TVE curve decays [103]. Regardless, these correlations provide the ability for significant components of TVE curve variation to be easily and accurately captured, thus individualising the generic TVE curve and minimising errors.

The 5 other parameters (x_1-x_3, $\dot{x}_1$, $\dot{x}_3$) were assessed across the same 38,106 heartbeats. Moderate variability was exhibited by all parameters. These parameters were fixed to the median values exhibited, which are shown in Table 3.1. Note that the fixed values for t_1 and t_3 were only employed in the fixed timing approach, which was used to create a point of comparison.

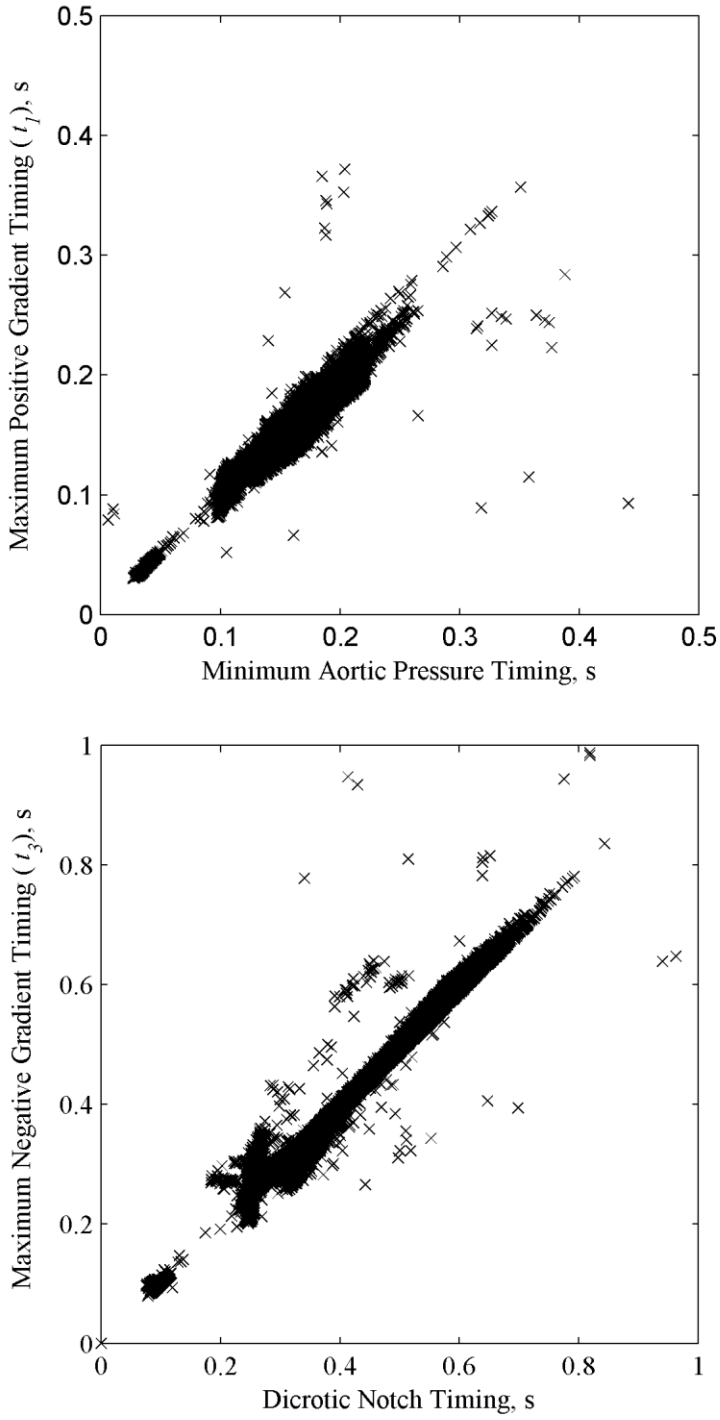

Fig. 3.5: Correlations between aortic pressure features and TVE peak gradient timing (t_1 and t_3). R = 0.972 and R = 0.997, respectively.

Table 3.1: Fixed TVE curve parameters, presented as median (25^{th} – 75^{th} percentile). Note that parameters are unit-less due to normalisation of both time and elastance.

Parameter	Parameter Value
x_1	0.34 (0.27 – 0.43)
$\dot{x_1}$	17.8 (10.6 – 24.2)
x_2	0.58 (0.45 – 0.69)
x_3	0.73 (0.64 – 0.81)
$\dot{x_3}$	-14.1 (-18.7 – -10.6)
t_1	0.22 (0.21 – 0.23)
t_3	0.68 (0.65 – 0.73)

3.3.3 Evaluation of Approach

The errors associated with dynamic timing, as opposed to fixed timing, in generating the TVE curve are shown in Table 3.2. The median overall error exhibited by the dynamic timing approach was 18%, less than half of the median 41% error exhibited by the fixed timing approach, and errors for the dynamic approach were, overall, significantly lower ($p < 0.05$, two-tailed Student's t-test). The median errors for both methods varied notably between pigs, from 15.8% to 21.7% for the dynamic and 34.8% to 43.5% for the fixed timings. Also of note is that the relative median errors do not correspond between the two methods. For example Pig D6 has the lowest median error for the dynamic timing (15.8%), yet not for the fixed timing (34.8%). Conversely, Pig D2 has the second highest median error for the dynamic timing (20.9%) and the lowest median error for the fixed timing (23.3%).

Table 3.2: Errors associated with the dynamic and fixed timing approaches, presented as median (25^{th} – 75^{th} percentile).

Pig (Test Cohort)	Dynamic Timing Error	Fixed Timing Error
D2	20.9% (19.3 – 24.3)	23.3% (21.1 – 25.8)
D4	18.2% (14.3 – 21.3)	40.4% (34.7 – 48.2)
D5	21.7% (15.3 – 28.1)	43.5% (34.6 – 49.0)
D6	15.8% (13.4 – 18.6)	34.8% (21.4 – 51.4)
Overall	18.0% (14.4 – 23.5)	41.0% (28.9 – 49.3)

3.4 Discussion

The dynamic approach produced relatively low errors of median 18% (IQR: 14.4% – 23.5%). This error was less than half of the error associated with the fixed TVE curve of 41% (IQR: 28.9% – 49.3%), and statistically significantly lower overall. This significant reduction in error highlights the disadvantage of generic TVE curves, and the advantage of individualising this input if it can be obtained, as here, from readily available data and established physiological relationships.

The fact that the approach was derived and validated over entirely independent cohorts of pigs lends further support to the applicability of this approach. Further, it is important to note that the experimental protocol employed incorporated a dobutamine infusion, which directly, rapidly and artificially alters cardiac elastance [104]. As such, while population values are established and validated over the same experimental protocol, this protocol includes a clinical intervention designed to directly and dramatically alter the fundamental cardiac elastance from which TVE is derived, and which different individuals are known to respond differently to [105].

Median errors varied notably pig-to-pig ranging from 15.8% to 21.7% for the dynamic approach and 34.8% to 43.5% for the fixed approach. This outcome implies that some inherent, pig specific property of the TVE curve is likely not being captured. A combination of sensitivity (Fig. 3.4) and variability (Table 3.1) suggests a significant amount of the remaining error is associated with the shoulder height x_2, which is in turn significantly influenced by the parameter V_d, set to 0 in this work. Thus, it is possible that identification of a subject specific V_d for each pig would reduce this difference, while retaining a more physiological than phenomenological approach to derivation of parameters.

Mention should be made here of the nature of the original definition of the TVE curve in [55]. Here it is suggested that the TVE curve, when combined with V_d, possesses a uniform shape and changes solely based on end-systolic elastance (E_{es}), the maximum magnitude of the non-normalised TVE curve. This assumption clearly contrasts with the notion that the form of the TVE curve can offer diagnostic information in [44, 89, 90, 99], and would support the approach presented here of using a fixed form for the TVE curve, though devoid of information from V_d. However, as the original TVE study [55] was performed over a limited number of heartbeats, subject to extremely controlled conditions, including the heart being essentially isolated from cardiac reflexes, controls, and systemic input, it seems likely that the TVE curve for an isolated heart may be uniform, but the complex network of cardiovascular control and reflex systems responding to various external stimuli provides the shape changes observed here and elsewhere.

As such, this approach's application leans more towards providing a quick, simple means of significantly improving the accuracy of the TVE curve as an input to a larger model of the entire circulatory system [93, 94]. Use of such a beat-to-beat TVE curve as an input can reduce both identification timing and overall simulation error in such models. While the TVE curve is also capable of providing information such as trends in cardiac work, as E_{es} typically remains constant for a constant inotropic state [57], the simplification of physiological behaviour here and use of a fixed form for the TVE curve means the approach is more likely to be useful as a simple, easy means of improving a TVE input into a model than as an independent diagnostic tool.

It is worth noting that the approach was able to maintain accuracy despite the pigs undergoing a range of manoeuvres that significantly impact cardiac state. These included vena cava occlusions with a fluid filled balloon, which cause a sharp decrease in cardiac preload [87], fluid infusions which can cause variation in stressed blood

volume [64] and dobutamine infusions which lead to an increase in heart contractility [104]. This outcome suggests the approach will be robust to the dynamic cardiac states often found in critically ill patients [44]. The use of clinically and readily available aortic pressure measurements means that this approach can be implemented in real-time for this cohort. Overall, this approach is able to provide additional, beat-to-beat, patient specific information in real-time without requiring additional, invasive instrumentation.

3.5 Summary

An existing approach for identifying the TVE curve on a beat-to-beat basis was validated and modified, using a combination of strong correlations ($R > 0.97$) to aortic pressure waveform features and population constants assessed across 38,106 heartbeats over a development cohort of 2 porcine specimens. Validation of the approach was accomplished using 54,410 heartbeats across an independent test cohort of 4 porcine specimens. The results of this validation showed a reduction in normalised area under the curve error from 41.0%, when using only population constant values, to a median of 18.0%. This approach has the potential to provide a simple means of significantly improving the accuracy of TVE inputs into a larger model. However, due to the simplification of cardiovascular behaviour, lack of V_d as an input and the use of a single, rigid shape for the driver function, diagnostics or other cardiovascular information directly derived from the TVE curve likely necessitate a more comprehensive model. The next chapter addresses the need for a subject specific V_d.

4

Ventricular Dead Space Volume

Ventricular dead space volume (V_d) is a somewhat ambiguous physiological term intimately associated with the time varying elastance (TVE) concept. V_d is representative of the subject specific volume within the ventricle not actively participating in ventricular function, but can only be established using highly invasive and demanding experimental procedures. As such, it is frequently assumed equal to zero in studies. A less demanding means of estimating this parameter would provide a means to improve the performance of a number of such models, and more accurately non-invasively estimate the TVE curve.

4.1 Background

V_d and the related ventricular volume at zero pressure (V_0) are important subject-specific parameters for normalising inter- and intra- subject variation in cardiovascular models, including the widely used end-systolic pressure-volume relation (ESPVR) and TVE models [55, 57, 58, 89, 90, 98]. V_d was originally conceptualised as an '*experimentally determined correction factor*' for the TVE model [55] with a pair of similar physiological definitions being established. V_d has been said to '*represent a functionally dead volume at which the ventricle cannot generate any supra-atmospheric pressure*' [55, 57], a definition generally denoted V_0 (referred to as V_0 henceforth). V_d has also been defined as the volume at which '*the ventricle cannot develop any systolic pressure*', which occurs at '*a volume coordinate only mildly less than* V_0 [57, 106]' (referred to as V_d henceforth). This second definition corresponds to

the intersection of the ESPVR and End-Diastolic Pressure-Volume Relation (EDPVR) curves, where the maximum (end-diastolic) and minimum (end-systolic) volumes for a given heartbeat are identical, and thus no volume or pressure change is developed across that heartbeat. The definitions of V_0 and V_d are illustrated in Fig. 4.1.

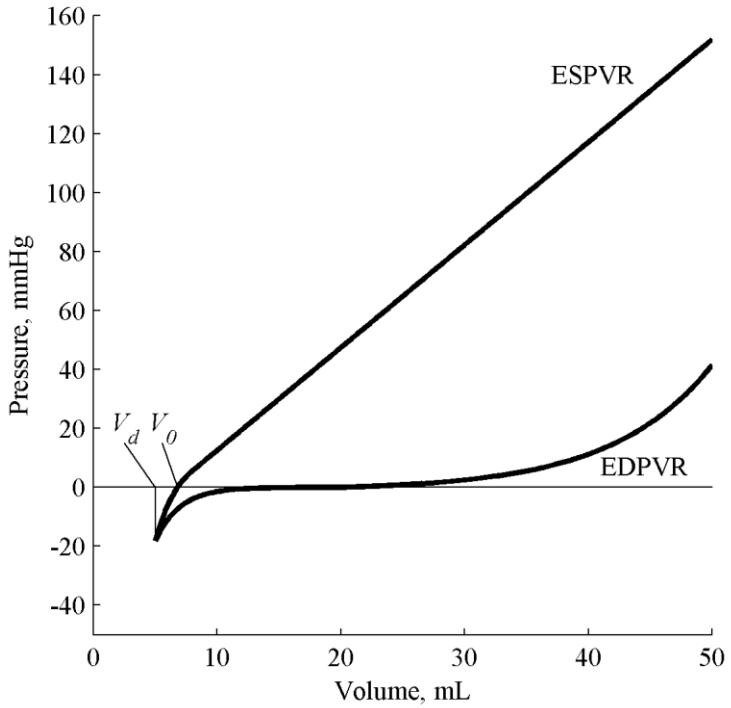

Fig. 4.1: The ESPVR, EDPVR, V_0 and V_d. Definitions as in [57].

In cardiac models based on the TVE concept, which are widely used in haemodynamic studies [55, 57, 58, 89, 90, 98], V_d and V_0 are used to account for variations in heart size, shape and efficiency between individuals and as an individual's condition changes. Specifically, V_d and V_0 represent a subject and condition dependent portion of measured ventricular volume that is not actively participating in ventricular function. As such, being able to estimate and account for V_d and V_0 on a subject and condition specific basis improves the physiological accuracy and the ability to accurate compare results from these models, where such models offer significant potential clinical benefits [89, 90, 107, 108]. Hence, this chapter presents new approaches to estimating

these values to better enable the use of TVE and associated models clinically and thus enhance their clinical impact.

In addition, the physical definitions of V_d and V_0, and their sensitivity to contractile state, suggests a potential direct use for these terms as a diagnostic aid [58, 109]. For example, one would expect an increase in V_d to suggest a heart behaving less 'efficiently' as a pump, and, for obvious reasons, a connection between these terms and the left ventricular ejection fraction (LVEF) [110]. Hence, this term alone may provide further diagnostics in addition to its use and need in other models from Chapter 3.

However, V_d cannot be directly measured without difficult experimental protocols due to the necessity of reducing the ventricle to atmospheric or sub-atmospheric pressure. Initial experiments validating the TVE model involved cross-circulated canine hearts [55, 98], a procedure which elegantly separates cardiac behaviour from systemic influences and allows reduction of the living heart to atmospheric pressure, but is clearly not applicable to an intensive care unit (ICU) patient**.** A less invasive alternative is the approximation of V_0, which has a similar value to V_d, via the ESPVR [109, 111]. However, this procedure typically relies on occlusion of the vena cava, a specialised intervention that places a significant added burden on both medical staff and patients, and is thus largely constrained to experimental studies. Further, the short time interval necessitated by such a procedure means that transient, rather than steady state, behaviour is captured, unless cardiac reflexes are suppressed, obfuscating the true ESPVR curve [112, 113], explored in Chapter 8. As such, there is no easy, practical means to assess V_d or V_0 in the ICU, where it might add clinical value.

This chapter presents a novel method for deriving V_d as physiologically defined in [106]: the volume at which '*the ventricle cannot develop any systolic pressure*'. It relies upon the extrapolation of a Frank-Starling curve (SV-V_{ed}) and its end-systolic equivalent (SV-V_{es}) to the point where stroke volume (SV) is 0, and '*the ventricle cannot*

develop any systolic pressure'. The method utilises common ICU procedures, such as mechanical ventilation recruitment manoeuvres, to develop this curve, and does not require specialised clinical intervention. The method is demonstrated across both a healthy, baseline case, as well as a compromised state after an endotoxin infusion to demonstrate the method's applicability to both healthy and compromised cardiovascular systems.

The method as presented here employs an invasive left ventricular catheter to measure end-diastolic (V_{ed}) and end-systolic (V_{es}) volume. Such volume measurements are increasingly available non-invasively via methods such as echocardiography [114], though it is important to note that the number of V_{ed} and V_{es} measurements required are demanding by the standards of modern echocardiography. While further validation and a modified protocol would be required, this method has the long-term potential to allow non-additionally invasive, patient-specific evaluation of V_d in a clinical environment, and thus an assessment of its clinical value beyond use in physiological models.

4.2 Methods

4.2.1 Experimental Data

This chapter makes use of the Protocol S data from 6 pigs, including the pig largely excluded due to data acquisition issues. The data from this pig was still usable, but extremely labour intensive to employ due to frequent gaps in the recorded data. However, due to the relatively simple, robust modelling required and the unusual and ambiguous nature of V_d, inclusion of this data in this chapter was deemed worthwhile. The waveform employed is continuously sampled left-ventricular volume (V_{lv}), providing invasively measured *SV*, V_{es} and V_{ed}. Data from the Protocol D pigs were not used in this chapter, as the fluid boli and dobutamine infusions present in Protocol D tended to induce sharp shifts in V_{es} and V_{ed}. In contrast, the more gradual fluid infusion

and RM driven shifts present in the Protocol S data were better suited to the methodology presented in this chapter.

4.2.2 Estimation of V_d

This method uses the definition of V_d as the volume at which '*the ventricle cannot develop any systolic pressure*' [57, 106]. V_{es}, V_{ed} and SV for each heartbeat were established from catheter data. This data was used to generate a Frank-Starling curve (SV-V_{ed}) and its end-systolic equivalent (SV-V_{es}) for each subject. Separate linear regression of the SV-V_{es} and SV-V_{ed} curves was performed using a total least squares algorithm [115]. Independent extrapolation of each curve to the y-axis should result in both converging to a single point at which $SV = 0$. At this point, no systolic pressure is developed over the course of a heartbeat, as $V_{ed} = V_{es}$, and V_d is the value of the ventricular volume y-intercept. Separate linear regression of the SV-V_{es} and SV-V_{ed} curves was chosen, as opposed to simultaneous regression with forced convergence of the two curves on the y-axis, as separate regression provides two separate V_d estimates, the agreement between which can be used to evaluate the physiological validity of the assumptions that drive the method.

4.2.3 Evaluation of Method

Ventricular Dead Space Volume (V_d) is extremely difficult to physically measure, and some ambiguity as to the exact definition of this value exists [57]. These difficulties make validation via a measured 'ground truth' V_d value impractical. As such, validation of the method used to derive V_d must rely on validating individual model assumptions and the physiological reasonability of the results. This validation process encompasses:

- Evaluation of the agreement between the separate V_d values derived from the SV-V_{es} and SV-V_{ed} curves for each pig. Theoretically, the two curves should

intersect at an identical V_d value if the linear approximation of the Frank-Starling curve holds.

- Assessment of the validity and strength of linear regression via Pearson's correlation coefficients, presented as *R* values, to ensure a linear, physiological relationship, rather than chance, creates the observed lines.
- Evaluation of the reasonability of the derived V_d values, both in terms of physiology and in comparison to invasively measured values presented in literature.

The analysis of data for each pig was separated into pre- and post- endotoxin infusion, as the development of sepsis should modify contractility and result in an increase in V_d. This hypothesis was evaluated using a one-tailed paired Wilcoxon Signed-Rank Test [116]. This non-parametric statistical test does not rely on data being normally distributed. A single value for V_d pre- and post- endotoxin infusion was provided from each of 6 pigs (n = 6). Overall, the method was employed across a total of 59,513 heartbeats worth of data, and 6 different animals in multiple circulatory states.

Once severe sepsis developed, the Frank-Starling curve generally collapsed to the extent nonlinear behaviour was present in the observable data range. Data gathered during this period of severe sepsis, the onset of which was defined as a drop in LVEF of greater than 33% for greater than 60 seconds [117], is excluded, as linear behaviour is a poor approximation to make at this point. This observable non-linear behaviour is illustrated by the Frank-Starling curves [46, 118], approximated by hand, and the 'circulatory collapse' region in Fig. 4.2, overlaid with data from Pig S2.

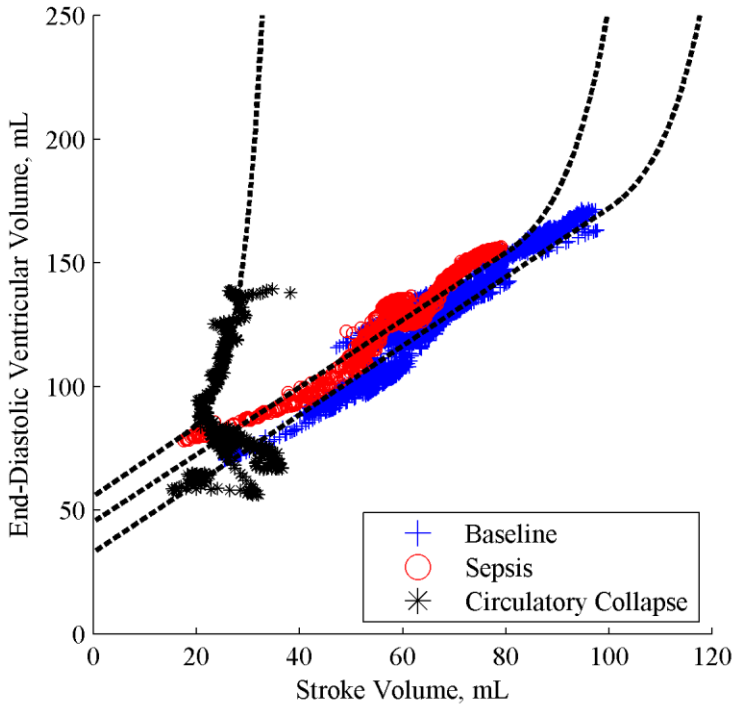

Fig. 4.2: Example Frank-Starling curves with data from Pig S2 overlaid. 6841 heartbeats, illustrative trend lines drawn by hand.

4.3 Results

Table 4.1 shows the absolute and relative values of V_d derived from the end-systolic $V_d(V_{es})$ and end-diastolic $V_d(V_{ed})$ curves, as well as the variation between these values. V_d values for each subject are specified separately for the pre- and post-endotoxin infusion periods. Due to the relatively small number of subjects, it is possible the data set is not normally distributed and thus overall values are presented as median (25^{th} percentile–75^{th} percentile).

Fig. 4.3 shows the SV-V_{es} and SV-V_{ed} curves used to derive V_d, and the corresponding regression lines and correlation coefficients for each pig, pre- and post- endotoxin infusion. The stroke and absolute volumes for each pig occupy a reasonably diverse range both inter- and intra- subject. The correlation coefficients, $R = 0.78$ and $R = 0.80$ average for pre- and post- endotoxin infusion respectively, are consistently high, again supporting the validity of a linear model over these periods and interventions.

Table 4.1: V_d and its variability, as determined by linear regression.

Pig		$V_d(V_{es})$[a], mL	$V_d(V_{ed})$[a], mL	ΔV_d, mL	ΔV_d, $\%V_d$	$V_{es}(0)$[b], mL	$V_d(V_{es})$, $\%V_{es}(0)$	$V_d(V_{ed})$, $\%V_{es}(0)$
S1	N[c]	26.8	27.5	0.7	2.7%	60.6	44.3%	45.5%
	S[c]	33.6	34.0	0.4	1.2%		55.5%	56.2%
S2	N	22.8	22.8	0.1	0.4%	49.3	46.2%	46.4%
	S	40.7	40.2	0.5	1.2%		82.6%	81.5%
S3	N	29.8	32.1	2.3	7.8%	61.6	48.3%	52.0%
	S	43.2	43.8	0.6	1.4%		70.1%	71.0%
S4	N	26.2	26.8	0.6	2.3%	52.6	49.8%	50.9%
	S	41.8	42.0	0.2	0.4%		79.4%	79.7%
S5	N	27.1	26.0	1.1	4.1%	51.1	53.1%	50.9%
	S	32.3	32.2	0.1	0.4%		63.2%	62.9%
S6	N	31.9	31.2	0.7	2.2%	71.2	44.7%	43.8%
	S	35.1	35.4	0.3	0.9%		49.3%	50.0%
All[d]	N	27.0 (26.2–29.8)	27.2 (26.0–31.2)	0.7 (0.6–1.1)	2.5% (2.2–4.1)	57.7	47.3% (44.7–49.8)	48.7% (45.5–50.9)
	S	37.9 (33.6–41.8)	37.8 (34.0–42.0)	0.4 (0.2–0.5)	1.1% (0.4–1.2)		66.7% (55.5–79.4)	67.0% (56.2–79.7)

[a] $V_d(V_{es})$ and $V_d(V_{ed})$ denote V_d values derived from the *SV*-V_{es} and *SV*-V_{ed} curves respectively.
[b] $V_{es}(0)$ denotes the baseline end-systolic volume, averaged over the first 10 heartbeats of the experiment.
[c] N denotes data from the pre-infusion (normal) region while S denotes data from the post-infusion (developing sepsis) region.
[d] 'All' values are presented as median (25^{th} percentile–75^{th} percentile).

The lower correlation coefficients for *SV*-V_{es} as compared to *SV*-V_{ed}, despite very similar distribution of data points around the respective linear trend lines, are primarily due to the often near horizontal gradients present in the *SV*-V_{es} trend lines. Specifically, Pearson's correlation coefficients 'punish' lower trend gradients as, in the extreme, a perfectly linear, perfectly horizontal trend does not mean one variable is correlated with another, and the associated correlation coefficient is 0, as opposed to 1 [119]. As such, these lower correlation coefficients do not represent a poorer linear fit, but a poorer guarantee of variable correlation, a concern alleviated here by the physiologically established nature of the relationship employed.

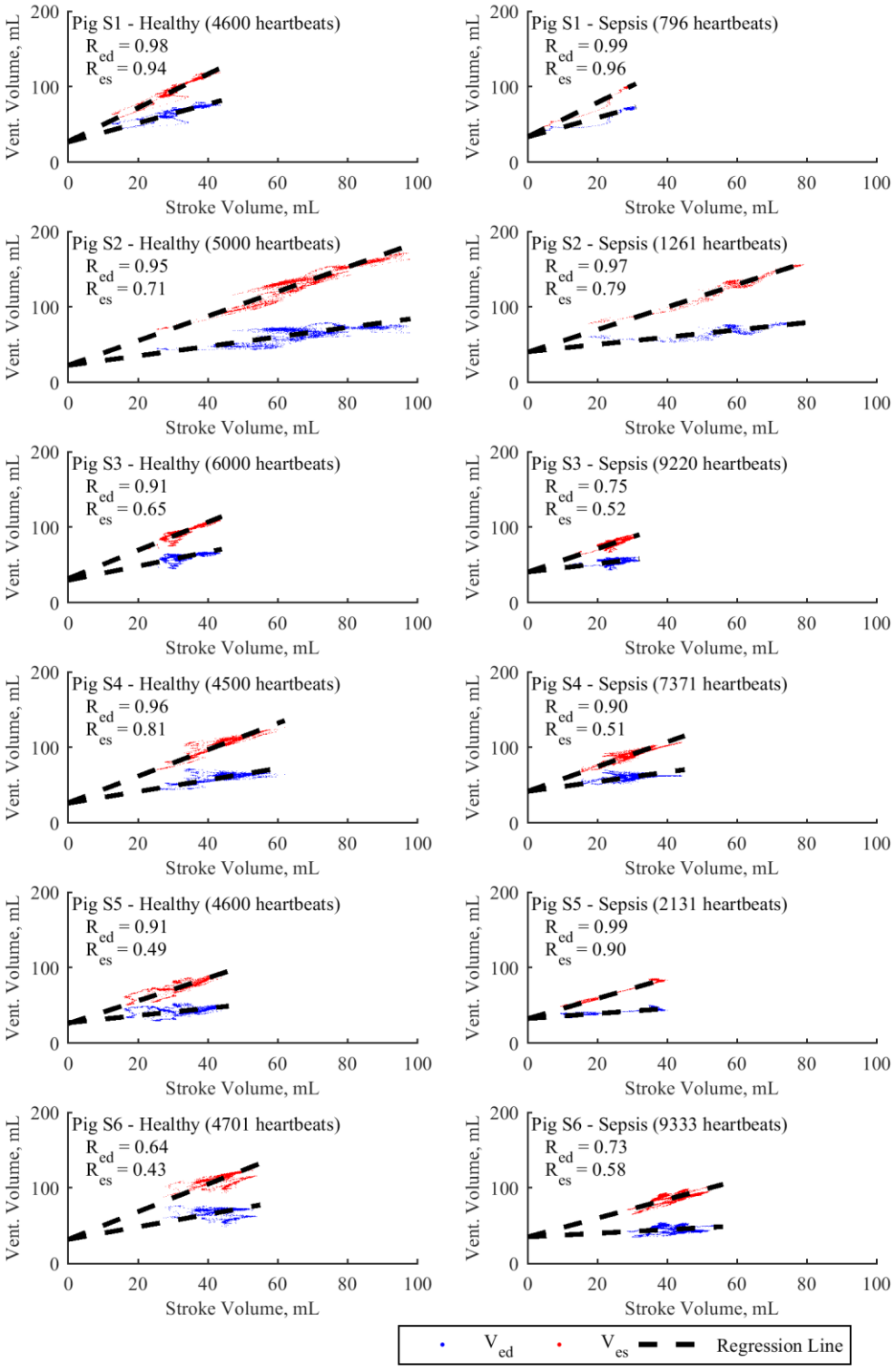

Fig. 4.3: Pre- (left) and post- (right) endotoxin infusion *SV-V*$_{ed}$, *SV-V*$_{es}$ curves and regression lines for each pig. Number of heartbeats and Pearson's correlation coefficients (*R*) presented in figure.

4.4 Discussion

4.4.1 Validation

One of the core assumptions made in determining V_d is that SV is a linear function of both V_{es} and V_{ed}. This assumption is somewhat physiologically intuitive, as both V_{es} and V_{ed} are intrinsically related and largely reliant on the same underlying factors, and such behaviour has been observed elsewhere [120]. However, one would expect some degree of independent variation, especially as sepsis and thus circulatory distress progresses. Fig. 4.3 shows consistently strong linear relationships for SV-V_{es} (R = 0.69 average) and SV- V_{ed} (R = 0.89 average) for all 6 Protocol S pigs undergoing a full progression from healthy to cardiac failure due to sepsis. This result implies that, while some independent variation in V_{es} and V_{ed} certainly occurs, the variables largely maintain a linear relationship even when the cardiac system is under considerable stress.

Another core assumption is that the relationship between SV, V_{es} and V_{ed} is not just linear in the observed range, but can be linearly extrapolated to SV = 0. Table 4.1 and Fig. 4.3 both show that independent linear extrapolation of the SV-V_{es} and SV-V_{ed} lines for each pig yields extremely consistent values for V_d with 7.8% variation at most, and an overall median absolute difference in paired V_d estimates of 2.1%. This low degree of variation across 6 separate subjects exhibiting a range of cardiac behaviour across a diverse and demanding clinical protocol provides strong support for this assumption. Further, the Frank-Starling Curve (SV-V_{ed}) is known to behave linearly in this region [46, 121], and linear behaviour of the SV-V_{es} curve may thus also be reasonably intuited.

Further supporting evidence of the validity of linear extrapolation is provided in the fact that the method yields extremely consistent, positive, values for V_d relative to V_{es}. These V_d values are 44.3-53.1% of the baseline V_{es} pre-infusion, and rise to 49.3-82.6% of the baseline V_{es} post-infusion. This consistency supports the idea that V_d varies

between subjects in a manner somewhat proportional to ventricular volume for a given set of cardiac conditions. The fact that this percentage range of baseline V_{es} is reasonably small for healthy behaviour provides the possibility to estimate baseline V_d from baseline V_{es}, although this range of values may be different for humans compared to pigs.

The derived values for V_d also agree with measured values provided in the literature. Although these literature studies typically use the $V_d = V_0$ definition for ventricular dead space, the two values have been shown to be similar [57, 106]. For example [109] presents several V_0 values for cross circulated dogs, and protocols involving preload, afterload and inotropic variation. The baseline preload experiment gives a range of 13-52% and the baseline afterload experiment a range of 46-83% of V_{es} for V_0, overlapping with the 44.3-53.1% of V_{es} range for V_d observed in this chapter. Observations in [58], a study conducted on humans, yield V_0 values for a normal contractile state in a 24-84% of V_{es} range for V_0, ignoring non-physiological negative results, across 5 subjects, again encompassing the 44.3-53.1% of V_{es} range for V_d observed in this chapter. Further, [58] also observed an increase in V_0 values from a baseline average value of 32 cc/m^2 to an average value of 46 cc/m^2 for individuals with intermediate and 100 cc/m^2 for individuals with poor contractile function, which agrees with the statistically significant increase in V_d observed in this chapter as sepsis developed. Other values presented in literature are similarly sized, positive values, as might be expected [111, 122]. Overall, this further data provides a strong body of evidence for the physiological validity of the results and thus the proposed methodology.

4.4.2 Response to Sepsis

In the period between endotoxin infusion and cardiac failure, V_d values rose in all cases from a range of 44.3-53.1% to 49.3-82.6%. This statistically significant increase in dead space volume corresponds to the decreased LVEF observed in sepsis patients, and

the myocardial depression associated with failure to survive sepsis [123]. This behaviour agrees well with the physiological definition of V_d, and supports its potential clinical use as a diagnostic aid. Importantly, in this region, the agreement between the two V_d values remained strong, and correlation coefficients remained high, suggesting the Frank-Starling curve remained in its linear region despite significant change in cardiac function

Directly prior to death, the Frank-Starling curve generally underwent a dramatic shift to the left and nonlinear behaviour was observable and strong (example in Fig. 4.2). This corresponds to the expected behaviour of the Frank-Starling curve as complete cardiac failure occurs [118]. This data, characterised by a decrease in LVEF of greater than 33% for longer than 60 seconds, was excluded from the 'post-endotoxin infusion' data as linear behaviour is a poor approximation to make at this point.

4.4.3 Limitations

There are some limitations to this study worth discussing. First, the study employs a left ventricular catheter to measure V_{ed} and V_{es}, the insertion of which is an invasive procedure that is not common practice in the ICU. Such volume measurements are increasingly available non-invasively via methods such as echocardiography [114], but the number of measurements required for this method is demanding by current echocardiography standards. Further, volume measurement, in addition to specialised invasive protocols, is also required for approximation of V_0 via the ESPVR [112, 113], which is the standard method available for finding a value similar to V_d. In contrast, the method presented here requires only common ICU interventions, primarily recruitment manoeuvres, to obtain a large enough range of data to fit a line. These interventions occur in normal care and are thus less burdensome to obtain. They also occur over a longer timescale meaning cardiac reflexes distort results less significantly compared to other methods.

Additionally, all data presented here is the result of the same protocol involving sepsis, a complex and varied condition [88], and several standardised interventions. While this data set encompasses several pigs and the full progression from healthy, baseline behaviour to cardiac failure, there are a huge range of possible cardiac conditions that could be tested. Thus, further validation over several of these conditions would be beneficial. Regardless, the underlying physiology and data supporting the development of this method has been discussed in detail, and would be expected to transfer to the majority of such conditions.

4.5 Summary

Overall, V_d is an important, subject specific, physiological value that is difficult to measure or accurately approximate, even when invasive instrumentation is available [57]. Thus, the method presented and validated in this chapter offers significant potential in its ability to provide a relatively easy, non-additionally invasive means of estimating V_d when ventricular volume measurements are available, without requiring a specific and highly involved protocol. Though any clinical application requires further studies and a modified protocol, this method offers the potential to aid in assessment of patient condition through its ability to normalise intra- and inter- patient variability in analysing and managing cardiovascular and circulatory dysfunction. Importantly for subsequent work, this method also provides a means of estimating V_d from baseline V_{es}, which was not previously possible.

5

End-Systolic and End-Diastolic Volume

In general, intensive care unit (ICU) instrumentation provides a better picture of cardiac pressure than of volume, while a number of significant cardiac metrics, such as end-diastolic volume (V_{ed}) as a surrogate for preload, time varying elastance (TVE) and pressure-volume (P-V) loops, rely on volume as an input. To more accurately estimate these metrics, additional volume information is required. The unstressed or 'dead space' ventricular volume (V_d) as discussed in Chapter 4 provides part of this picture, as do recent advances allowing the estimation of stroke volume (SV) from aortic pressure (P_{ao}) [108, 124]. Beat-by-beat upper and lower limits on ventricular volume would thus provide the last piece in the puzzle required to fully estimate the ventricular volume profile.

5.1 Background

Two important cardiovascular biological markers in the intensive care unit (ICU) are preload and afterload. Afterload serves as an indicator of the pressure downstream from the left ventricle, and is sensitive to alterations in valve function and arterial tone [46]. Afterload is approximated in the ICU via the typically measured, resulting P_{ao} [68]. Preload, representing the loading conditions upstream from the heart, is sensitive to venous blood pressure and return, which are in turn sensitive to circulatory volume and venous tone [46].

Preload is typically represented by V_{ed} [62], but this value is not typically measured in the ICU as the required instrumentation is too invasive. As a result, clinical approximation is difficult. In fact, volume and flow measurements, in general, are rarely taken in the ICU [108], resulting in a relative abundance of pressure measurements, but an incomplete picture of cardiac behaviour without volume or flow.

Recent work has provided a means of approximating the beat-to-beat cardiac *SV* under typical ICU instrumentation [108]. *SV* provides a beat-to-beat indicator of the how much heart volume is changing, but must be combined with a beat-to-beat absolute maximum or minimum value to provide a more complete picture of cardiac volume behaviour, and thus allow approximation of cardiac preload. There is thus a need to relate either end-systolic volume (V_{es}) or V_{ed} to existing pressure measurements. An existing and frequently used example of such a relationship is the end-systolic pressure-volume relation (ESPVR) [58, 91, 125]. However, this relation relies upon several subject specific parameters that are measurable in an experimental environment, but too invasive to measure clinically.

This chapter investigates the viability of using a modified ESPVR to provide a beat-by beat approximation of V_{es}, allowing, in concert with *SV*, approximation of V_{ed} (preload) and a more complete picture of cardiac volume behaviour. This modified ESPVR relies on continuous heart rate and aortic pressure data, and initial parameters being fixed during a brief ~10 heartbeat echocardiography calibration during which non-invasive volume measurements are available [126]. Such short echocardiography readings are becoming increasingly available clinically [127], enabling the research presented in this chapter. This method thus has the potential to aid in the provision of a more complete picture of cardiac behaviour under normal ICU instrumentation without additional invasive measurements or procedures.

5.2 Methods

5.2.1 Experimental Data

This chapter makes use of the 5 Protocol S pigs as a development cohort and the 6 Protocol D pigs as a validation cohort. The waveforms employed include continuously sampled P_{ao} as a method input, and continuously sampled left-ventricular volume (V_{lv}) to provide invasively measured V_{es} and V_{ed}. Due to the lack of available equipment, baseline catheter readings were used as surrogates for baseline echocardiography readings, but it's important to note both methods show comparable performance and correlation to gold standard MRI data [128-130].

5.2.2 The ESPVR

The ESPVR is typically expressed [57]:

$$P_{es} = E_{es} \times (V_{es} - V_0) \tag{5.1}$$

where P_{es} is the end-systolic pressure, E_{es} the end-systolic elastance and V_0 the ventricular volume at zero pressure. This relationship represents the ventricular volume corresponding to a given ventricular pressure when the heart is fully contracted (end-systole).

The exact nature of E_{es} is somewhat controversial. It has been argued that it is constant for a given contractility [55], although there is evidence suggesting it varies as a result of loading conditions [131, 132]. As the intent is to track V_{es} through changes in contractility, a fixed value for E_{es} is clearly not appropriate for ICU monitoring, or for an experimental data set encompassing sepsis and dobutamine, where contractility is directly and dramatically varied due to changes in both condition and drug therapy.

5.2.3 Proposed Method

While a number of the components of ESPVR are not measured under typical ICU instrumentation, it is possible to replace these values with physiologically similar and more easily obtained measurements. ESPVR is thus re-factored:

$$P_{DN} = E_{es} \times (V_{es} - V_d) \tag{5.2}$$

where:

- P_{es} is replaced by P_{DN}, the Dicrotic notch pressure in the aorta, as the aorta sits directly downstream from the left ventricle. Thus, aortic and left-ventricular pressure are very similar, with a slight difference due to aortic valve resistance, during systole. As real-time aortic pressure is typically available in the ICU, P_{DN} provides a readily available surrogate for P_{es}.
- V_0 is replaced by V_d, as the two are often used interchangeably, and have similar physiological roles and values [57, 89, 90]. V_d can be more easily estimated than V_0, via a relationship with baseline V_{es} as presented in Chapter 4 [59]:

$$V_d = 0.48 \times V_{es}(Baseline) \tag{5.3}$$

where the factor 0.48 is generated using the average baseline V_d value from Chapter 4 (which ranges from 0.44 – 0.53). Finally, the fact that E_{es} changes as patient contractility and, potentially, loading conditions vary, needs to be accounted for. The decision was made to approximate E_{es} using a power relationship with heart rate (*HR*) for several reasons. First, changes in *HR* and E_{es} are staple cardiovascular system responses to changing conditions [46]. As continuous monitoring of *HR* in the ICU is commonplace, it provides a partial, if incomplete, picture of cardiovascular system response, which is typically mathematically sympathetic with changes in E_{es}. For example, the neural regulatory baroreflex acts by either increasing or decreasing both E_{es} and *HR*, rather than acting independently on the two [46]. Second, a power

relationship was selected as it suits a mathematically sympathetic relationship and is sufficiently simple, provided the exponent is fixed *a-priori*, that it can be uniquely determined during a short, ~10 heartbeat echocardiography calibration.

Thus, this relationship captures, in a simplified manner, physiological elements and suits the need for method simplicity and ease of use. The fully modified ESPVR relationship thus reads:

$$V_{es} = \frac{P_{DN}}{E_C \times HR^n} + V_d \tag{5.4}$$

where E_C is a subject-specific coefficient with units mmHg.s^3/mL, representing the subject specific coupling between *HR* and E_{es}, and *n* is an exponent to be determined and then fixed *a-priori*. Thus, in the model implementation, P_{DN} and *HR* are inputs that are measured every heartbeat, the exponent *n* is fixed *a-priori*, and V_d and E_C are fixed for the duration of monitoring during the calibration phase, where V_{es} is being measured. The results section presents an assessment of the increase in errors associated with the transition from a subject specific to an *a-priori* value of *n*.

5.2.4 Method Development

Linear least squares, performed using MATLAB (R2014a, 64-bit, The Mathworks, Natwick, MA, USA) and the 'lsqlin' function, was used to determine a subject specific exponent *n* that minimised method errors for each of the 5 Protocol S pigs. Note that E_C can be analytically determined for a given *n* during the echocardiography calibration, and is thus a dependent parameter. The overall process for determining the approximate beat-to-beat V_{es} curve using the *a-priori* exponent, *n*, is defined:

1. Determine V_d (Eq. 5.3) and E_C (Eq. 5.4) from a 10 heartbeat 'calibration' period, where V_{es} is measured, simulating an echocardiography reading.

2. Determine V_{es} for each subsequent heartbeat based on the fixed values (V_d and E_C) and heartbeat specific measured values (HR and P_{DN}).

Overall, direct evaluation of the effectiveness of the method was accomplished across all 5 Protocol S and 6 Protocol D pigs in several ways:

- Using Pearson's correlation coefficients (R), which allow evaluation of the method's capability to capture trends in V_{es} over the course of the two protocols investigated, and thus provide benefits in monitoring patient condition.
- Using the absolute percentage error for each pig, which allows an evaluation of the ability of the method to accurately approximate the exact value of V_{es}, and thus the suitability of this method for use as a component of a larger model.
- Via direct visual evaluation of the trendlines, which is only possible due to the relatively small number of subjects (N = 11), but does provide a means of evaluating the temporal and procedure based variations in method effectiveness.

A comparison across these metrics was made between V_{es} curves estimated using subject specific exponent, n, and V_{es} curves estimated using an *a-priori* fixed exponent, n, which provides an indication of how much method accuracy is lost in the reliance on an *a-priori* exponent.

5.2.5 The Method in Context

While the previous section details a validation of the process from which the method is derived, this section focuses on comparing this method to alternative assumptions sometimes used in literature [57, 89, 90]. This analysis thus places the method in context. This section specifically looks at the impact on error of the two major assumptions made in this method:

1. That V_d can be expressed as a function of baseline V_{es}, as in Eq. 5.3
2. That E_{es} can be expressed as a function of HR, as in Eq. 5.4

Direct evaluation of the tracking of V_{es} using different forms of ESPVR allows validation of both of these assumptions. In particular, 3 different methods of tracking V_{es} were compared:

1. **Fixed E_{es} and neglected V_0:** The standard ESPVR (Eq. 5.1) with $V_0 = 0$ (a commonly used assumption [57, 89, 90])
2. **Fixed E_{es} and fixed V_0:** The standard ESPVR (Eq. 5.1) with $V_0 = V_d$ (allowing assessment of the validity of Eq. 5.3)
3. **Dynamic E_{es} and fixed V_0:** The ESPVR as used in the proposed method (Eq. 5.4) with $V_0 = V_d$, and E_{es} as a function of HR (allowing assessment of the validity of Eq. 5.4)

5.3 Results

5.3.1 Method Development

Table 5.1 provides an overview of the subject specific exponents, n, provided by linear least squares, along with the associated correlation coefficients and error values for tracking V_{es} across the development cohort of Protocol S pigs. Correlation coefficients are generally high with an overall average of $R = 0.87$, and errors generally low with an average of medians of 3.2%, suggesting the model is effectively able to capture the dynamic nature of E_{es}. It was decided, for simplicity, to set the *a-priori* value of $n = 3$ based on these results.

Table 5.2 provides a similar overview of the subject specific exponents for the validation cohort of Protocol D pigs. While these were not used in model development, the provision of these errors and exponents allows a more comprehensive evaluation

of model performance. As can be clearly seen, and as mentioned in Chapter 2, Pig D1 is an outlier, though interestingly retains a relatively good correlation coefficient. While results from Pig D1 are included throughout this chapter, they are excluded from mean calculations. Overall correlation coefficients are high, with a mean value of 0.85. Further, overall error values are relatively low, but notably higher than for Protocol S ($p < 0.05$, two-tailed Student's t-test) due to the disruptive nature of dobutamine on the coupling between E_{es} and HR [11, 66, 69-72].

Table 5.1: Tracking V_{es} with subject specific n for Protocol S: correlation coefficients and errors, presented as median (25^{th} – 75^{th} percentile).

Pig	Exponent (n)	Correlation (R)	Magnitude of Error*, %
S1	3.06	0.93	1.7% (0.9 – 3.0)
S2	3.98	0.94	2.9% (1.5 – 4.8)
S3	2.06	0.87	4.6% (2.2 – 7.2)
S4	2.63	0.80	4.7% (2.1 – 8.2)
S5	4.13	0.81	2.3% (0.9 – 7.7)
Mean	3.17	0.87	3.2% (1.5 – 6.2)

*Magnitude here refers to the fact that the absolute value of the percentage error is taken prior to summary statistics being calculated, thus these errors are not representative of a bias and negative and positive errors do not cancel out.

Table 5.2: Tracking V_{es} with subject specific n for Protocol D: correlation coefficients and errors, presented as median (25^{th} – 75^{th} percentile).

Pig	Exponent (n)	Correlation (R)	Magnitude of Error, %
D1	-5.46	0.82	11.2% (5.4 – 24.4)
D2	1.86	0.89	11.2% (2.7 – 24.6)
D3	1.93	0.88	11.5% (5.8 – 22.0)
D4	2.74	0.87	13.7% (8.5 – 22.6)
D5	3.55	0.91	15.7% (5.6 – 82.6)
D6	0.98	0.60	6.6% (2.8 – 13.2)
Mean	2.21	0.83	11.7% (5.1 – 33.0)

Table 5.3 provides an overview of the correlation coefficients and error values associated with tracking V_{es} using an *a-priori* exponent $n = 3$, as would be done clinically. Overall, there is only a slight increase in error, from 7.5% to 10.6% (mean of median values), and a slight decrease in correlation coefficients, from $R = 0.85$ to R

= 0.84 (mean). There is only once case (Pig D6) in which there is a large increase in error between Tables 5.1/5.2 and Table 5.3. The notable difference in error values between the sepsis and dobutamine protocol pigs is also present in Table 5.3 values ($p < 0.01$, two-tailed Student's t-test). The higher correlation coefficients for pigs D5, D6 and S1 in Table 5.3 as compared to Tables 5.1 and 5.2 are due to the regression process' focus on minimising percentage error rather than maximising correlation coefficient. Specifically, it is possible for a non 1-1 relationship to provide higher correlation coefficients, but this will never be optimal in linear least squares or, indeed, for this model.

Table 5.3: Tracking V_{es} with *a-priori* $n = 3$: correlation coefficients and errors, , presented as median (25^{th} – 75^{th} percentile).

Pig	Correlation (R)	Magnitude of Error, %
D1	0.29	75.1% (17.5 – 109.5)
D2	0.83	14.1% (3.1 – 26.0)
D3	0.84	15.2% (9.6 – 23.3)
D4	0.86	13.3% (9.0 – 23.3)
D5	0.92	18.4% (7.5 – 85.3)
D6	0.66	23.3% (12.2 – 28.2)
S1	0.94	1.8% (1.0 – 3.2)
S2	0.91	6.4% (4.6 – 9.8)
S3	0.84	4.5% (2.7 – 7.4)
S4	0.79	4.7% (2.1 – 8.1)
S5	0.80	4.2% (2.2 – 7.8)
Mean	0.84	10.6% (5.4 – 22.2)

Figs. 5.1 and 5.2 visualise the approximation of V_{es} for each subject across both protocols. It is clear that there are a diverse range of subject specific responses to the various elements of each protocol, which are generally effectively tracked, with the exception of the outlier Pig D1, by the method with only a minor decrease in performance when shifting from a subject specific to an *a-priori* exponent value. The sharp, vertical, and long-term changes in V_{es} exclusive to Fig. 5.1 demonstrates the effect of dobutamine in rapidly altering cardiac behaviour and E_{es}. In contrast, V_{es} in Fig. 5.2 tends to change more gradually as sepsis develops over the course of the

experiment. These latter results indicate the method accurately captures expected, induced changes in V_{es}, and does so in a subject specific fashion, capturing subject specific response to condition and care.

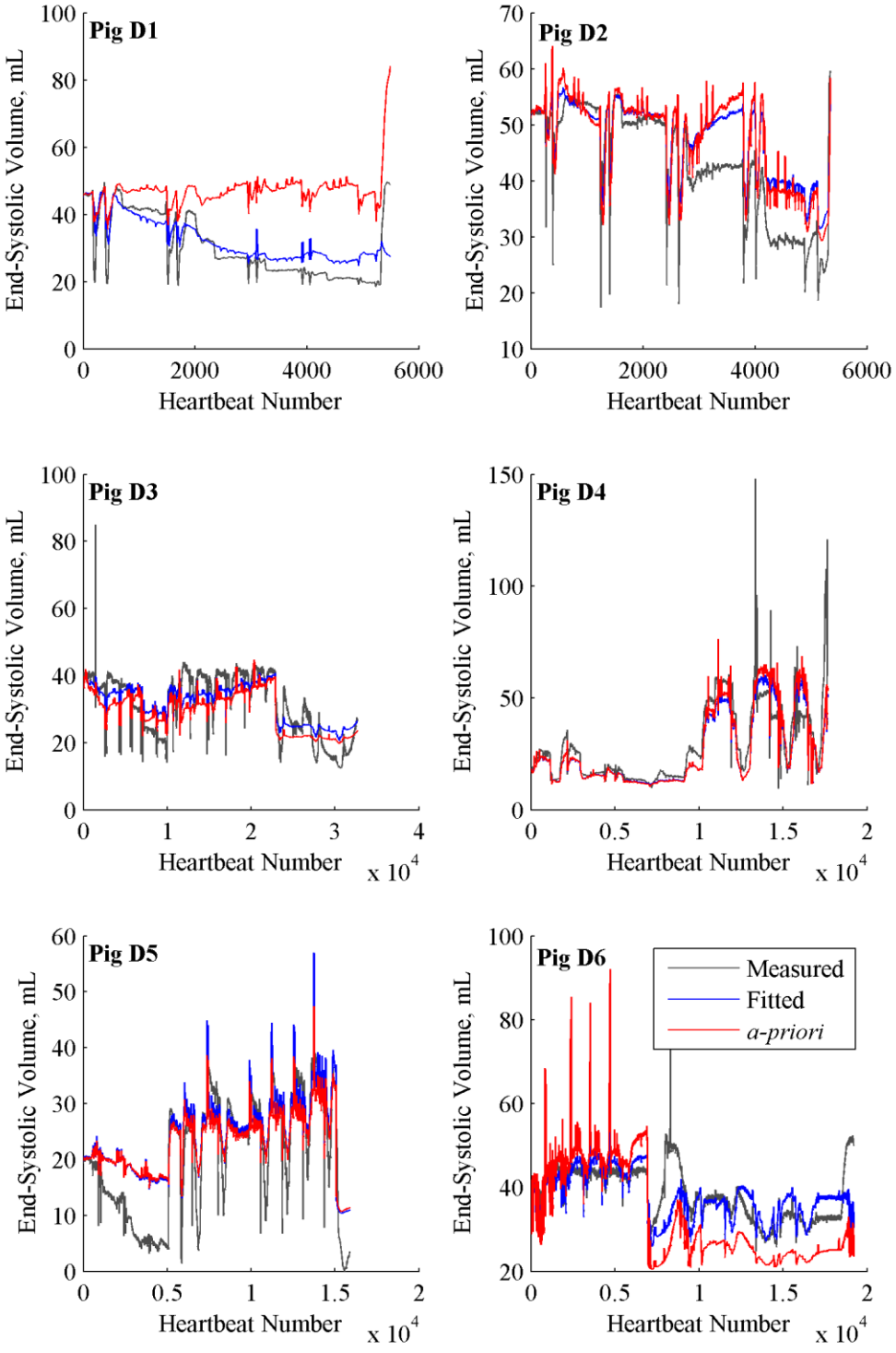

Fig. 5.1: V_{es} trends and tracking for protocol D (dobutamine).

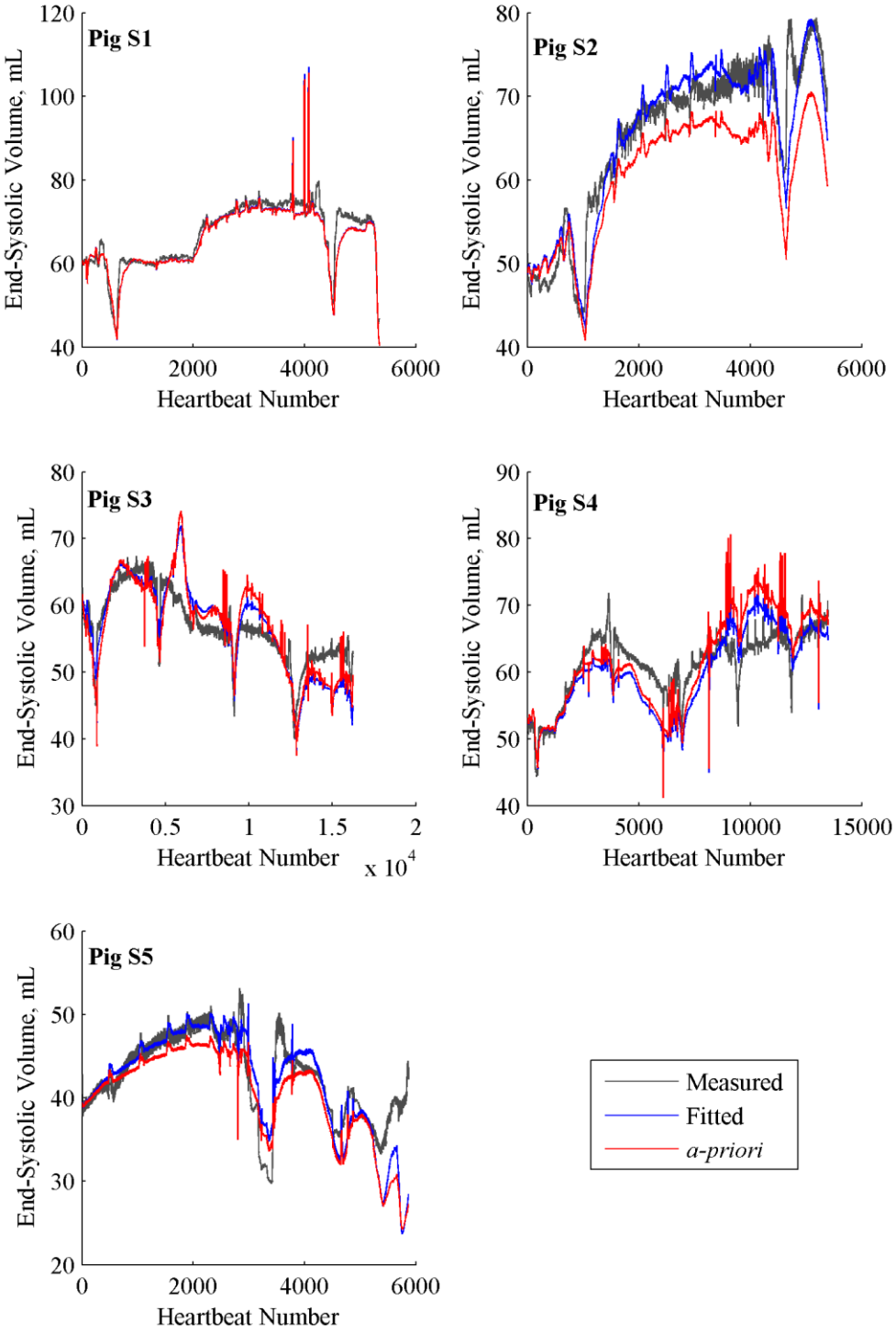

Fig. 5.2: V_{es} trends and tracking for protocol S (sepsis).

5.3.2 The Method in Context

Table 5.4 shows the percentage error associated with the 3 methods specified to track V_{es} in Section 5.2.5 across the 5 Protocol S pigs. Moving from neglected V_0 (Method 1) to fixed V_0 (Method 2), via Eq. 5.3, shows a modest reduction in overall error ($p < 0.05$, paired two-tailed Student's t-test), especially 75th percentile error which falls from 46.4% to 34.5%. Introduction of dynamic E_{es} (Method 3) as opposed to fixed E_{es} (Method 2), via Eq. 5.4, shows a notable reduction in overall error ($p < 0.01$, paired two-tailed Student's t-test), and a significant reduction in median errors from 18.5% to 10.6%. It is worth noting that statistically significant differences despite large, overlapping error distributions is due to the paired nature of the data. On certain heartbeats all methods perform poorly, on others all perform well, but some methods perform better than others consistently across both extremes. Overall, these results support the validity and usefulness of Eqs. 5.3 and 5.4, along with their associated assumptions, in the tracking of V_{es}.

Table 5.4: Magnitude of error associated with different methods of tracking V_{es}, presented as median (25th – 75th percentile). Method 3 corresponds to the method used in Section 5.3.1 with an *a-priori* $n = 3$.

Pig	1. Fixed E_{es}, neglected V_0	2. Fixed E_{es}, fixed V_0	3. Dynamic E_{es}, fixed V_0
D1	13.8% (2.1 – 23.4)	41.4% (6.9 – 66.7)	75.1% (17.5 – 109)
D2	5.2% (1.6 – 29.8)	13.5% (2.4 – 15.0)	14.1% (3.1 – 26.0)
D3	30.1% (11.1 – 61.2)	24.1% (5.0 – 55.0)	15.2% (9.6 – 23.3)
D4	14.9% (7.2 – 37.2)	23.6% (11.9 – 29.5)	13.3% (9.0 – 23.3)
D5	34.0% (21.1 – 81.6)	36.0% (22.3 – 73.5)	18.4% (7.5 – 85.3)
D6	18.8% (8.5 – 37.8)	15.1% (3.4 – 48.4)	23.3% (12.2 – 28.2)
S1	4.6% (0.7 – 23.9)	8.7% (0.6 – 14.7)	1.8% (0.2 – 9.0)
S2	19.5% (2.1 – 39.1)	23.4% (2.1 – 34.0)	6.5% (1.8 – 16.5)
S3	12.2% (4.2 – 45.0)	5.6% (0.2 – 16.6)	4.5% (0.5 – 12.7)
S4	30.7% (7.3 – 42.7)	23.3% (2.9 – 29.3)	4.7% (0.4 – 13.6)
S5	12.4% (1.1 – 65.4)	11.7% (0.9 – 32.7)	4.2% (0.4 – 23.4)
Mean	18.2% (6.5 – 46.4)	18.5% (5.2 – 34.5)	10.6% (4.5 – 26.1)

Note the values quoted from the final row of Table 5.4 are an average of the 25th percentile, median and 75th percentile error for the pigs rather than an overall 25th percentile, median and 75th percentile error. The decision was made to represent population values in this way as the overall median is less representative than the average median due a differing number of heartbeats recorded for different pigs.

The comparative behaviour of these 3 methods is well illustrated in Fig. 5.3, which shows the tracking of V_{es} for Pig S1. Method 1 agrees reasonably well with measured V_{es} during normal behaviour, but diverges significantly from measured V_{es} during recruitment manoeuvres and the onset of severe sepsis, where there are large vertical changes in V_{es}. Method 2 accurately captures these large vertical changes in V_{es}, reducing the large 75th percentile error in Method 1. Method 3 retains the tracking of large vertical changes in Method 2, and tracks normal behaviour more effectively by accounting for changes in E_{es}, significantly reducing median error.

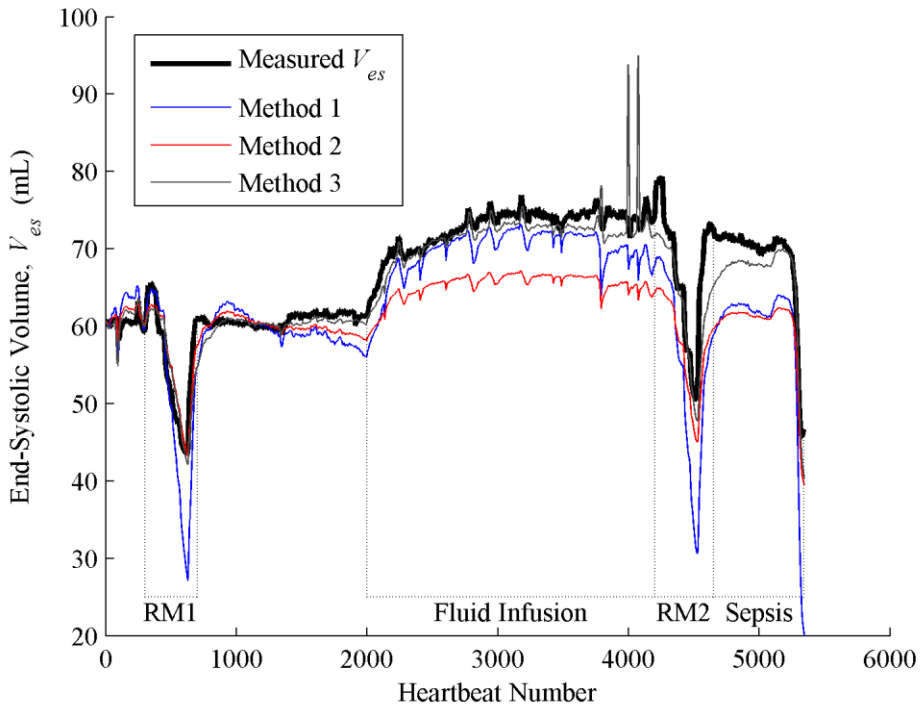

Fig. 5.3: Tracking of V_{es}. Comparison between the three methods in Section 5.2.5 for Pig S1 versus directly measured V_{es}.

5.4 Discussion

5.4.1 Method Development

As seen in Table 5.3, the correlation coefficients across the 2 protocols and 10 pigs excluding D1 are reliably good, with a mean value of 0.84 and a minimum value of 0.66. This result suggests the method effectively captures trends in V_{es}. The ability to track trends in V_{es} allows, in concert with *SV*, for tracking of preload which is important for patient diagnostics and monitoring purposes. That these high correlation coefficients are sustained across 10 subjects and 2 protocols encompassing elements such as sepsis and dobutamine, which dramatically alter cardiac function, provides a good initial validation of the method.

While the ability to track trends is important for monitoring changes in patient condition, the ability to approximate the actual value of V_{es} is important for the method to be used as a component of larger models, and in providing a more complete picture of cardiac volume behaviour in the ICU. Table 5.3 shows the method is able to continuously estimate the value of V_{es} relatively effectively, with a mean median error of 10.6%, and mean 75th percentile error of 22.2%. Again, this accuracy is sustained over a number of subjects and a pair of different and demanding clinical protocols, suggesting the method is able to adapt to both short and long term changes in patient condition due to disease or drug therapy.

From Fig. 5.1, and as previously discussed in Chapter 2 and further discussed in Chapter 7, Pig D1 appears to suffer from sensor drift over the duration of the experiment. While the overall shape of the V_{lv} waveform, changes in *SV* as discussed in Chapter 7, and inter-variable relationships remain present, both V_{es} and V_{ed} show a steady, inexplicable drift downwards over the course of the experimental period, accounting for the radically different fitted exponent (n = -5.46) and high error values

generated when using n = 3, despite low errors in estimating the P-V loop of this pig in Chapter 7.

With the exception of Pig D1, the considerable variation in the subject specific values of n across the two cohorts, which ranged from 0.98 (Pig D6) to 4.27 (Pig S5), only resulted in a minor increase in error and decrease in correlation coefficients with the use of the *a-priori* value of n = 3, derived from the Protocol S data. A comparison between Tables 5.1/5.2 and Table 5.3 shows the largest decrease in correlation coefficient is a relatively minor reduction from R = 0.89 to R = 0.83. A similar comparison of error values shows minor increases in error between Tables 5.1/5.2 and Table 5.3 in most cases, with the only major increase occurring for Pig D6.

Pig D6 had the lowest subject specific exponent (n = 0.98) and poorest correlation coefficient when that subject specific exponent was used (R = 0.60). Fig. 5.2 shows using a value of n = 3 causes an overestimation of the decrease in V_{es} that results from a dobutamine infusion at about heartbeat 7000. However, the method still predicts the direction of change correctly, as well as appearing to accurately model the behaviour prior to and after the dobutamine infusion. This suggests that the low subject specific exponent may be driven primarily by the large shift induced by the dobutamine infusion as opposed to behaviour either beforehand or afterwards. Given the ability of the method to capture dobumatine shifts accurately for the other 5 pigs in Fig. 5.2, this case seems to be an exception, rather than the rule.

There is a distinct overall increase in error values, although not a concordant decrease in R values, from the Protocol S development cohort to the Protocol D validation cohort. This result is to be expected, both due to value of n being selected based on Protocol S, and the fact that dobumatine induces sharp changes in E_{es}, disrupting the sympathetic relationship between E_{es} and HR. This disruption in the relationship between E_{es} and HR makes the Protocol D pigs an excellent and challenging validation

cohort, as well as an unsuitable development cohort, due to such external disruption in the relationship between E_{es} and HR not being typical behaviour.

It is important to note that, despite the disruption the sympathetic relationship fundamental to the model developed in this chapter, overall error error values for both Protocol D and Protocol S are within acceptable levels. The method is still able to capture trends accurately, though the exact magnitude of the patient response to dobutamine is difficult to predict, as in Pig D6, resulting in the observed increased error associated with Protocol D. Thus, the ability of the method to estimate the value of V_{es} would benefit from recalibration after the administration of drugs such as dobutamine, although the method performs well enough, regardless.

5.4.2 The Method in Context

A direct evaluation of the effectiveness of three different ESPVR equations set out in Section 5.2.5 in tracking V_{es} allowed validation of assumptions that:

- That V_d can be derived from V_{es} as in Eq. 5.3 (implemented in Method 2)
- That E_{es} can be expressed as a function of HR as in Eq. 5.4 (implemented in Method 3)

Method 1 serves as a control and uses a simplified ESPVR, assuming $V_0 = 0$ and E_{es} is constant. This method tracks V_{es} reasonably well, yielding an overall median error of 18.2% across all 10 pigs compared to V_{es} as directly measured. The assumption that V_0 can be neglected is often used due to a combination of V_0 being difficult to measure directly, as it requires a significant artificial reduction in ventricular pressure [106], and V_0 typically being relatively small [58]. This assumption is largely supported by these results, as an 18.2% median error seems acceptable when weighed against the type of highly invasive and involved protocol traditionally required to determine V_0.

However, as shown in Fig. 5.3, this 18.2% median error fails to capture the extremely large inaccuracies associated with using Method 1 to track sudden changes in V_{es} due, for example, to recruitment manoeuvres or the onset of severe sepsis. This failure to track sudden changes leads to a significantly larger 75th percentile error of 46.4% for Method 1. This high error when sudden changes occur is of clinical concern in an ICU or cardiac surgery clinical scenario, where sudden changes and accurate, rapid determination of patient responses to these sudden changes is extremely important [46].

Method 2 introduces the assumption that V_d can be derived from baseline V_{es}, as in Eq. 6.4, and that V_d can be used as a surrogate for V_0. There is a minor, but important physiological distinction between the two values: V_0 is the ventricular volume at zero pressure, while V_d is the volume at which the ventricle cannot develop any systolic pressure [57]. However, the purpose of both terms is to account for the subject-specific inactive volume within the ventricle, and the two values have been shown to be similar for a given subject [57].

Method 2 results in a notable decrease in 75th percentile error compared to Method 1 from 46.4% to 34.5%, and is able to track sudden changes in V_{es} significantly more effectively, as shown in Fig 5.3. Overall, Method 2 is associated with a modest decrease in overall error ($p < 0.05$, paired two-tailed Student's t-test), but does result in a modest increase in median error compared to Method 1 from 18.2% to 18.5%. Both Method 1 and Method 2 fail to capture the dynamic nature of E_{es}, thus, large errors are reduced, but overall accuracy is not greatly improved. Regardless, these results provide support for the validity of Eq. 5.3, and the use of V_d as a surrogate for V_0 in this method. The fact these error reductions are sustained over significant changes in cardiac output and ejection fraction as sepsis develops suggests the absolute value of V_d does not change significantly enough under such conditions to detract from method accuracy.

Method 3 further assumes that E_{es} can be expressed as a function of *HR*. This assumption is unusual, but is supported by the results. The full method sees a further, significant reduction in overall error compared to Methods 1 and 2 ($p < 0.01$ in both cases, paired two-tailed Student's t-test), as well as a large reduction in average median error compared to both Methods 1 and 2, from 18.2% and 18.5% to 10.6% in Table 5.4. This result suggests general tracking of trends in V_{es} is being significantly improved, also supporting the validity of expressing E_{es} as a function of *HR*. This behaviour can also be observed in Fig. 5.3. This result, combined with the minimal addition in method complexity required to include *HR*, which is very easy to measure, provides a strong case for the use of Method 3.

However, it is still important to note the power law relationship between E_{es} and *HR* expressed in Eq. 5.4 is a significant simplification of actual cardiac behaviour. The cardiac system uses a large variety of responses to maintain cardiac output. The cubic ($n = 3$) used to approximate E_{es} changes as a function of *HR* attempts to mathematically approximate the sympathetic nature of some of these responses. However, the relationship between *HR* and E_{es} varies between subjects, as accounted for by calibration, and as time and condition change.

5.4.3 Limitations

There are a couple of limitations to this study that should be noted. First, the proposed method does require an echocardiography calibration to provide subject specific initial parameters. While echocardiography is non-invasive, and becoming increasingly commonplace in the ICU [127], the method still cannot be implemented entirely without an increase in the workload of clinicians. Second, the method was validated across a limited data set. While effort was made to ensure the experimental protocols encompassed a variety of procedures, conditions and drugs with a variety of effects,

this still represents only a fraction of the range of cardiac behaviour possible in an ICU. As such, further validation over more diverse data sets and subjects is needed.

Specifically, there are several interventions that specifically alter either *HR* or contractility. Examples include inotropes, which increase contractility and were part of the validation, and vagus nerve stimulation [133], which decreases *HR*. The method's ability to adapt to inotropes, albeit with some increase in error, suggests the method is capable of tracking changes through such interventions. Further, given that such interventions are instigated by a clinician, it would be relatively easy to recalibrate the method directly after an intervention should the method be shown to require it.

5.5 Summary

Management of cardiovascular disease in the ICU would benefit from better extraction of relevant cardiac metrics from the wealth of data regularly available in such an environment. A method was developed to allow clinical approximation of V_{es} beat-to-beat, using a modified ESPVR, brief echocardiography calibration and continuous P_{ao} and *HR* data. This method was validated across 11 pigs and 2 protocols, covering sepsis, dobutamine infusion, recruitment manoeuvres and fluid infusions. The method was able to track trends in V_{es} effectively across both protocols, with a mean correlation coefficient of $R = 0.84$. The method was also able to approximate the exact value of V_{es} effectively, with a mean-median magnitude of error of 10.6%, although these errors were consistently higher for the protocol involving dobutamine than sepsis. Overall, this method, combined with an existing method that provides *SV*, allows for a more complete picture of cardiac volume behaviour to be established in the ICU, including metrics such as preload. This method thus also provides the ability to non-additionally invasively estimate the V_{lv} profile in an ICU setting, which is a focus of the following chapter.

6

Time Varying Elastance Revisited

With the additional benefits of non-additionally invasive estimation of unstressed or 'dead space' ventricular volume (V_d) as described in Chapter 4, and end-systolic (V_{es}) and end-diastolic (V_{ed}) volumes as described in Chapter 5, it is time to revisit the Time Varying Elastance (TVE) curve, first presented in Chapter 3. This chapter develops a more complex means of estimating the TVE curve without directly assuming a shape for the waveform. This method is thus more appropriate for the potential diagnostic use of the TVE curve, and provides a significant increase in method accuracy and complexity.

6.1 Background

As established in Chapter 3, the TVE curve is an important means of expressing cardiac dynamics [55], with potential applications as an input into larger models [93-97] or for direct diagnostic use [44, 89, 90, 99]. While the original definition of the TVE curve suggests a uniform curve scaled solely by end-systolic elastance (E_{es}) and t_{max} [55], the presence of large amounts of modern data and a more intact circulatory system in subjects appears to result in changes in the shape of the curve itself, potentially due to cardiovascular control and reflexes. These shape differences may provide information with diagnostic benefits [44, 89, 90, 99].

Chapter 3 provided a TVE curve matching the definition in [55], with a consistent shape, but adjustable timing and magnitude. This chapter seeks to provide a more

complex means of estimating the TVE curve. It leverages the physiological estimation methods developed in Chapters 4 and 5, without assumptions of a constant shape and with more connection to underlying physiology to provide a non-additionally invasive estimate of the TVE curve for potential diagnostic use.

This chapter thus presents a novel, minimally invasive method for deriving the TVE curve beat-by-beat. The method focuses on combining simple physiological assumptions with clinically available catheter waveforms to individually simulate the pressure and volume components that define the TVE curve, rather than generating the TVE curve itself. Importantly, this approach avoids the need to directly assume a shape for the TVE curve, as it is instead generated from these underlying waveforms. It is thus better equipped to capture variations in TVE shape over time and condition, as well as the corresponding alterations in intra-beat cardiac behaviour.

Using only clinically feasible measurements mean the method has the potential for real-time implementation at the patient bedside, without requiring additional, invasive instrumentation. Such a TVE curve could be used to provide additional, patient specific information on intra-beat behaviour and inter-beat variation in the functioning of the heart. Finally, monitoring the TVE curve, associated metrics, and their evolution over time could add significant new data and insight to improve diagnosis and treatment.

6.2 Methods

6.2.1 Proposed Method

The TVE curve is defined:

$$e(t) = \frac{P_{lv}(t)}{V_{lv}(t) - V_d} \tag{6.1}$$

where P_{lv} is the pressure in the left ventricle and V_{lv} is the volume in the left ventricle [55, 57]. Thus, the TVE curve is defined by two time-varying waveforms (P_{lv} and V_{lv}) and one constant (V_d). Once again, these values can be measured directly, but doing so is not clinically feasible [66], so a surrogate estimation is required.

The proposed method approximates these waveforms (V_{lv}, P_{lv}) and constant (V_d) using four clinically available inputs, as shown in Fig. 6.1 Continuous aortic pressure (P_{ao}) and heart rate (HR) are widely available. Continuous femoral pressure (P_{fe}) can easily be measured under clinical conditions, but is not a typical intensive care unit (ICU) measurement [73]. Finally, baseline V_{es} requires a short, baseline echocardiography, which is increasingly available, clinically [127].

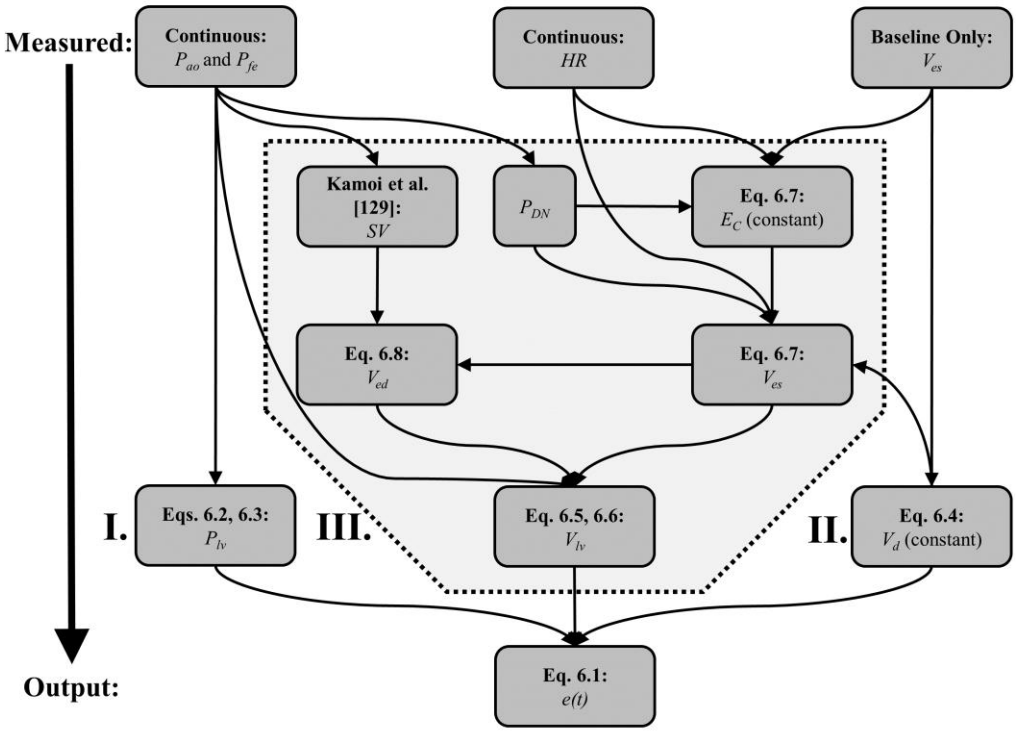

Fig. 6.1: Flowchart of the proposed method. Roman numerals indicate different method regions.

The overall goal of this method is to use the clinically available inputs P_{ao}, P_{fe}, HR and baseline V_{es} to determine the outputs P_{lv}, V_d and V_{lv}, and thus the TVE curve $e(t)$ as set out in Fig. 6.1 and Eq. 6.1. This resulting TVE curve can be experimentally validated

against the TVE curves derived from experimentally measured P_{lv} and V_{lv} in animal models. The availability of a nearby continuous pressure measurement (P_{ao}) forms an effective basis for the continuous approximation of P_{lv}, and the availability of a baseline volume measurement (V_{es}) forms an effective basis for the approximation of baseline V_d, comprising Regions I and II in Fig. 6.1.

There is no continuous volume measurement available for continuous approximation of V_{lv}. However, the methods presented in Chapters 4 and 5 can be used to provide volume information from clinically available data. Thus, these methods form the basis for the shaded central Region III in Fig. 6.1, which is considerably more complicated than Regions I and II.

While the overall method involves approximating two output waveforms (V_{lv}, P_{lv}) from two similar input waveforms (P_{ao} and P_{fe}), it's important to note all four waveforms (P_{lv}, V_{lv}, P_{ao}, P_{fe}) have distinct features. Different regions of behaviour are governed by different physiological phenomenon, and these waveforms have been extensively characterised [46]. As such, all four waveforms are heavily interconnected and information rich, making this task more reasonable than it might first appear.

6.2.1.1 Determining P_{lv} from P_{ao} (Region I, Fig. 6.1)

During systole (Region P1, Fig. 6.2), the aortic valve opens as blood is ejected from the heart. Thus, P_{ao} is approximately equivalent to P_{lv} with a slight phase lag (δ) and a pressure drop. While this pressure drop is non-negligible in conditions such as aortic stenosis [46], valve dysfunction of any kind is present in just 3.61% of cardiovascular disease mortalities in the US [1]. Further, such conditions are typically chronic in nature, relatively easily diagnosed [134] and evolve slowly, while the method is designed to monitor short term changes in an ICU environment. As such, this

assumption should not significantly affect the methods' applicability to the vast majority of the target cohort.

During diastole (Region P2-3, Fig. 6.2), the aortic valve closes as the ventricle relaxes and fills with blood, and P_{lv} and P_{ao} diverge providing little direct information to estimate P_{lv}. However, relaxation and filling are largely passive [46], so a generic exponential function can be used to approximate diastolic P_{lv}. These generic exponential functions consist of an exponential decay in early diastole (Region P2, Fig. 6.2) as the ventricle relaxes, followed by an exponential increase (Region P3, Fig. 6.2) as the ventricle begins to contract.

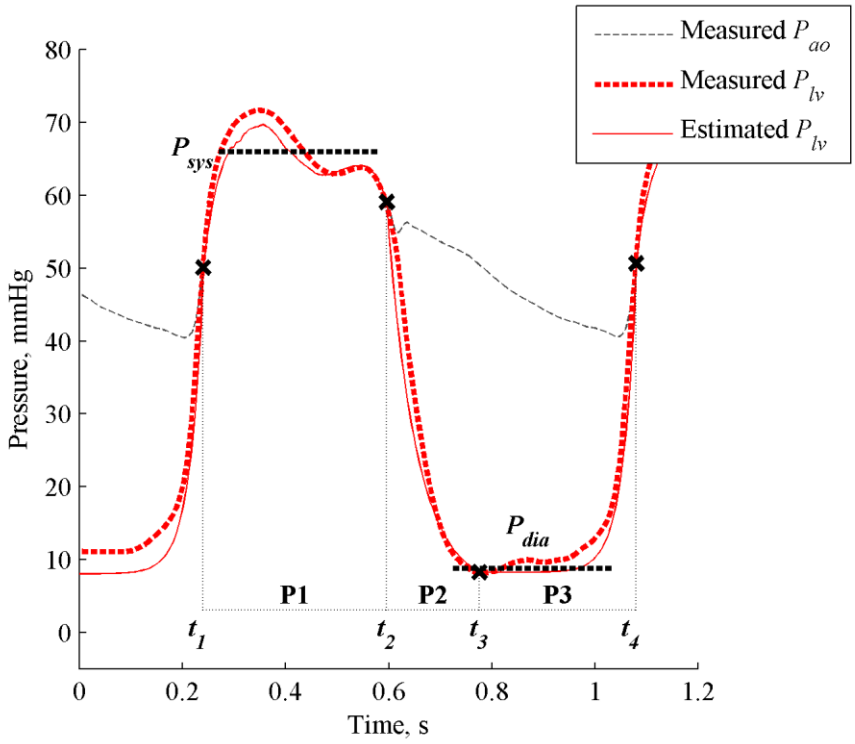

Fig. 6.2: P_{lv} estimated via P_{ao} compared to invasively measured P_{lv}. P_{sys} denotes the mean-systolic pressure and P_{dia} denotes the mean-diastolic pressure. Note P_{ao} has been shifted left by δ.

While atrial contraction contributes significantly to late diastolic filling, ventricular elastance remains largely passive in late diastole [46]. Thus, the TVE curve is typically at its baseline value until the beginning of ventricular contraction in early systole.

While atrial function affects the magnitude of the driver function, which is normalised in this work, and may affect its shape, this effect is indirect as the driver function represents the impact of contraction in driving pulsatile blood from the heart to the arterial system. Further, with the decreasing popularity of pulmonary artery catheters [49], none of the typically available instrumentation in an ICU provides a clear picture of atrial behaviour. As such, while the exponential in Region P3 is broadly intended to capture ventricular filling, no specific atrial behaviour component is integrated into this model, and there is no readily available data to do so directly

Per Fig. 6.2, P_{lv} for the n_{th} heartbeat is defined:

$$t_1^p = t\left(\frac{dP_{ao}}{dt}_{max}\right)_n - \delta \tag{6.2a}$$

$$t_2^p = t\left(\frac{dP_{ao}}{dt}_{min}\right)_n - \delta \tag{6.2b}$$

$$t_4^p = t\left(\frac{dP_{ao}}{dt}_{max}\right)_{n+1} - \delta \tag{6.2c}$$

$$t_3^p = (1-\tau)t_2 + \tau t_4 \tag{6.2d}$$

$$P_{lv}(t) = \begin{cases} P_{ao}\left(t_1^p + \delta < t < t_2^p + \delta\right) & t_1^p < t < t_2^p \\ \rho + \left(P_{ao}\left(t_2^p\right) - \rho\right)e^{-\alpha_1\left(t - t_2^p\right)} & t_2^p < t < t_3^p \\ P_{lv}\left(t_3^p\right) + \left(P_{ao}\left(t_3^p\right) - P_{lv}\left(t_3^p\right)\right)e^{\alpha_2\left(t - t_3^p\right)} & t_3^p < t < t_4^p \end{cases} \tag{6.3}$$

where τ is the relative length of early-diastole decrease in P_{lv} (Region P2, Fig. 6.2) to late-diastole/early-systole increase in P_{lv} (Region P3, Fig. 6.2), ρ is the asymptotic minimum pressure during diastole in the left ventricle, α_1 governs the rate of decrease from $P_{lv} = P_{ao}$ at end-systole towards $P_{lv} = \rho$ (Region P2, Fig. 6.2), α_2 governs the rate of increase from $P_{lv} \approx \rho$ in diastole to $P_{lv} = P_{ao}$ at early-systole (Region P3, Fig. 6.2),

and δ is the lag between P_{lv} and P_{ao}. Due to the lack of available measured information apart from P_{ao} at the beginning and end of diastole, the exponentials are generated using the generic values in Table 6.1, derived from a combination of observed experimental behaviour and expected behaviour discussed in medical literature, which give an approximation of the typical, passive physiological behaviour.

Table 6.1: Parameter values for estimation of P_{lv} [135].

Parameter	Parameter Value
τ	0.38
ρ	6 mmHg
α_1	17.5 s^{-1}
α^2	37.5 s^{-1}
δ	0.008 s

6.2.1.2 Determining V_d from baseline V_{es} (Region II, Fig 6.1)

This approach leverages the method established in Chapter 4 for estimating V_d from baseline ventricular volume measurements [59]. Defining V_d as a percentage of baseline V_{es} allows approximation of baseline V_d during the initial echocardiographic reading where measured V_{es} is available. While V_d has been shown to change with condition, there is no practical means of capturing this change short of additional echocardiography measurements. Thus, while intermittent measures are feasible, in this chapter V_d is fixed at a baseline value.

$$V_d = 0.48 \times V_{es} \tag{6.4}$$

6.2.1.3 Determining V_{lv} from P_{ao}, HR and V_d (Region III, Fig 6.1)

Unlike pressure, little volume or flow information is readily available from the typical, clinically available instrumentation. Estimating V_{lv} thus relies on the methods presented in Chapters 4 and 5 for estimating ventricular volume information from clinically available pressure inputs. V_{lv} was estimated by combining beat-by-beat estimations of

the timing and height of the peaks and troughs of the waveform and a piecewise sine wave. The piecewise sine wave comprises a systolic region (Region V1, Fig. 6.3), where volume falls as blood is ejected, and a diastolic region (Region V2, Fig. 6.3), where volume rises during filling, with a 90° phase shift at the beginning of systole. Physiologically, a set of exponentials would potentially be more representative [46], but the piecewise sine wave achieves similar results with considerably fewer variables to define its shape, reducing the number of parameters to be determined.

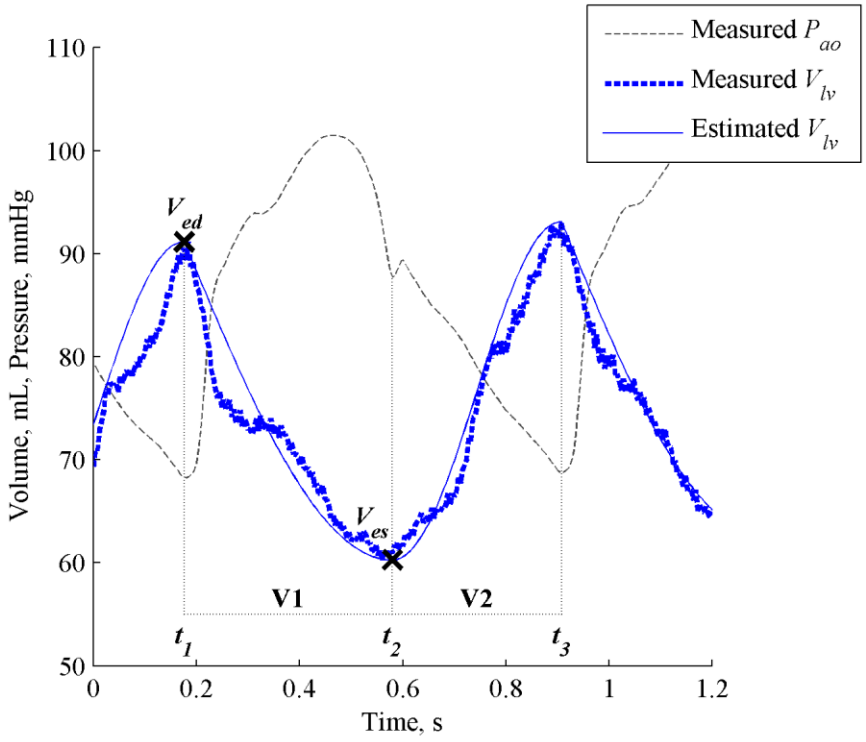

Fig. 6.3: V_{lv} estimated via P_{ao} compared to invasively measured V_{lv}.

V_{lv} changes are pressure driven, so P_{ao} is used to determine timing of peaks and troughs in V_{lv}:

$$t_1^v = t\left(P_{ao_{min}}\right)_n - \delta \tag{6.5a}$$

$$t_2^v = t(P_{DN})_n - \delta \tag{6.5b}$$

$$t_3^v = t\left(P_{ao_{min}}\right)_{n+1} - \delta \tag{6.5c}$$

Determining the magnitude of the beat-by-beat troughs (V_{es}) is accomplished using the method set out in Chapter 5 to estimate V_{es} beat-by-beat under clinical conditions (Eq. 6.7). Determining the magnitude of the beat-by-beat peaks (V_{ed}) is accomplished by combining V_{es} with existing research approximating beat-by-beat Stroke Volume (*SV*) from clinical data [124]. This approach uses pulse wave velocity from P_{ao} and P_{fe} to uniquely identify a three-element Windkessel model based on the reservoir-wave concept. This subject specific Windkessel model can then be used to convert measured P_{ao} into an estimated *SV* beat-by-beat, with a 95% limit of agreement error of 26% [124]. Beat-to-beat left ventricular volume is thus estimated:

$$V_{lv}(t) = \begin{cases} (V_{ed})_n + ((V_{es})_n - (V_{ed})_n)\sin\left(\dfrac{\pi(t - t_1^v)}{2(t_2^v - t_1^v)}\right) & t_1^v < t < t_2^v \\ (V_{es})_n - ((V_{ed})_{n+1} - (V_{es})_n)\left(\dfrac{1}{2}\cos\left(\dfrac{\pi(t - t_2^v)}{(t_3^v - t_2^v)}\right) - \dfrac{1}{2}\right) & t_2^v < t < t_3^v \end{cases} \tag{6.6}$$

where:

$$V_{es} = \frac{P_{DN}}{(E_c \times HR^3)} + V_d \tag{6.7}$$

$$V_{ed} = V_{es} + SV \tag{6.8}$$

where Eq. 6.7 expresses the relationship between E_{es} and *HR* developed in Chapter 5.

6.2.1.4 Summary of Proposed Method

The overall derivation of the TVE curve can be summarised:

Initially or Intermittently:

1. Calculate V_d using Eq. 6.4 and baseline V_{es} (Region II, Fig. 6.1)

2. Calculate E_C using Eq. 6.7, P_{DN}, HR, V_d and baseline V_{es} (Region III, Fig. 6.1)

Every heartbeat:

1. Estimate P_{lv} using Eq. 6.2, Eq. 6.3 and P_{ao} (Region I, Fig. 6.1)
2. Determine V_{es} using Eq. 6.7, P_{DN}, HR, V_d and E_C (Region III, Fig. 6.1)
3. Determine SV using Kamoi et al. [124], P_{ao} and P_{fe}
4. Determine V_{ed} using Eq. 6.8, V_{es} and SV (Region III, Fig. 6.1)
5. Estimate V_{lv} using Eq. 6.5, Eq. 6.6, P_{ao}, V_{es} and V_{ed} (Region III, Fig. 6.1)
6. Calculate and normalise the TVE curve $e(t)$ using Eq. 6.1

The required clinical measurements include:

- Continuously sampled P_{ao}
- Continuously sampled P_{fe}
- Continuously sampled HR
- A baseline, 10-heartbeat V_{es}

All these measurements are either in widespread clinical use or possible to implement clinically without excessive burden on either clinicians or patients.

6.2.2 Analysis and Validation

The proposed method was validated on experimentally gathered data. A range of input (P_{ao}) and output (V_{lv}, P_{lv}) waveforms were continuously measured via catheter. This data allowed validation of individual model assumptions through comparison with directly measured output waveforms, as well as validation of the overall method through comparisons between the TVE curve as calculated using simulated and directly measured V_{lv} and P_{lv} wave forms.

6.2.2.1 Experimental Data

This chapter makes use of the 5 Protocol S pigs that were not subject to exclusion. The waveforms employed include continuously sampled P_{ao} and P_{fe} as method inputs, and continuously sampled P_{lv} and V_{lv} to provide the invasively measured TVE curve. The data set encompasses 46,318 heartbeats across 5 Piétrain pigs. A diverse clinical protocol provides the ability to assess intra- and inter- subject variability across a large amount of invasive and non-invasive measurements. Together they enable rigorous assessment and validation of the method.

6.2.2.2 Model Validation

The overall method presented here is designed to simulate the TVE curve beat-by-beat, without requiring invasive instrumentation of the heart or real-time image-based monitoring, neither of which is clinically or ethically feasible in care. As such, validation of the method relies on comparison of the simulated TVE curve to the invasively measured, 'true' TVE curve, which is calculated using the catheter measured V_{lv} and P_{lv} waveforms for a single beat. This comparison is achieved by calculating the magnitude and signed 'error area' between the measured and simulated TVE curve, according to Eqs. 6.9 and 6.10:

$$\varepsilon_{mag} = \frac{\int_{t=0}^{1} |e_{sim}(t) - e_{meas}(t)|}{\int_{t=0}^{1} (e_{meas}(t))} \tag{6.9}$$

$$\varepsilon_{sgn} = \frac{\int_{t=0}^{1} (e_{sim}(t) - e_{meas}(t))}{\int_{t=0}^{1} (e_{meas}(t))} \tag{6.10}$$

where ε_{sim} and ε_{meas} are the simulated and measured TVE curves, respectively, t is normalised time set to 1 for every heart beat to enable comparison over different beats, and ε_{mag} and ε_{sgn} and denote the magnitude and signed errors respectively. This approach is identical to the approach used in Chapter 3, enabling direct comparison.

6.3 Results

The overall purpose of this model is to track the shape of the TVE curve, and how this shape changes when circulatory behaviour changes. Table 6.2 shows the area under the curve errors, ε_{mag} and ε_{sgn}, for all 5 Protocol S pigs. The median error is relatively small at 11.4%, suggesting the method is effective, and the interquartile range relatively narrow at 9.2% – 14.7%, suggesting the method is consistent. The method does not demonstrate a significant bias ($p > 0.05$, one sample Student's t-test relative to a population bias of 0), with an average median of -2.5%, and an interquartile range of -6.1% – 0.8. This method shows a statistically significant reduction in median errors relative to the method presented in Chapter 3 ($p < 0.01$, two-tailed unpaired Student's t-test).

Table 6.2: TVE curve percentage area under the curve errors (ε_{mag} and ε_{sgn}) associated with proposed method (identifying V_{es} and V_{ed}), presented as median (25^{th} – 75^{th} percentile)

Pig	Mag. Percentage Error (ε_{mag})	Signed Percentage Error (ε_{sgn})
S1	11.6% (9.0 – 14.4)	-4.9% (-7.0 – -2.6)
S2	9.4% (7.8 – 11.6)	2.3% (-1.4 – 6.6)
S3	11.4% (9.4 – 15.6)	-7.8% (-12.6 – -4.5)
S4	11.1% (9.5 – 13.0)	-7.5% (-9.3 – -5.7)
S5	13.4% (10.5 – 19.0)	5.2% (-0.3 – 10.1)
Mean	11.4% (9.2 – 14.7)	-2.5% (-6.1 – 0.8)

Table 6.3 shows, as a point of comparison, the area under the curve errors associated with the method if the directly measured values for V_{es} and V_{ed} are used. Using these measured values removes the majority of Region III, Fig. 6.1 (Eqs. 6.4 and 6.7-6.8) from the overall method, where a lot of relatively significant assumptions are made. The errors in Table 6.3 are very comparable to those in Table 6.2, with an overall modest reduction in average median error (11.4% to 10.2%) and bias (-2.5% to -2.2%), as expected when measuring V_{es} and V_{ed} directly and invasively, rather than estimating them. Hence, the assumptions made had very little impact on error when removed.

Table 6.3: TVE curve percentage area under the curve error (ε_{mag} and ε_{sgn}) associated with using measured V_{es} and V_{ed} values, presented as median (25^{th} – 75^{th} percentile)

Pig	Mag. Percentage Error (ε_{mag})	Signed Percentage Error (ε_{sgn})
S1	11.5% (9.0 – 13.3)	-5.6% (-8.1 – -2.7)
S2	8.5% (7.3 – 10.1)	-0.7% (-3.7 – 2.2)
S3	8.1% (7.1 – 9.1)	-2.7% (-4.7 – -0.6)
S4	11.4% (9.5 – 13.5)	-7.8% (-9.9 – -5.6)
S5	11.3% (9.8 – 13.5)	6.0% (2.8 – 9.0)
Mean	10.2% (8.5 – 11.9)	-2.2% (-4.7 – 0.5)

Fig. 6.4 shows a variety of measured and modelled TVE curve shapes for each of the 5 pigs, capturing both intra- and inter- subject variability. For each figure, Panel I shows a baseline waveform, Panel II a waveform during a RM and Panel III a waveform after endotoxin infusion has occurred and sepsis develops. The range of shapes and inter-pig variability indicated that assuming a generic population or cohort TVE curve as in Chapter 3 is not particularly valid, and is further supported by the range of intra-pig variability evidenced and captured by the method presented here. There are a variety of shoulder heights, relative gradient and maximum/minimum gradient timings that result in TVE curves with distinct shapes, variations which are well captured by the method. These TVE curves were also selected to demonstrate a range of error values similar to the interquartile error range for that pig (Table 6.2). Thus, these drivers are reasonably representative of the overall ability of the method to capture TVE curve shapes, despite different overall shapes for each pig and changes in shape as condition changes.

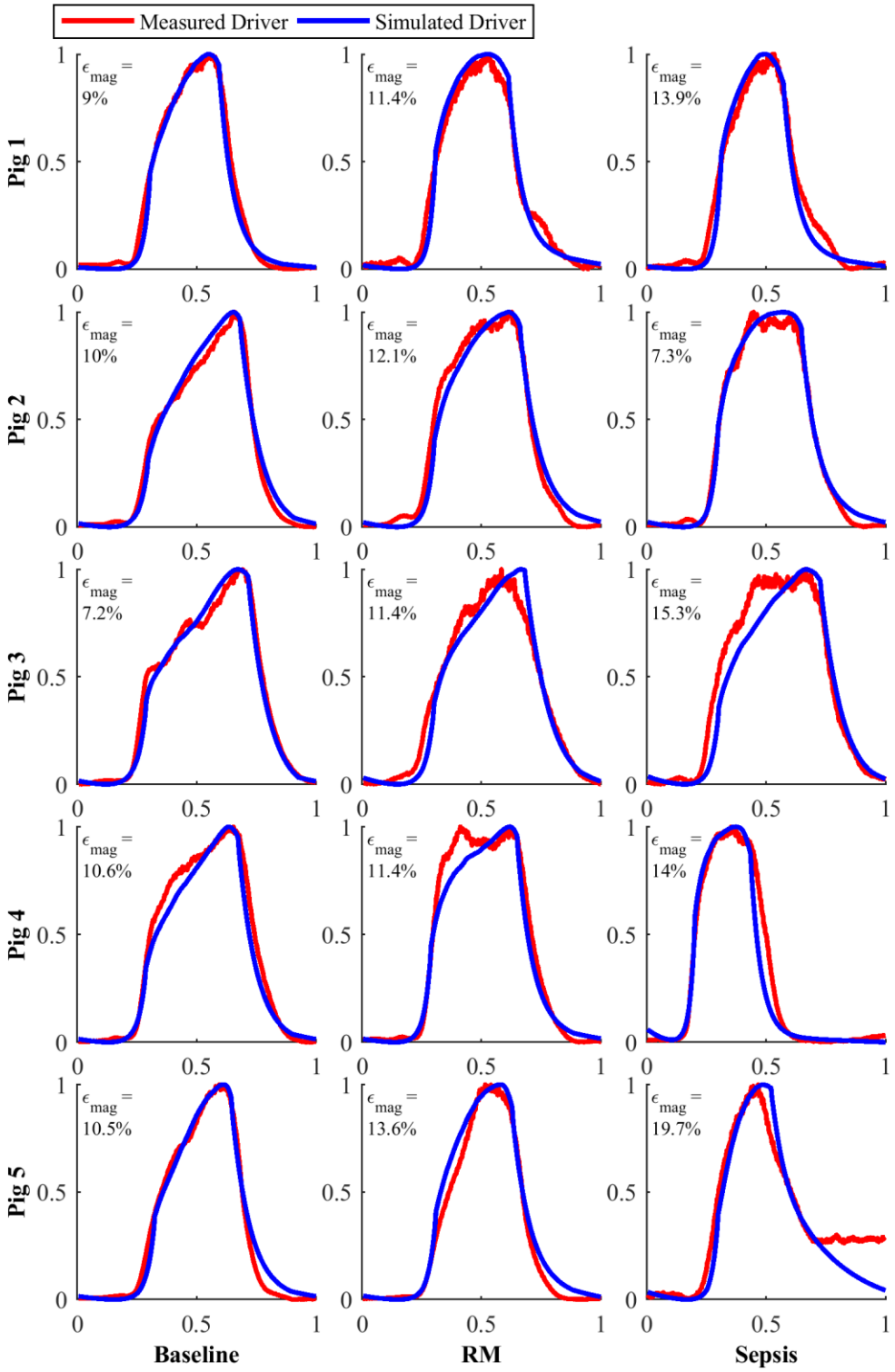

Fig. 6.4: Example TVE curves for each pig. A range of error values and cardiac states are shown.

6.4 Discussion

6.4.1 Model Validation

Estimating the TVE curve using the proposed method resulted in a relatively low median magnitude error area, ranging from 9.4% to 13.4% (Table 6.2) across all pigs, and yielded a statistically significant reduction in median errors relative to the method presented in Chapter 3 ($p < 0.01$, two-tailed unpaired Student's t-test). This narrow range of median magnitude errors implies the method is able to consistently and effectively capture inter-subject variations in TVE curve behaviour, suggesting it is generalizable to other subjects. This inter-subject variability is demonstrated well by various baseline drivers shown in Fig. 6.4. All 5 pigs demonstrate relatively distinct baseline TVE curve shapes, showing a considerable level of inter-subject variability impossible to capture with a generic cohort or population based TVE curve that relies on a basic assumed shape as in Chapter 3 [89, 90].

The simulated TVE curve also had a relatively narrow average interquartile error range of 9.2% to 14.7% (Table 6.2), suggesting the method is able to relatively consistently and effectively capture inter-subject variations in TVE curve behaviour. Examples of the variation in TVE curve shape intra- and inter- subject are provided in Fig. 6.4. Accurate capture of relative changes and trends in patient behaviour are extremely important, as these changes are critical in assessing whether a patient is recovering, responding to treatment, or is not responding and in need of a change in treatment.

Most pigs demonstrated notable changes and intra-pig variability in driver shape during recruitment manoeuvres and as sepsis developed. A couple of the more unusual driver shapes were not fully captured. For example, Panel 2 of Pig S4 in Fig. 6.4, where the driver measured driver displayed two peaks and the simulated driver only one.

The simulated TVE curve demonstrated consistently low signed area error, at -2.5% (IQR –6.1% to 0.8%), shown in Table 6.2. This result shows the method only slightly underestimates the TVE curve, supported further by 2 pigs having a slight positive bias and the other 3 a slight negative bias. This outcome further supports the ability of the TVE curve to accurately capture both intra- and inter- subject variability over time and condition.

In assessing the impact of assumptions on the TVE curve, a comparison of Table 6.2, using approximated V_{es} and V_{ed}, and Table 6.3, using measured V_{es} and V_{ed}, show very similar error values. For example, overall median error fell from 11.4% to 10.2% and overall bias from -2.5% to -2.2%, only a modest reduction in error. This result implies that the body of assumptions and equations in Region III, Fig. 6.1 concerned with the approximating the V_{es} and V_{ed} for simulation of V_{lv} do not result in a large increase in error compared to using measured V_{es} and V_{ed}. The assumptions made in areas of the method not involving simulating V_{es} and V_{ed} are relatively minimal, mostly involving using P_{ao} to determine waveform timing. As such, it would seem that much of the error associated with this method is the result of assuming equations for parts of the two waveforms being reconstructed (P_{lv} and V_{lv}), as shown in Figs. 6.2 and 6.3. Thus, the assumptions employed in Region III, Fig 6.1 appear to function as intended, and further reduction in error would probably require increased method complexity or an increase in the clinically available data.

An important point to consider is the fact the TVE curve is consistently normalised to a duration and amplitude of 1.0, as it is designed specifically as an indicator of how the heart is behaving relatively over the course of a beat, to be coupled with a lumped metric (E_{es}) indicating the overall strength of that heartbeat [55, 89, 90]. This normalisation does mean that some of the errors associated with the various assumptions and approximations made throughout the method are reduced, and that

indicators of absolute cardiac work and its changes, for example, are not able to be directly extracted from the TVE curve created. Fortunately, the driver does not exist alone, the intent is that the shape of the TVE curve, indicative of transient, relative cardiac behaviour, be used alongside other existing metrics, such as Cardiac Output or Stroke Volume [108, 136], indicative of lumped, absolute cardiac behaviour, to provide further diagnostic information.

6.4.2 Limitations

There are study limitations that should be considered. First, all data presented is derived from a single protocol involving a single, but complex and varied [88], condition (sepsis). This data set encompasses several pigs, a full progression from healthy, baseline behaviour to cardiac failure and clinically standard ventilation and fluid interventions. Nevertheless, there is a much larger range of possible cardiac conditions, and further validation over several of these would be beneficial. However, the method already detects changes in haemodynamics, including those due to circulatory or cardiac muscle changes during sepsis in this study. Thus, the ability to detect changes due to inotropes should be similar to what is presented for the range of behaviours already observed in sepsis. Further, given inotrope infusions are determined and performed by a clinician, it would be possible to recalibrate the method directly after such an infusion to adjust to the new inotropic state if it proved necessary. Overall, the underlying physiology and data supporting the development of this method has been discussed in detail, and would be expected to generalise well to a wider range of conditions, as there are no intervention or condition specific assumptions made.

The method also requires validation on human subjects to ensure the methodology as presented here remains physiologically accurate, though the strong similarities between porcine and human physiology and the effectiveness of porcine models are well established [137, 138]. Equally, only an animal model, as used here, allows the direct

validation against cardiac measured TVE curves, which would not be possible in humans. Thus, only an animal trial allows this important first validation.

The method does require an initial calibration via echocardiography or similar means. Echocardiography equipment is increasingly available in modern ICUs [127]. Further, echocardiography is non-invasive and the calibration period required is relatively short, requiring approximately 10 heartbeats. However, the requirement of such a calibration still prevents the method from being fully implementable without modest additional clinical workload using normal ICU instrumentation.

6.5 Summary

The TVE curve is an important, but difficult to clinically measure, expression of internal cardiac dynamics that captures the heart's ability as a pump and can evolve over time, condition and patients. A novel, minimally invasive method for deriving the TVE curve beat-by-beat, by combining simple physiological assumptions with readily available catheter waveforms to individually simulate the components of the TVE curve, is proposed. This method was assessed across a cohort of 5 Piétrain pigs undergoing a progression from healthy behaviour to cardiac failure due to sepsis. The TVE curve generated by the method was shown to effectively track a directly measured function throughout the experiments, with low overall median magnitude (11.4%) and signed (-2.5%) area under the curve errors. There is the potential for this method to provide real time, patient specific information on intra-beat behaviour and inter-beat variation in the heart, at the patient bedside, without requiring additional, invasive instrumentation. However, due to the nature of the TVE curve, this method is limited to providing shapes and trends, rather than absolute values of particular cardiac metrics.

7

The Pressure-Volume Loop

While clinical estimation of time varying elastance (TVE) has promise, the lack of an absolute value component or current clinical metrics directly derived from the TVE curve makes it worth exploring clinical estimation of another cardiac metric based off the same inputs. The pressure volume (P-V) loop uses absolute values and is situated at the core of the concepts of elastance, ventricular dead space, and cardiac contractility. Non-invasive estimation of the P-V loop is considerably more demanding than the TVE curve, but concordantly provides significantly more information and easily derivable cardiac metrics due to the lack of waveform normalisation during the calculation process.

7.1 Background

A fundamental expression of cardiac dynamics and function is the left ventricular P-V loop [46] (Fig. 7.1), comprising: Filling; Contraction; Ejection; and Relaxation, a closed 'loop' describing the heartbeat. The area inside the P-V loop is the stroke work (*SW*), an important metric sensitive to cardiac dysfunction, corresponding to work done by the ventricle ejecting blood into the aorta [53, 54]. As discussed in Chapter 2, the positions of the upper left and lower right corners are points on the end-systolic pressure-volume relation (ESPVR) and end-diastolic pressure-volume relation (EDPVR) [55, 56] respectively, as is the unstressed or 'dead space' ventricular volume (V_d) [59]. The P-V loop thus provides information about contractility, which is also sensitive to changes in cardiac function and state.

Clinical estimation of these relationships and associated properties is a major research area, typically focused on an individual component or relationship, such as ESPVR [91, 139], EDPVR [140] or preload recruitable stroke work (*PRSW*) [141, 142]. Thus, current methods do not provide all the information from the full P-V loop. Further, lacking direct left-ventricular pressure (P_{lv}) and volume (V_{lv}) measurements, these methods frequently rely on continuous echocardiography, which is currently impractical [143]. There has been no work associated with minimally invasive estimation of the P-V loop using currently available, but indirect, catheter data.

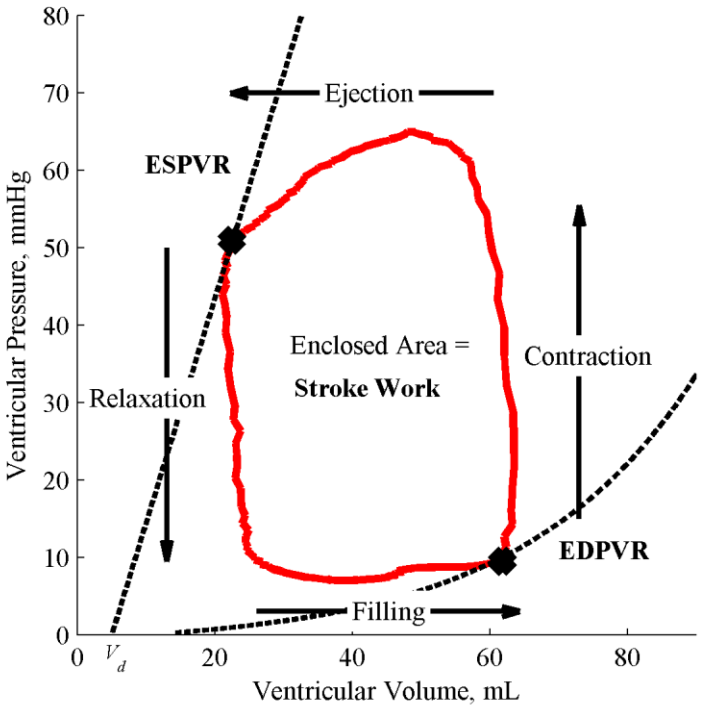

Fig. 7.1: Annotated, experimental P-V loop. The slight pressure decrease in ejection is due to the open chest experiment [144, 145].

This chapter applies the method presented in Chapter 6 for minimally invasive beat-by-beat estimation of the V_{lv} and P_{lv} profiles to obtain the left ventricular P-V loop. Using clinically available measurements enables potential real-time clinical implementation without additionally invasive instrumentation.

7.2 Materials and Methods

7.2.1 Proposed Method

The left ventricular P-V loop combines V_{lv} and P_{lv}. As has been previously mentioned, direct measurement is highly invasive and not ethically feasible, clinically [66]. As such, this chapter employs the method developed in Chapter 6 to estimate P_{lv} and V_{lv} from four clinically available inputs, shown in Fig. 7.2. As before, continuous aortic pressure (P_{ao}) and heart rate (HR) are widely available. Continuous femoral pressure (P_{fe}) can easily be measured under clinical conditions, but is not a typical ICU measurement [73]. Finally, baseline end-systolic volume (V_{es}) require a short, baseline echocardiography, which is increasingly available, clinically [127]. Importantly, this approach is distinct from existing methods used for estimation of clinical metrics derived from the P-V loop [91, 139-142] relying on continuous echocardiography throughout the duration of monitoring. The short, baseline echocardiography reading of V_{es} minimises demands on specialist time and allows sharing of equipment across several ICU patients.

While this method is largely identical to the method presented in Chapter 6 [135], there are significant differences in the nature of estimating TVE and P-V loops. Specifically, TVE is calculated using the relative magnitude of the P_{lv} and V_{lv} waveforms over time and involves significant processing of those waveforms that effectively filters some potential sources of error. Normalisation of TVE to a peak value of 1.0 may also limit the impact of some of these sources of error.

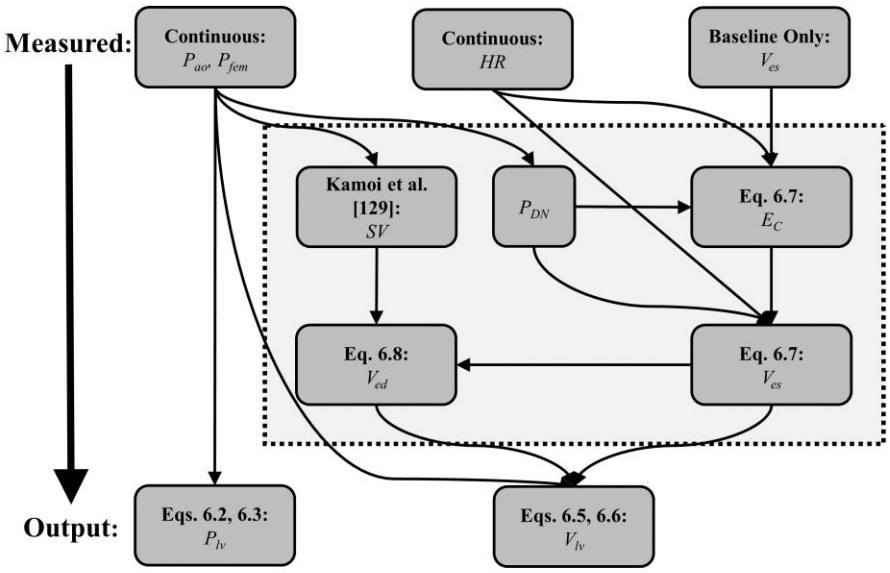

Fig. 7.2: Summary flowchart of proposed method.

In contrast, obtaining P-V loops requires the absolute values of the two waveforms over time, and even relatively small errors that would not necessarily effect TVE could lead to significant deviation of analytical and clinical metrics calculated from these loops. Thus, the two rely on different components of waveform information, and have different established roles and benefits in clinical literature, where there is often a greater reliance on the analytical and subjective assessment of P-V loops. This chapter thus constitutes a major extension of the applicability of the aforementioned method, and requires an entirely separate validation to ensure its accuracy and potential clinical applicability to this new context.

7.2.1.1 Summary of Proposed Method

P-V loop estimation from Fig. 7.2 (see Section 6.2.1 for a detailed description of the method) is summarised:

Initially or Intermittently:

1. Calculate V_d using Eq. 6.4 and baseline V_{es} from echocardiography
2. Calculate E_C using Eq. 6.7, P_{DN}, HR and baseline V_{es} from echocardiography

Every heartbeat:

1. Simulate P_{lv} using Eq. 6.2, Eq. 6.3 and P_{ao}
2. Determine V_{es} using Eq. 6.7, P_{DN}, HR and E_C
3. Determine SV using Kamoi et al. [124], P_{ao} and P_{fe}
4. Determine V_{ed} using Eq. 6.8, V_{es} and SV
5. Simulate V_{lv} using Eq. 6.5, Eq. 6.6, P_{ao}, V_{es} and V_{ed}
6. Use P_{lv} and V_{lv} to generate the P-V loop

The required clinical measurements include:

- Continuously sampled P_{ao}
- Continuously sampled P_{fe}
- Continuously sampled HR
- A baseline, 10-heartbeat V_{es}

All of which are either in widespread clinical use or possible to implement clinically without excessive burden on either clinicians or patients.

7.2.2 Analysis and Validation

Performance was evaluated over two experimentally gathered data sets, encompassing 142,169 heartbeats from 11 Piétrain pigs across 2 protocols designed to provide diverse cardiac conditions [59, 83]. Each data set included direct measurements of method inputs (P_{ao}, P_{fe} and HR) and outputs (V_{lv}, P_{lv}), allowing direct validation on a beat-by-beat basis of model generated P-V loops versus invasively measured left-ventricular P-V loops.

7.2.2.1 Experimental Data

This chapter makes use of the 6 Protocol D and 5 Protocol S pigs that were not subject to exclusion. The waveforms employed include continuously sampled P_{ao} and P_{fe} as method inputs, and continuously sampled P_{lv} and V_{lv} to provide surrogate baseline echocardiography V_{es} readings as well as an invasively measured P-V loop for validation.

7.2.2.2 Model Validation

This method approximates beat-by-beat left ventricular P-V loops using clinically available P_{ao}, HR, P_{fe}, and baseline V_{es} measurements. Validation compares beat-by-beat model derived and invasively measured 'true' P-V loops. Specifically, the P-V loop's enclosed area or stroke work and the absolute P-V loop values/position, assessed by:

- **Diastolic and Systolic Pressures:** Direct comparison of invasively measured and estimated mean-systolic (P_{sys}) and mean-diastolic (P_{dia}) pressures. Mean pressures were used due to the presence of plateaus of high and low pressures in the P_{lv} waveform (Fig. 6.2). Results are expressed as overall percentage error quartiles, with inter-pig averages calculated using the mean of quartiles due to inter-pig variations in experimental monitoring length.

- **Diastolic and Systolic Volumes:** Direct comparison of invasively measured and estimated V_{es} and V_{ed}. Because V_{lv} has distinct peaks and troughs, these individual points are compared (Fig. 6.3). Results are expressed as overall percentage error quartiles, with inter-pig averages calculated using the mean of quartiles due to inter-pig variations in experimental monitoring length.
- **Stroke Work:** Direct comparison of the area enclosed by invasively measured P-V loop, calculated using admittance catheter data, and estimated P-V loop, calculated using the methodology described in this chapter, (SW_M and SW_E), as well as a simplified, clinically used *SW* approximation [76, 121, 141]:

$$SW_S = SV \times MSP \tag{7.1}$$

  where *MSP* is the mean-systolic pressure in the aorta. Results are expressed as overall percentage error quartiles, with inter-pig averages calculated using the mean of quartiles due to inter-pig variations in experimental monitoring length.
- **Changes in Stroke Work:** The ability to track *SW* trends is assessed by trend compass [146], comparing time dependent signals (SW_M and SW_E) over 180 heartbeat (~3min) clinically relevant intervals. The trend compass assesses trend accuracy independent of point accuracy and does so in terms of the accuracy of the slope or trend between points, which is clinically relevant as such trends are often used to titrate care when they are used to assess a patient-specific response to care or disease. The trend angle is defined for a given heartbeat *n*:

$$A = [t(n+180) - t(n) \quad SW_E(n+180) - SW_E(n)] \tag{7.2a}$$

$$B = [t(n+180) - t(n) \quad SW_M(n+180) - SW_M(n)] \tag{7.2b}$$

$$\theta = \cos^{-1}\left(\frac{A \cdot B}{\|A\|\|B\|}\right) \tag{7.3}$$

where θ, derived from a rearranged normalised dot product, is an indication of the angle between the two vectors. These angles, paired with the magnitude of the measured variable (SW_M) are plotted on a radial plot. Note that in this chapter the magnitude of $t(n+180) - t(n)$ was normalised to be equal to the overall mean of SW_M and SW_E, thus providing scale invariance and a comparable 'difference and mean' ratio to that used in a Bland-Altman plot [147].

Pearson's correlation coefficients (R) are also evaluated. As the data set presented here is large (142,169 heartbeats), these correlation coefficients were re-calculated with only every 1 in 1000 and then 1 in 2000 beats from the first recorded heartbeat included to assess the sensitivity of the correlation coefficients to the size of the data set.

Overall, individual validation of P_{sys}, P_{dia}, V_{sys} and V_{dia} against direct measures allows individual evaluation of the effectiveness of the assumptions employed in the method, allowing a further, clearer evaluation of efficacy and potential errors of the method described in Chapter 6.

7.3 Results

7.3.1 Pressures and Volumes

Table 7.1 shows errors estimating P_{sys} for both protocols (median: 3.7-11.7% for Protocol D; median: 1.5-12.1% for Protocol S), suggesting assuming P_{ao} represents P_{lv} is effective during systole. Table 7.1 shows higher errors estimating P_{dia} (median: 10.7% - 32.9% Protocol D; median: 6.4% - 23.8% Protocol S), which is expected due to the fixed nature of the approximation in Eq. 6.3. However, P_{dia} is frequently an order

of magnitude smaller than P_{sys}, thus higher percentage errors do not necessarily translate into significant absolute errors. There was a weak correlation between errors in P_{sys} and P_{dia} (R = 0.04) due to the fundamental differences between how the two are estimated.

Table 7.1: Percentage errors for pressure estimation of P_{dia} and P_{sys}. Presented as median (25^{th} – 75^{th} percentile) for Protocol D, Pigs D1 – D6 and S, Pigs S1 – S5.

Pig	Number of Heartbeats	Mag. Error*: Diastolic Pres. (P_{dia})	Mag. Error*: Systolic Pres. (P_{sys})
D1	5,480	22.1% (8.3–58.2)	3.7% (3.2–4.3)
D2	5,343	15.2% (7.9–21.9)	8.1% (7.8–8.6)
D3	32,626	32.9% (14.7–87.0)	7.9% (7.1–8.8)
D4	17,584	19.0% (10.9–27.2)	11.7% (10.2–12.7)
D5	15,874	10.7% (4.9–18.1)	11.1% (10.4–11.9)
D6	18,944	29.3% (13.7–70.7)	4.8% (4.1–5.5)
Mean (D)	15,975	21.5% (10.1–47.2)	7.9% (7.1–8.6)
S1	53,46	23.3% (8.5–30.7)	7.1% (4.8–10.4)
S2	5,382	6.4% (2.9–12.9)	1.5% (0.6–2.6)
S3	16,233	13.4% (5.8–19.8)	1.7% (1.1–2.6)
S4	13,507	17.4% (12.8–26.2)	12.1% (10.1–13.7)
S5	5,870	23.8% (14.9–31.2)	2.2% (1.3–4.2)
Mean (S)	9,268	16.9% (9.0–24.2)	4.9% (3.6–6.7)
Mean (D&S)	12,926	19.4% (9.6–36.7)	6.5% (5.5–7.7)

*Magnitude here refers to the fact that the absolute value of the percentage error is taken prior to summary statistics being calculated, thus these errors are not representative of a bias and negative and positive errors do not cancel out.

Estimated V_{es} is a function the assumptions described in Chapter 5 for deriving ESPVR (Eq. 6.7). Table 7.2 shows associated median errors of 13.5-75.2% (Protocol D) and 2.0-6.6% (Protocol S), where Pig D1 is an outlier with 72.5% with the next highest protocol D error being 18.7%. Given the generally small value of V_{es}, moderate percentage errors do not necessarily translate into significant absolute errors. Estimated V_{ed} is a function of the assumptions associated with V_{es} combined with those associated with deriving the SV as in Kamoi et al. [124]. The expected increase in error due to additional assumptions is partially offset by the fact that V_{ed} is, on average, significantly larger than V_{es}. Thus, V_{ed} errors in Table 7.2 (Protocol D: 6.5-25.5%; Protocol S: 4.5-13.2%) are lower for Protocol D but higher for Protocol S than those for V_{es}. Again,

Pig D1 is an outlier with next highest at 12.6%. There was a notable correlation between errors in V_{ed} and V_{es} (R = 0.80, Protocol D and R = 0.83, Protocol S), which is expected as V_{es} is a linear input in the estimation of V_{ed}. Overall, Tables 7.1 – 7.2 suggest the method effectively locates P-V loops, and thus the method described in Chapter 6 not only captures the relative but also absolute behaviour of P_{lv} and V_{lv} effectively.

Table 7.2: Percentage errors for volume estimation of V_{es} and V_{ed}. Presented as median (25^{th} – 75^{th} percentile) for Protocol D, Pigs D1 – D6 and S, Pigs S1 – S5.

Pig	Number of Heartbeats	Mag. Error: Systolic Vol., V_{es}	Mag. Error: Diastolic Vol., V_{ed}
D1	5,480	75.2% (17.9–110.5)	25.5% (9.9–39.0)
D2	5,343	14.5% (3.1–27.2)	8.7% (2.3–17.1)
D3	32,626	15.4% (9.6–23.6)	9.5% (5.3–13.3)
D4	17,584	13.5% (8.6–22.5)	6.5% (2.3–12.2)
D5	15,874	17.9% (7.1–84.7)	12.6% (7.1–17.6)
D6	18,944	18.7% (13.3–30.7)	9.9% (6.0–18.7)
Mean (D)	15,975	25.9% (9.9–49.9)	12.1% (5.5–19.7)
S1	5,346	2.0% (1.0–3.3)	4.5% (1.5–8.8)
S2	5,382	6.6% (4.4–9.9)	13.2% (4.9–17.5)
S3	16,233	4.5% (2.6–7.6)	6.2% (2.9–12.0)
S4	13,507	4.7% (2.2–8.1)	5.6% (3.1–11.0)
S5	5,870	4.3% (2.5–8.1)	5.3% (3.0–9.9)
Mean (S)	9,268	4.4% (2.5–7.4)	7.0% (3.1–11.8)
Mean (D&S)	12,926	15.0% (7.7–30.6)	9.5% (4.7–16.1)

7.3.2 Stroke Work

Errors for estimated SW_E and simplified SW_S (Eq. 7.1), relative to invasively measured SW_M, are in Table 7.3. In 29 of 33 quartiles (25^{th}, 50^{th} and 75^{th} for 11 pigs), SW_E had lower errors than SW_S. Table 7.3 also shows correlation coefficients between SW_E and directly measured SW_M with overall R = 0.73 (Dobutamine) and R = 0.84 (Sepsis), suggesting the method effectively tracks changes in condition. Table 7.4 shows that these correlation coefficients remain relatively steady even when the number of data points is reduced drastically. In both protocols, one pig has a significantly lower R value than the rest (Pig D3, R = 0.14 and Pig S2, R = 0.58). Errors in SW_E were most strongly

correlated with errors in P_{sys} (R = 0.70), with other correlations being poor (P_{dia}, R = 0.04, V_{es}, R = -0.03, V_{ed}, R = 0.16).

Table 7.3: Percentage errors for stroke work estimation. Presented as median (25th – 75th percentile) for Protocol D, Pigs D1 – D6 and S, Pigs S1 – S5.

Pig	Mag. Error: Est. Stroke Work (SW_E)	Mag. Error: Simp. Stroke Work (SW_S)	Corr. Coeff. (R)
D1	3.5% (1.6–5.7)	8.9% (4.7–15.5)	0.90
D2	26.0% (21.6–30.2)	33.7% (28.8–41.0)	0.94
D3	32.6% (18.7–46.8)	43.7% (19.1–74.6)	0.14
D4	30.0% (17.9–63.7)	61.5% (37.9–90.2)	0.68
D5	27.8% (13.9–42.6)	40.1% (26.4–57.0)	0.70
D6	17.2% (5.9–34.5)	22.7% (11.9–37.1)	0.80
Mean (D)	22.9% (13.3–37.3)	35.1% (21.5–52.6)	0.73
S1	15.6% (5.3–21.3)	30.6% (7.5–39.1)	0.95
S2	16.4% (10.4–20.7)	14.3% (7.6–24.0)	0.58
S3	24.6% (12.4–42.9)	43.1% (22.5–67.6)	0.88
S4	41.2% (14.2–61.1)	57.4% (25.0–74.8)	0.84
S5	20.8% (17.5–55.6)	8.9% (4.7–96.4)	0.92
Mean (S)	23.6% (12.0–40.3)	30.9% (13.5–60.4)	0.84
Mean (D&S)	23.2% (12.7–38.6)	33.2% (17.8–56.1)	0.77

Table 7.4: Correlation coefficients for reduced data sets

Data Set	R, all data	R, 1 in 1000	R, 1 in 2000
D	0.73	0.75	0.75
S	0.84	0.79	0.74
D & S	0.77	0.76	0.75

Figs. 7.3 – 7.4 present trend compasses comparing estimated SW_E and invasively measured SW_M with percentage of trends having $\text{abs}(\theta) < 0.0997° = \tan^{-1}(0.1)$, or 1 part in 10 gradient error [146]. The upper semicircle represents increasing SW_M trends, and the lower, decreasing SW_M trends. The right semicircle represents overestimation ($\Delta SW_E > \Delta SW_M$), and the left underestimation ($\Delta SW_E < \Delta SW_M$) of the trend. Protocol D had 84.4 – 93.1% in this band and Protocol S, 80.4 – 92.1%. Thus, while errors may be greater, trend accuracy is strong over clinically relevant periods and a range of changes of condition.

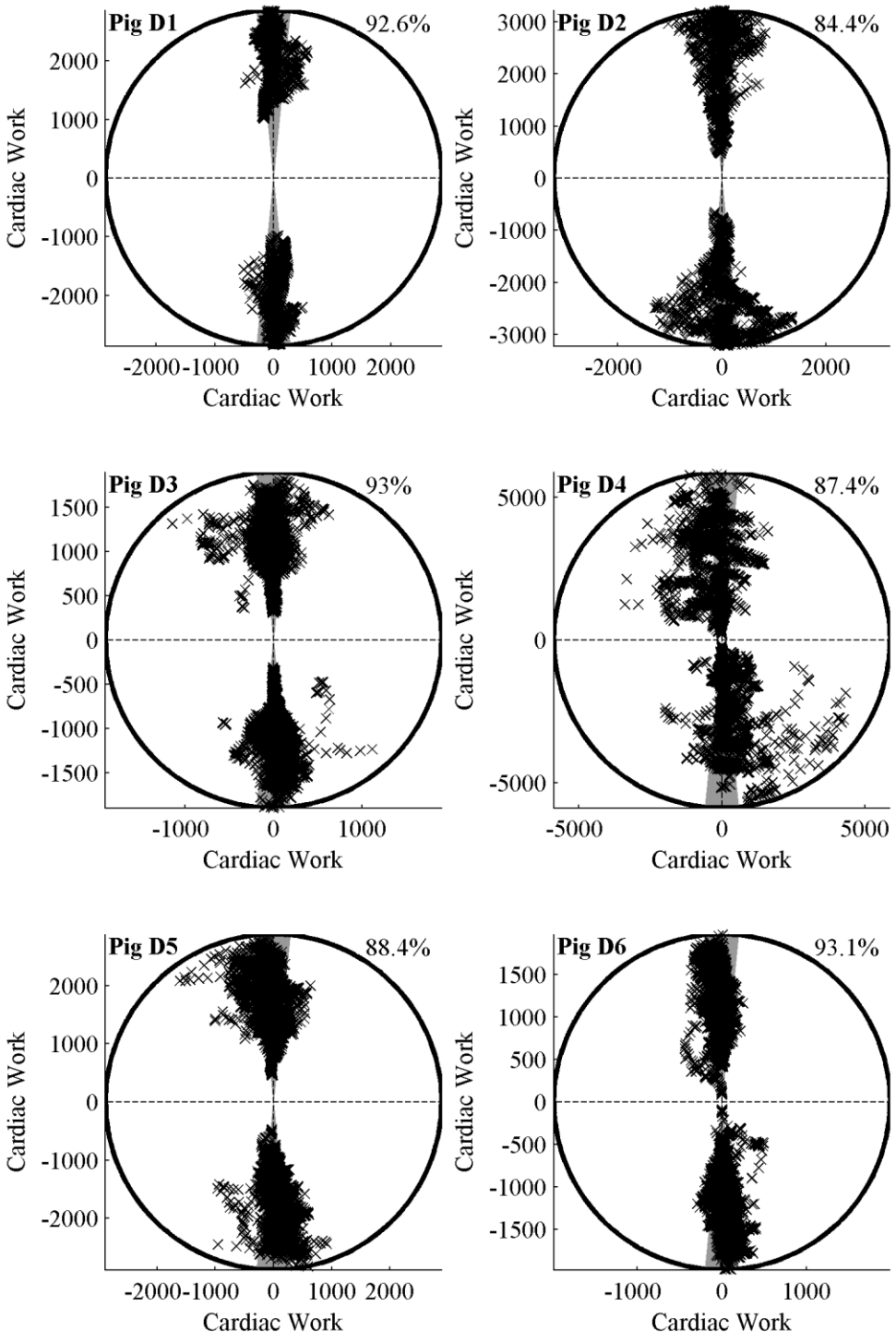

Fig. 7.3: Trend compass plots for estimated and measured stroke work, Dobutamine (Protocol D) Pigs.

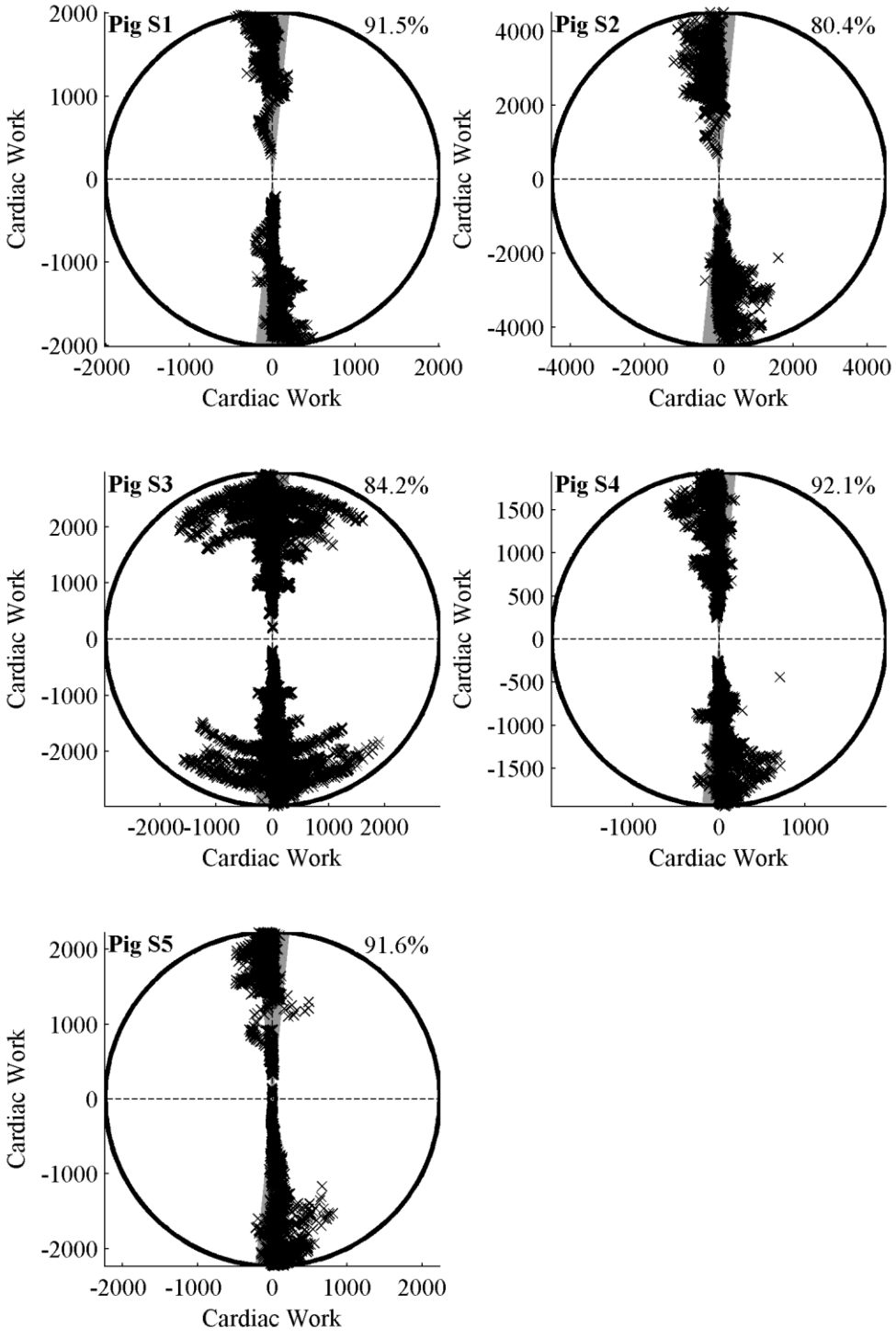

Fig. 7.4: Trend compass plots for estimated and measured stroke work, Sepsis (Protocol S) Pigs.

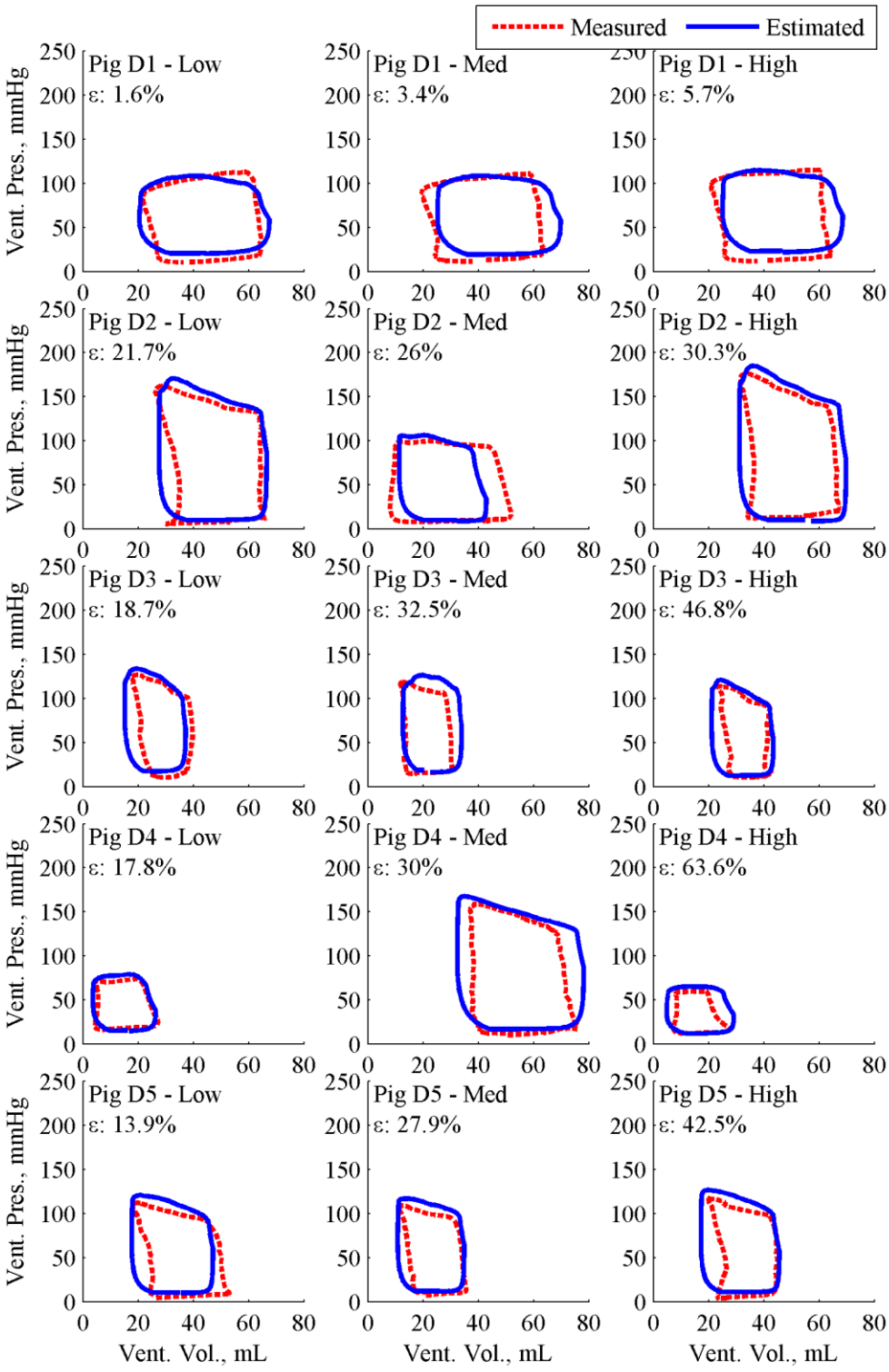

Fig. 7.5: Example P-V loops for different error quartiles, Dobutamine (Protocol D) Pigs, where ε is the percentage error in stroke work associated with the particular P-V loop.

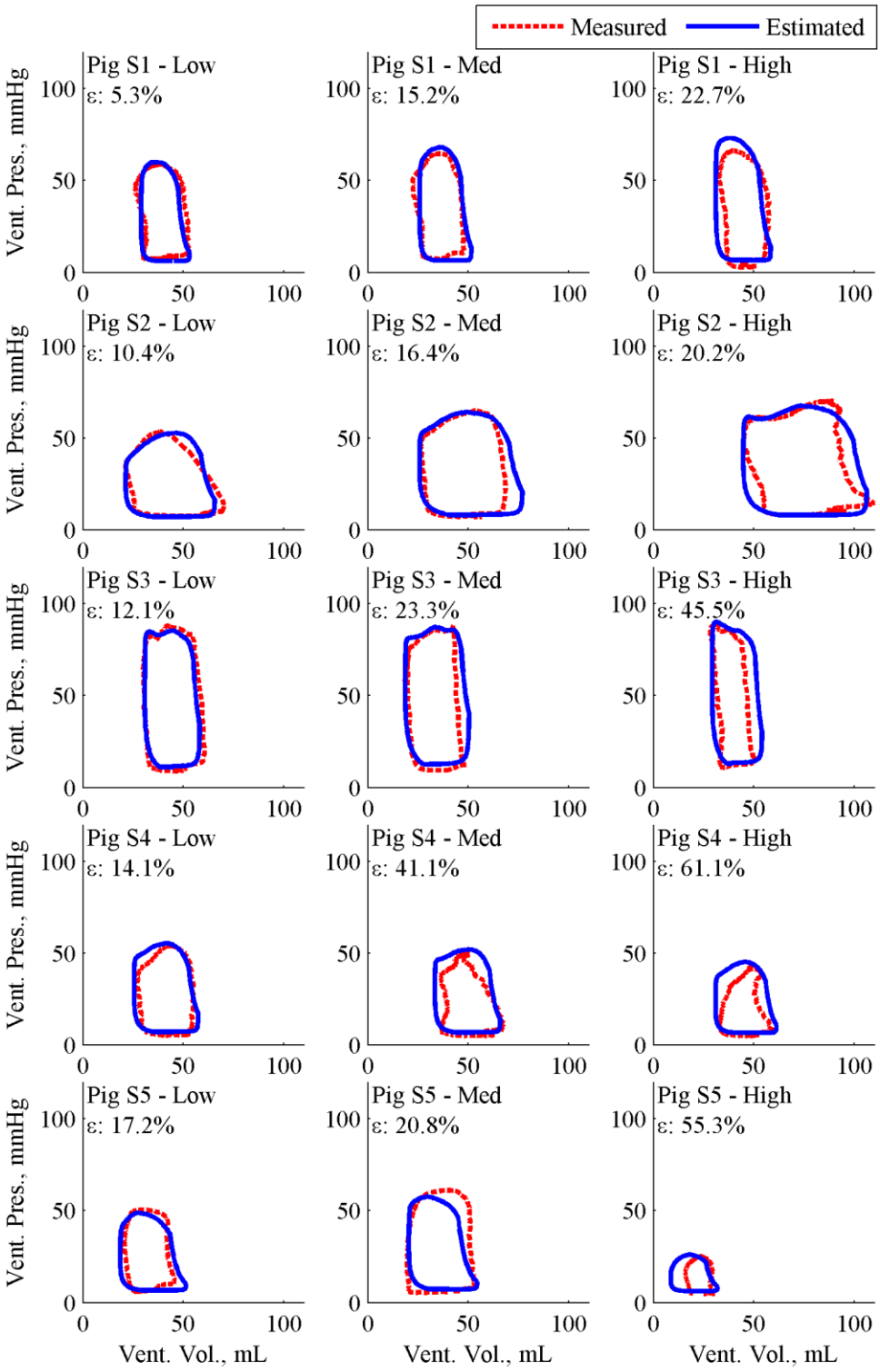

Fig. 7.6: Example P-V loops for different error quartiles, Sepsis (Protocol S) Pigs. Where ε is the percentage error in stroke work associated with the particular P-V loop.

Figs. 7.5 – 7.6 present demonstrative P-V loops for both protocols, as examples of quartiles of lumped *SW* estimation error in Table 7.3, thus illustrating the qualitative range of errors. Significant inter- and intra- subject variability is present, but overall errors are not qualitatively large and supported by strong trend accuracy in Figs. 7.3 – 7.4. Overall, these results show the method's ability to approximate subject specific shape and location of P-V loops.

7.4 Discussion

7.4.1 Pressure and Volume

Comparing invasively measured and estimated pressures and volumes in Tables 7.1 – 7.2 assesses both method efficacy and, in isolation, the impact of underlying assumptions in a manner impossible when analysing TVE as in Chapter 6. Low errors in Table 7.1 suggest P_{ao} and P_{lv} remain similar in systole, while the aortic valve is open, even during administration of drugs and the progression of sepsis significantly altering cardiac function. P_{sys}, is the only measured (P_{ao}) edge of the P-V loop, resulting in expected lower errors in Table 7.1, and thus assuming P_{ao} and P_{lv} remain similar holds well.

P_{dia}, results from assuming a set of fixed exponential waveforms, due to lack of available pressure data during diastole. Errors were thus higher and varied more between pigs in Table 7.1. However, since P_{dia} is roughly an order of magnitude smaller than P_{sys}, larger percentage errors translate to less significant absolute errors and do not significantly affect the method's ability to position a P-V loop.

V_{es}, was estimated using a modified ESPVR encompassing several assumptions. Median errors in Table 7.2 show significant differences ($p < 0.05$, two-tailed Student's t-test) between protocols D and S, possibly due to the use of dobutamine (Protocol D), which artificially alters the elastance used/found in estimating V_{es}, as well as due to an

outlying Pig D1. However, excluding this outlier, errors for both protocols were within acceptable levels.

V_{ed} was estimated using estimated V_{es} and estimated SV from Kamoi et al. [124], combining error contributions from both. This issue is partially offset by the fact $V_{ed} > V_{es}$, resulting in lower overall errors for Protocol D and slightly higher, but still very low, errors for Protocol S in Table 7.2, after removing outlier Pig D1. Excluding D1, median errors throughout estimation of V_{es} and V_{ed} do not exceed 20%, suggesting effective volumetric location of the P-V loop.

Interestingly, Pig D1 has low SW errors (Table 7.3) and effective trend tracking (92.6%, Fig. 7.3), implying actual shape and changes in shape of the P-V loop were well captured with some measure of bias. Large errors in V_{es} and V_{ed} may be due to a zeroing or sensor drift error in the volume catheter during this experiment. This possibility is supported by the percentage error in V_{ed} for Pig D1 being 3 times lower than for V_{es}, in contrast to most other pigs where this percentage error is 1.5 - 2 times lower. This discrepancy suggests a large part of error for Pig D1 is a steady offset or bias, which would be significantly reduced by a larger magnitude V_{ed}, as opposed to random error whose size depends on the measured value. Since a great deal of clinical management is titrated based on changes in measured state, this issue is significantly ameliorated by very good trend correlation.

Existing single-beat estimation methods for ESPVR [139] and EDPVR [140] rely on continuous echocardiography to provide continuous SV and ejection fraction data, which are currently cost prohibitive for standard ICU use [143]. Other measurements are also often required, such as arm cuff pressures [139]. The method presented here avoids such requirements by employing echocardiography only for a short calibration period, reducing associated costs, complexity and demands on specialist time. More

importantly, this method provides a unified set of cardiac dynamic information, in contrast to a single relationship.

7.4.2 Stroke Work

Table 7.3 compares errors between method estimated SW_E and a common, simplified approximation, SW_S with directly measured value. Error in SW_E was lower than SW_S in 29 of 33 quartiles assessed, suggesting this method's added complexity provides greater accuracy. Overall, average errors are 22.9% for Protocol D and 23.6% for Protocol S, with Figs. 7.3 – 7.4 and Table 7.2 showing strong correlation and trend accuracy. These results are significant, as they suggest the method effectively tracks changes in patient condition, despite errors, which is extremely important in in titrating care in the ICU.

Errors in SW_E were most strongly correlated to errors in P_{sys} (R = 0.70), with other correlations being poor (R = -0.03 to 0.16). This was of interest as estimation of P_{sys} involves directly copying a section of P_{ao} and assuming it is representative of P_{lv}. As a large amount of the method's information is derived from P_{ao}, it is possible that differences between P_{lv} and P_{ao} while the aortic valve is open and the two should be at their most similar, uncluttered by any mathematical process, provide a reasonable predictor, albeit one unavailable clinically, of overall method accuracy for a given subject.

Pig D3 exhibited significantly lower correlation (R = 0.14), which is not upheld by the trend compass in Fig. 7.3 with 93.0% within the specified θ band. The likely cause of this discrepancy is the long experimental time of Pig D3 (32,626 heartbeats), involving long periods without interventions where natural variation and noise dominate. R values punish 'horizontal' trend regions, as two variables that don't change aren't

necessarily correlated [119], while a trend compass makes no distinction and tracks trends independent of point accuracy [146].

Figs. 7.5 – 7.6 illustrate the range of results for P-V loops in different error quartiles in Table 7.3. The large variations in loop size in Fig. 7.5 for Pigs D2 and D4 show the significant effect of dobutamine on the circulatory system. Similar large variations in loop size in Pigs S4 and S5 (Fig. 7.6) demonstrate the significant effect of sepsis on cardiac function. Overall, these figures demonstrate the ability of the method to capture the diverse range of locations and shapes the P-V loop can take across different subjects and conditions. Finally, in several cases, the high percentage errors are due to overestimation of relatively small SW_M values (Pigs D4, S4, S5). Even in cases where error in SW_E is relatively high, the method is qualitatively reasonably able to locate and approximate the P-V loop shape and offers very good trend tracking.

There exist single-beat methods to estimate *PRSW* with strong correlation to measured *SW*, using non-invasive measurements and echocardiography [141]. This approach performed well using invasive measurements in dogs [141] and in humans. However, using non-invasive measurements reduced strong correlations to $R = 0.66$ or $R = 0.71$ when subject specific baseline ventricular properties were incorporated (associated percentage errors aren't reported) [142], which is lower than the overall method presented here ($R = 0.77$). Further, this other method requires more expensive, continuous echocardiography [143], as opposed to a short echocardiography calibration. Finally, it also does not provide the unified set of absolute pressure, volume and P-V contour information provided by the method presented here.

7.4.3 Limitations

Inevitably, there are limitations. First, the proposed method requires two inputs that are not widely available in the ICU, although readily obtained clinically. Specifically, a

short, non-invasive echocardiography calibration period of approximately 10 heartbeats and continuous P_{fe} as an input for the SV model [124], where it is used to estimate pulse wave velocity. While availability of echocardiography is becoming increasingly widespread in the ICU [127], this requirement still represents a modest additional clinical workload relative to normal ICU instrumentation. P_{fe} can be invasively measured clinically [73], but typically is not measured because it does not provide relevant additional information over P_{ao} barring specific cases. However, combining P_{ao} and P_{fe} to approximate SV adds new data and capability that may change this perception. Alternatively, P_{fe} can be ignored at the cost of some accuracy, as without P_{fe} one of the Windkessel elements must be fixed based on population values [108]. Existing studies show a shift from a 90% limit of agreement of less than ±10 ml[124] to a 90% limit of agreement of −12.4 to 14.3 ml [108] in *SV* estimation.

The data in this study is the product of a limited set of protocols and range of conditions. However, deliberately challenging protocols were selected, encompassing the complex and varied progression of sepsis [88], infusions of dobutamine to provide the largest possible disruptions to model assumptions about contractility, and several clinically standard interventions including recruitment manoeuvres. These are part of a far greater possible range of cardiac conditions, and the ability of the method to detect the effects of intra-ventricle conditions such as an ischemic attack, in addition to systemic conditions, should be validated with future work. However, such intra-ventricle conditions would be expected to affect diastolic/systolic timing and/or cardiac output, all of which influence the method through the medium of measured P_{ao}, and thus be potentially detected with this method although it was not possible to validate that possibility in this study. Hence, the overall physiology and assumptions employed developing this method are expected to generalise well, as no condition or intervention specific assumptions were made.

Finally, validation on human subjects is required before the method can be considered for clinical validation or use in observational and/or intervention studies.

7.5 Summary

The method developed in Chapter 6 was validated for the minimally invasive beat-by-beat estimation of the left ventricular P-V loop. This validation was performed across 142,169 heartbeats of data from 11 Piétrain pigs that were subject to two distinct protocols encompassing sepsis, dobutamine administration and clinical interventions. The method demonstrated the ability to effectively locate the P-V loop, with overall median errors for V_{es} of 15.0%, V_{ed} of 9.5%, P_{sys} of 19.4% and P_{dia} of 6.5%, and to estimate *SW* effectively, with an overall median error of 23.2%. Further, the method was shown to be able to effectively track changes in *SW*, with a trend compass in band performance of 80.4% to 93.1%, and an average *R* value of 0.77. While the method requires further validation, specifically on human subjects, it has demonstrated potential as a means of providing additional insight into cardiac behaviour, both in the form of TVE curves and P-V loops, at the patient bedside.

8

The ESPVR

The end-systolic pressure-volume relation (ESPVR) has been present throughout this thesis. As was discussed in Chapter 4, linear extrapolation of the ESPVR to the volume axis provides V_0, ventricular volume at zero pressure. Providing a sufficient range of ESPVR values for this extrapolation is a popular experimental method for approximating this parameter, but requires inducing a significant drop in cardiac output. This chapter provides an overview of the results of estimating V_0 using the experimentally standard vena cava occlusion method, and frames the results against those in Chapter 4 and literature surrounding the ESPVR in general.

8.1 Background

The ESPVR is an important cardiac relation with a strong presence throughout this thesis. The ESPVR can be used to evaluate the contractile state of the heart, as well as the response of the heart to changing circulatory conditions for a given contractile state [57]. ESPVR, generally represented as a linear pressure-volume relationship, can also be extrapolated to the volume axis to determine V_0, the volume of the heart at zero pressure, which is similar to V_d, the unstressed or 'dead space' ventricular volume, as discussed in Chapter 4. V_0 and V_d are important aspects in normalising models of cardiac behaviour across different subjects or contractile states, as this volume is 'non-functional' and thus does not represent cardiac work [111].

However, the linearity of the ESPVR only holds when either the curve is developed over a timescale sufficiently long for cardiac reflexes to not exert significant influence, or if cardiac reflexes are suppressed, for example by β-blockade as in [112] or ganglionectomy as in [113]. This issue presents something of a conundrum, as slowly but significantly reducing cardiac output (*CO*) over sustained period of time effects the cardiovascular system and can fail to provide a clinically desired 'snapshot' of contractile state due to the longer timescale. Similarly, suppression of cardiac reflexes through drugs or surgery significantly alters cardiovascular system behaviour and thus influences experimental results. The vena cava occlusion, favoured for its ability to cause a short, sharp drop in *CO* without long term effects on the subject, falls within the timescale where the influences of cardiac reflexes are significant and curvilinear behaviour can be observed if cardiac reflexes are not suppressed [112, 148, 149].

A potential workaround is to apply a curvilinear model to this short term ESPVR, potentially allowing determination of V_0 while avoiding the disadvantages presented above. This approach has been attempted in previous studies involving canine subjects and quadratic models, and shifts from negative, non-physiological V_0 values from linear models to small, positive, physiologically realistic V_0 values from quadratic models noted [112, 148]. However, as noted in one of these papers, '*a clear drawback of the parabolic equation, however, is that it lacks any inherent theoretical basis*' [148]. Further, these studies do not present end-systolic volume (V_{es}) values that allow for comparison with the method presented in Chapter 4, nor do they compare V_0 and V_d as a means of further validation.

This work examines data from repeated vena cava occlusion manoeuvres and compares a linear model with a nonlinear exponential model of the ESPVR in a case where reflexes are unsuppressed. An exponential model has a greater physiological precedence than a quadratic model, due to the general prevalence of exponentials in

physiological modelling as exemplified by the fact that EDPVR, a sister relationship to ESPVR, is typically expressed as an exponential [46]. Further, an exponential model behaves in a more physiological manner than a quadratic when extrapolated.

The vena cava occlusion manoeuvres take place over a large pressure range and number of heartbeats in a number of different pigs, providing a broad range of data. The unique aspects of this study are the number of heartbeats per pig across multiple occlusion manoeuvres available, the exploration of exponential modelling of the ESPVR as compared to the linear or quadratic models typically employed [150] and the use of porcine data as opposed to canine or rat data, which is important due to the close physiological resemblance of pigs to humans [151]. Further, these results are framed against baseline V_{es} values and compared to those obtained for V_d in Chapter 4.

8.2 Methods

8.2.1 Experimental Data

This chapter makes use of the 6 Protocol D pigs that were not subject to exclusion. The waveforms are continuously sampled left-ventricular pressure (P_{lv}) and volume (V_{lv}) over the course of multiple vena cava occlusions of between 10 and 20s duration, which are used to develop the ESPVR. Overall 1177 heartbeats during these vena cava occlusion manoeuvres were analysed. Data from the Protocol S pigs were not used in this chapter, as vena cava occlusions were not performed as part of this protocol.

8.2.2 Modelling the ESPVR

During vena cava occlusion manoeuvres end-systolic pressures and volumes were determined by finding and recording the maximum ratio of pressure to volume for each heartbeat. Two models were used for determining ESPVR and V_0. The first is the traditional linear model, which was used as a means of comparison and to confirm a

significant departure from linear behaviour was being observed due to the action of cardiac reflexes:

$$P_{es} = E_{es}(V_{es} - V_0) \tag{8.1}$$

where P_{es} represents end-systolic pressure and E_{es} end-systolic elastance. The second model used was the exponential model:

$$P_{es} = P_{\infty}\left(1 - \mathrm{e}^{-m(V_{es} - V_0)}\right) \tag{8.2}$$

where P_{∞} is the asymptotic pressure and m an indication of the steepness of the exponential curve.

The exponential model was selected as it captured observed nonlinear ESPVR behaviour with more physiological accuracy than previously employed quadratic curves, which can behave in a non-physiological manner when extrapolated. Both curves were fitted by using the Levenberg-Marquardt Algorithm to minimise the geometric mean deviation (GMD) [152]. Use of the GMD accounts for the fact that both the volume and pressure measurements taken are equally subject to measurement error. Linear and exponential ESPVR curves were compared based on Pearson's correlation coefficient (R) values. Both the linear and exponential fit were evaluated using the correlation between measured P_{es} and P_{es} as determined via Eq. 8.1 (linear) and Eq. 8.2 (exponential) from measured V_{es}. This process ensured the comparison was a fair comparison between two linear, 1-1 fits, as R is designed for linear correlations. The resulting V_0 values were also compared with values presented in literature, and with the values for V_d provided in Chapter 4.

8.2.3 Statistical Comparison of Models

The Akaike information criterion (AIC) is a method of estimating the loss of information involved with using a model to represent a data set [153]. It presents a trade-off between goodness of fit against model complexity, and can be expressed for a least squares problem:

$$AIC = n \log\left(\frac{RSS}{n}\right) + 2K \tag{8.3}$$

where n is the number of data points in the sample set, RSS is the residual sum of square errors and K is the number of parameters in the model. Lower values of the AIC are considered indicators of a more effective model than higher values.

8.3 Results

Combined end-systolic pressures and volumes for each pig, with linear and exponential fits, are shown in Fig. 8.1. Of note is the nonlinear behaviour in all pigs except Pig D6, and the fact that the curves for different positive end-expiratory pressure (PEEP) levels largely conform to a single exponential model. Also of note is the unusual behaviour of Pig D4, which appears to undergo a change in contractile state between PEEP 10 and 15 and thus is split into two model lines. Example pressure-volume (P-V) loops are overlaid on each plot.

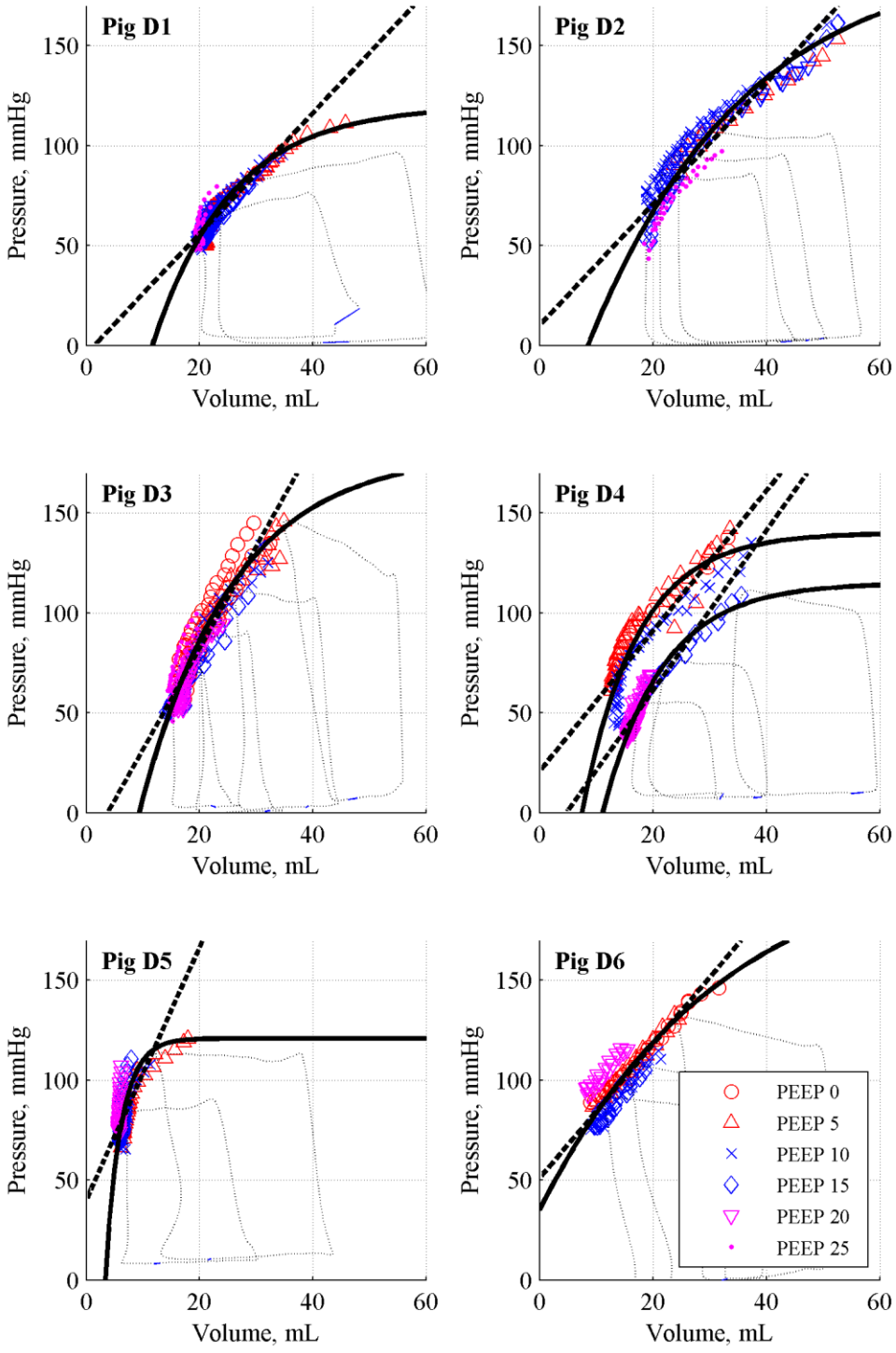

Fig. 8.1: ESPVR linear and exponential model lines for Pigs D1 – D6, example P-V loops are overlaid.

The linearised correlation coefficients for each pig along with V_0 and AIC values are presented in Table 8.1.

Table 8.1: Correlation coefficients and V_0 values for linear (V_0, Lin) and exponential (V_0, Exp) ESPVRs.

Pig	R, Exp. Model	R, Lin. Model	V_0, Exp. Model, mL	V_0, Lin. Model, mL	AIC, Exp. Model	AIC, Lin. Model	No. Beats
D1	0.943	0.929	11.67	1.43	614.4	703.3	276
D2	0.951	0.939	8.56	-3.29	560.9	595.2	154
D3	0.929	0.923	9.38	3.78	981.3	1020.1	266
$D4_1$	0.926	0.900	7.47	-5.87	428.5	467.1	111
$D4_2$	0.978	0.947	11.1	4.73	146.8	216	89
D5	0.717	0.708	3.31	-6.33	571.9	624.7	153
D6	0.873	0.882	-5.72	-15.22	435.5	437.5	124

Finally, the V_0 values provided by the exponential model presented relative to baseline V_{es} in Table 8.2, to allow comparison with those results from Chapter 4.

Table 8.2: V_0 from exponential ESPVR expressed as a percentage of baseline V_{es} (V_0, $\%V_{es}(0)$).

Pig	V_0, Exp. Model, mL	Baseline $V_{es}(0)$, mL	V_0, $\%V_{es}(0)$
D1	11.67	45.8	25.5%
D2	8.56	52.1	16.4%
D3	9.38	39.0	24.0%
$D4_1$	7.47	18.2	41.1%
$D4_2$	11.10	18.2	61.1%
D5	3.31	8.5	38.9%
D6	-5.72	20.0	-28.6%

8.4 Discussion

The exponential model demonstrates a reasonably consistent, if modest, overall improvement in correlation coefficient ($p < 0.05$, two-tailed, paired Student's t-test), with only Pig D6 demonstrating a higher linear than exponential correlation coefficient in Table 1. Further, the exponential fit provided more physiologically reasonable, positive values for V_0 in 6 out of 7 cases, while the linear fit provided non-

physiological, negative V_0 values in 4 of 7 cases. Negative V_0 values are an acknowledged issue with linear ESPVR when generated rapidly [57], especially where cardiac reflexes are active. The exponential fits appear to go some way towards alleviating this issue, similar to the results of a quadratic fit, as previously reported [112, 148].

The AIC values for the exponential model in Table 1 are consistently, if modestly, lower than those for the linear model ($p < 0.01$, two-tailed, paired Student's t-test). This result suggests that, even accounting for the additional parameter available to the exponential model, the exponential model provides an improvement in performance over the linear model. The combined AIC values, R values, and V_0 values support the validity of an exponential model to account for nonlinear behaviour of the ESPVR in cases where cardiac reflexes are not supressed.

The exponential model also performs in a more physiological manner as the boundary conditions are approached. Exponential models tend towards a positive asymptotic pressure as volume increases, rather than increasing indefinitely (linear) or potentially decreasing (quadratic). Indeed, the end-diastolic pressure-volume relation (EDPVR) is represented by an exponential curve [46].

With the exception of Pig D6, the V_0 values presented range from 16.4-41.1% of baseline V_{es} for the Protocol D pigs. These result agree well with V_0 values reported in literature, for example 13-52% of baseline V_{es} in cross circulated dogs [109], and 24-84% of baseline V_{es}, ignoring non-physiological negative results, in humans [58]. Other literature [111, 122] reports similarly sized, positive values, as might be expected. Further, V_0 values presented here agree reasonably well with 44-53% of baseline V_{es} reported for the Protocol S pigs in Chapter 4. It is possible that the exponential method presented in this chapter underestimates V_{es} in some cases, as the method in presented Chapter 4 is more rigorous and reliant on a more robust pair of redundant linear

extrapolations rather than a single, significant, nonlinear extrapolation. Regardless, the exponential method does notably improve V_0 estimation over the linear ESPVR under the conditions presented.

As noted above, Pig D6 exhibits performance different from the other subjects. This pig demonstrated negative V_0 values for both linear and exponential fits, larger correlation coefficients for linear than exponential fits and visually apparent linear behaviour. However, it is possible this behaviour is the result of the occlusion manoeuvres failing to move the P-V loops far enough left for curvilinear behaviour to become apparent in this specific pig, or due to the pig's cardiac reflexes failing to perform effectively. This linearity also accounts for the negative V_0 produced by the exponential fit, as the lack of the steeper gradient closer to the x-axis results in an exponential with extremely low curvature, approaching linear behaviour.

Pig D4 exhibits an apparent change in contractile state between PEEP 15 and PEEP 20, with two quite separate, but distinctly curvilinear, ESPVR lines. As these two regions are able to be distinctly separated both in terms of PEEP level and temporally, the data was split into its two separate sections for model fitting. While this split increases overall R values, the core purpose of this paper is to compare linear and exponential R values, rather than obtaining a high R value. Thus, this approach is justified. It is worth noting that both of the exponential V_0 values are positive and agree reasonably well, while the linear V_0 values vary greatly and go from negative to positive. During the second occlusion manoeuvre at PEEP 15, the balloon used to occlude the vena cava failed to fully deflate, raising the possibility that it remained partially inflated for the remainder of the experiment, thus potentially causing the observed behaviour.

Fitting a single ESPVR curve through data corresponding to different PEEP levels in a given specimen is unusual and provides for some interesting observations. ESPVR is supposedly relatively independent of cardiac preload and afterload [154, 155], and

dependent mainly on the contractile state of the individual. However, this assumption has been the subject of ongoing debate [57, 109, 156], and, as PEEP effects both preload and afterload [157], it is possible PEEP changes cause shifts in ESPVR. The data shown in Fig. 8.1 shows slight variability in ESPVR with PEEP changes, with no discernible trend as pressure increases (Pig D6, for example, shifts to the left as PEEP rises, while Pig D2 shifts to the right). This result agrees well with other animal studies, which show ESPVR is not altered significantly by PEEP [125, 158].

Use of an exponential ESPVR curve to model cases where cardiac reflexes are unsuppressed has interesting potential implications. While the difference between a linear and exponential ESPVR is minimal over the physiological range typically observed in an ICU, the exponential curve slightly shifts the expected cardiac response to changing circulatory conditions for a contractile state. A more significant change is in terms of providing more accurate estimates of V_0 or V_d, as the two curves behave quite differently when extrapolated to the volume axis. While not as robust as the method presented in Chapter 4, this result has the potential to improve the accuracy of V_0 estimation from the ESPVR when generated from short term interventions while cardiac reflexes are active.

8.5 Summary

The ESPVR has been observed to behave in a curvilinear fashion when generated over a short time span with cardiac reflexes not supressed, as in an ICU patient. Experiments were conducted encompassing 41 vena cava occlusion manoeuvres at a variety of PEEPs across 6 porcine specimens, and ESPVR assessed for each pig. The ESPVR curves were found to conform better to an exponential fit in 6 out of 7 cases, and provide more physiologically reasonable positive V_0 values in 6 out of 7 cases, while the linear fit produced positive V_0 values in only 3 out of 7 cases. This overall outcome

conforms to the notion that ESPVR is nonlinear where cardiac reflexes are not supressed, and provides an improved means of estimating V_0 under such conditions.

9

Arterial Transfer Functions

An alternative means of looking at the circulation of blood is through direct waveform energetics. In this chapter, rather than manually creating a deterministic, physiologically relevant model, the pressure waveforms in the circulatory system are treated as inputs and outputs for a non-physiological transfer function based mathematical model, with the results interpreted in the frequency domain. This approach requires no *a-priori* physiological assumptions beyond what is located 'upstream' and 'downstream', but implicitly assumes an overall linear behaviour between the two signals. It is thus more focused on the direct observation, interpretation and analysis of the available data.

9.1 Background

Transfer functions relate the outputs of a system to their inputs, and are popular in a wide variety of fields [159]. Transfer functions are expressed in the frequency domain, rather than the time domain, and are defined for linear time-invariant systems. While real world systems often do not strictly conform to the definition of 'linear time-invariant', within certain boundaries their behaviour generally can be expressed as such. Transfer functions are used to mathematically analyse system behaviour and predict response to a wide range of inputs, for example a building's seismic response [160, 161], as well as to design systems to certain performance criteria [162].

For a discrete-time system, with an input $x(t)$ and output $y(t)$, the transfer function can be expressed:

$$H(s) = \frac{Y(s)}{X(s)} \tag{9.1}$$

where $H(s)$ is the transfer function and $Y(s)$ and $X(s)$ are the system output and input, respectively, transformed onto the complex s-plane, which is used to express system behaviour in the frequency domain. Provided the inputs and outputs are periodic, the transformation from time to frequency domain can be achieved using Fourier transforms [163].

Transfer functions can be applied to biological systems, including the circulatory system. Prior work investigated transfer functions between inter-beat averages of airway pressure, aortic pressure split into diastolic, systolic and pulsatile components, and heart rate [164, 165]. These works primarily focus on longer term trends and the circulatory system's auto-regulation mechanisms. Additional results exist using transfer functions to estimate the aortic pressure waveform from a peripheral pressure waveform [166]. However, there is currently no work exploring the diagnostic potential of intra-beat cardiovascular pressure wave transfer functions.

This chapter explores the ability of intra-beat transfer functions to provide diagnostic information across an animal trial dataset encompassing the development and progression of sepsis. In general, intra-beat transfer functions are applicable to any combination of two pressure or volume waveforms within the same region (systemic or pulmonary) of circulation. As sepsis primarily effects the systemic circulation, transfer functions between aortic pressure (P_{ao}) and femoral pressure (P_{fe}) are investigated here.

9.2 Methods

An experimental animal trial data set including the progression of sepsis was employed in this chapter. Sepsis typically results in a decrease in systemic resistance due to capillary leakage [88]. Thus, clear changes in a systemic intra-beat pressure wave transfer function are anticipated.

9.2.1 Experimental Data

This chapter makes use of the 5 Protocol S pigs that were not subject to exclusion. The waveforms employed include continuously sampled P_{ao} and P_{fe}, used as the input and output waveforms for the transfer functions.

9.2.2 Data Processing

As experimentally gathered data from a biological system is not strictly linear time-invariant, some post-processing is required to obtain suitable waveforms. First, waveforms were grouped into sets of 8, to provide a sufficient window length to capture lower frequency influences, such as the breathing cycle, given the 250 Hz sampling rate and average 60 bpm cardiac cycle. Second, for each of these sets of 8 heartbeats, the late-diastolic region of the first heartbeat (Region D, Fig. 9.1) was adjusted via a shear transform to match the beginning of the corresponding region for the final heartbeat. This transform is illustrated in Fig. 9.1 by the dashed horizontal line, where only a single heartbeat instead of 8 is shown for ease. The shear transform provides a repeating sequence of heartbeats without any step changes, a 'periodic' waveform suitable for a Fourier transform. These operations were performed for both P_{ao} and P_{fe}, though only P_{ao} is shown in Fig. 9.1.

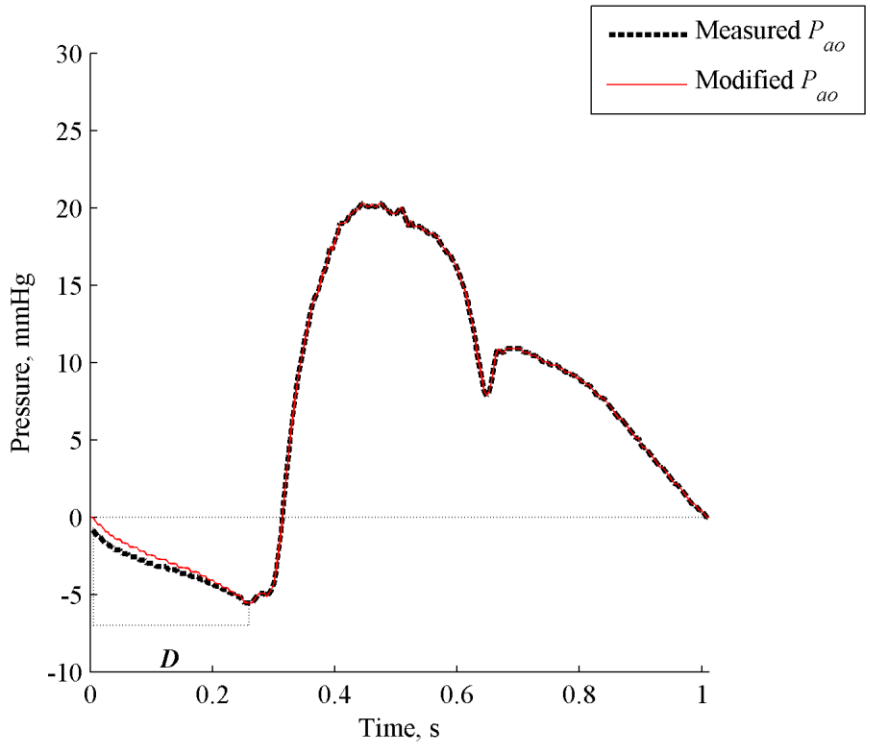

Fig. 9.1: Modification of P_{ao}. Only one heartbeat is shown for clarity, though this operation actually performed between the 1st and 8th heartbeat of a set.

The set of 8 heartbeats was then adjusted such that the signal began and ended at zero, and zero padded to a length of 4096 samples. This process provides a frequency resolution of approximately 0.06 Hz, covering an effective range from 0 – 125 Hz, yielding sufficient frequency resolution and range to easily separate breathing cycles set at 0.25 Hz by the ventilator, and heartbeats at ~1 – 2 Hz. Zero padding was used instead of a broader windowing function as a broad window risks including significant changes in P_{ao} or P_{fe}, resulting in a signal that changes too dramatically to be approximated by a periodic function. Fourier transforms were performed using the MATLAB 'fft' function (R2014a, 64-bit, The Mathworks, Natwick, MA, USA).

9.2.3 Data Presentation

As the cardiovascular system is not linear time-invariant in the long term, this method generates a large number of short term transfer functions, which can evolve over time. Presentation of such a large number of transfer functions was performed in two

different fashions. The first manually divides the data into sections between interventions, where the system should behave in an approximately linear time-invariant form. The transfer functions within each region are averaged, providing a small set of representative transfer functions. This approach results in far fewer transfer functions to be displayed, at the cost of averaging large areas of data where changes may be occurring in the shorter term. However, it allows the results to be presented in a 2-D profile, which aids interpreting the data. The second approach plots a full 3-D surface plot, showing the evolution of the transfer functions and phase plots over the course of the experiment for each pig. This approach provides a full indication of the evolution over time of the transfer function, but is more difficult to interpret than the profile plot in the first approach.

9.3 Results

Fig. 9.2 presents the transfer functions between P_{ao} and P_{fe}, divided into regions over the clinical trial by hand. The transfer functions progress from a light to a dark cyan throughout the pre-sepsis procedures, with recruitment manoeuvres (RMs) denoted by dashed lines, and then magenta to red throughout the post-sepsis procedures, with RMs again denoted by dashed lines. The vertical dashed lines denote average breathing and heartbeat frequencies from left to right, respectively. Of note are the peaks and harmonics occurring at roughly 2 Hz, 4 Hz and 8 Hz, which occur relatively consistently across pigs. Beyond a frequency of about 8 Hz, the data is overwhelmed by signal noise.

Fig. 9.3 presents the phase angle between P_{ao} and P_{fe}, divided into regions by hand. There is a slight phase lag present at approximately the heartrate, and this phase lag steadily increases with frequency. Due to the extremely large phase lag occurring at higher frequencies, the scales of Fig. 9.3 have been limited to aid interpretability.

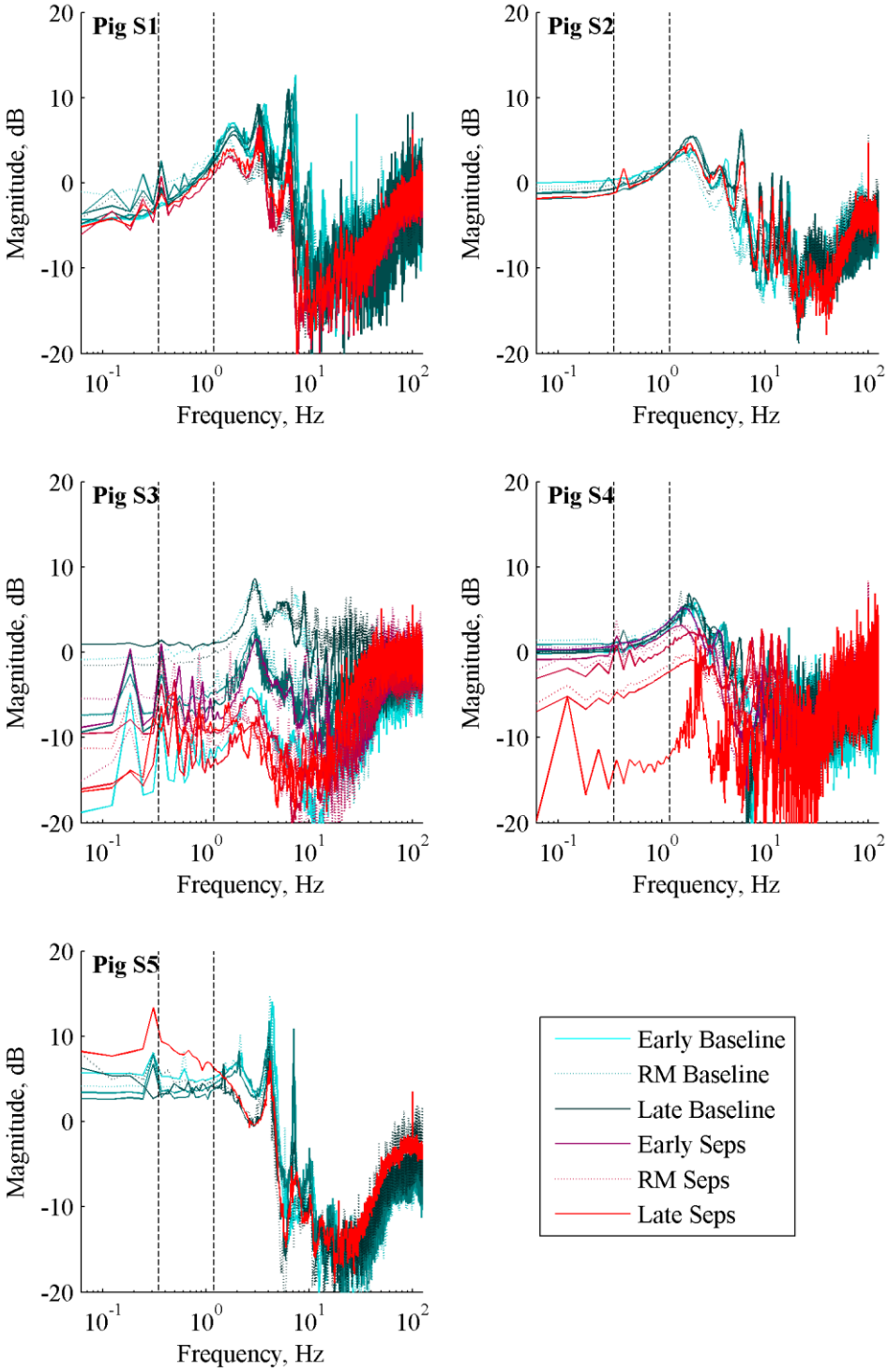

Fig. 9.2: Transfer function regional profile magnitude plots for Pigs S1 – S5.

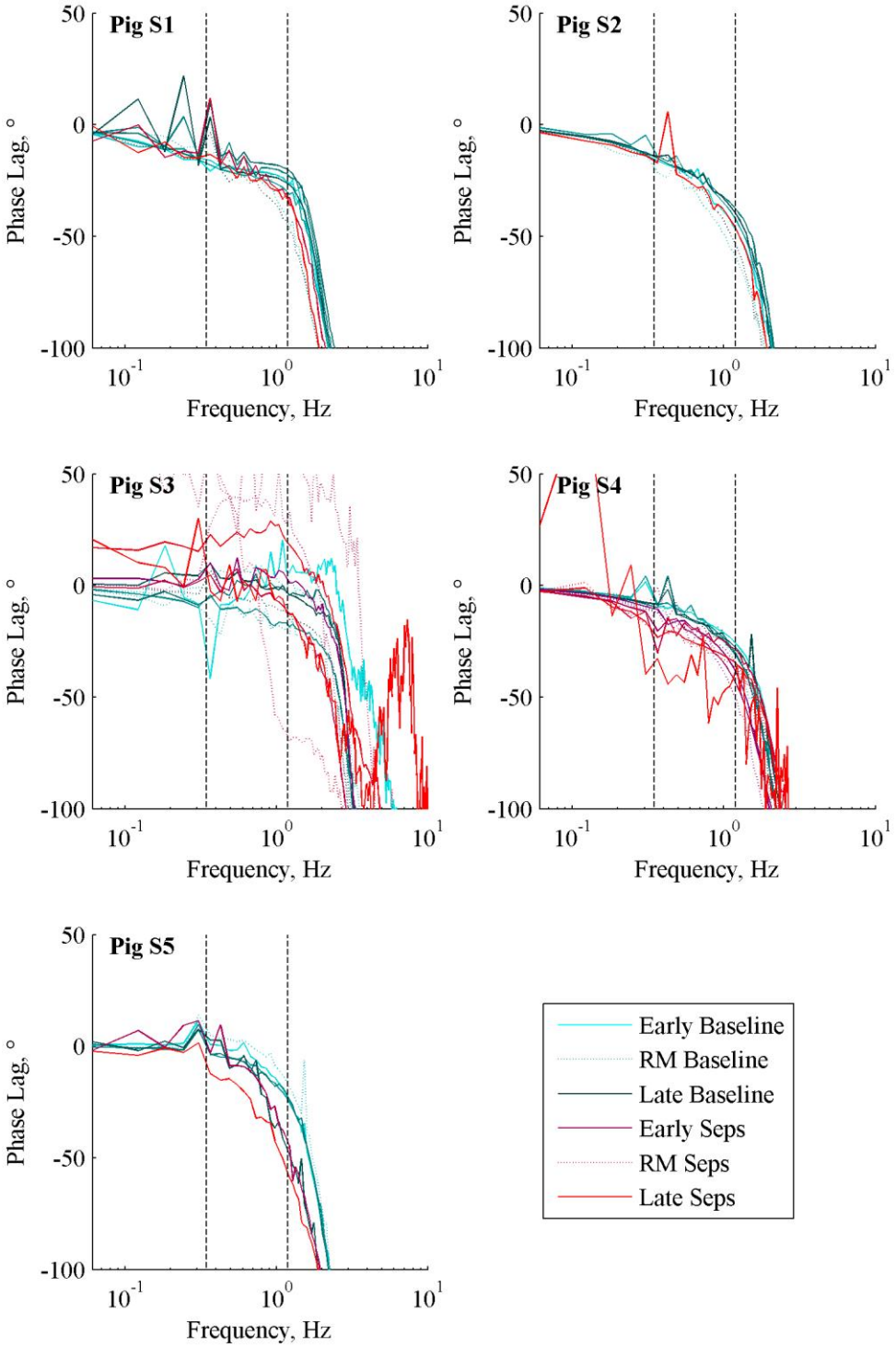

Fig. 9.3: Transfer function regional profile phase plots for Pigs S1 – S5.

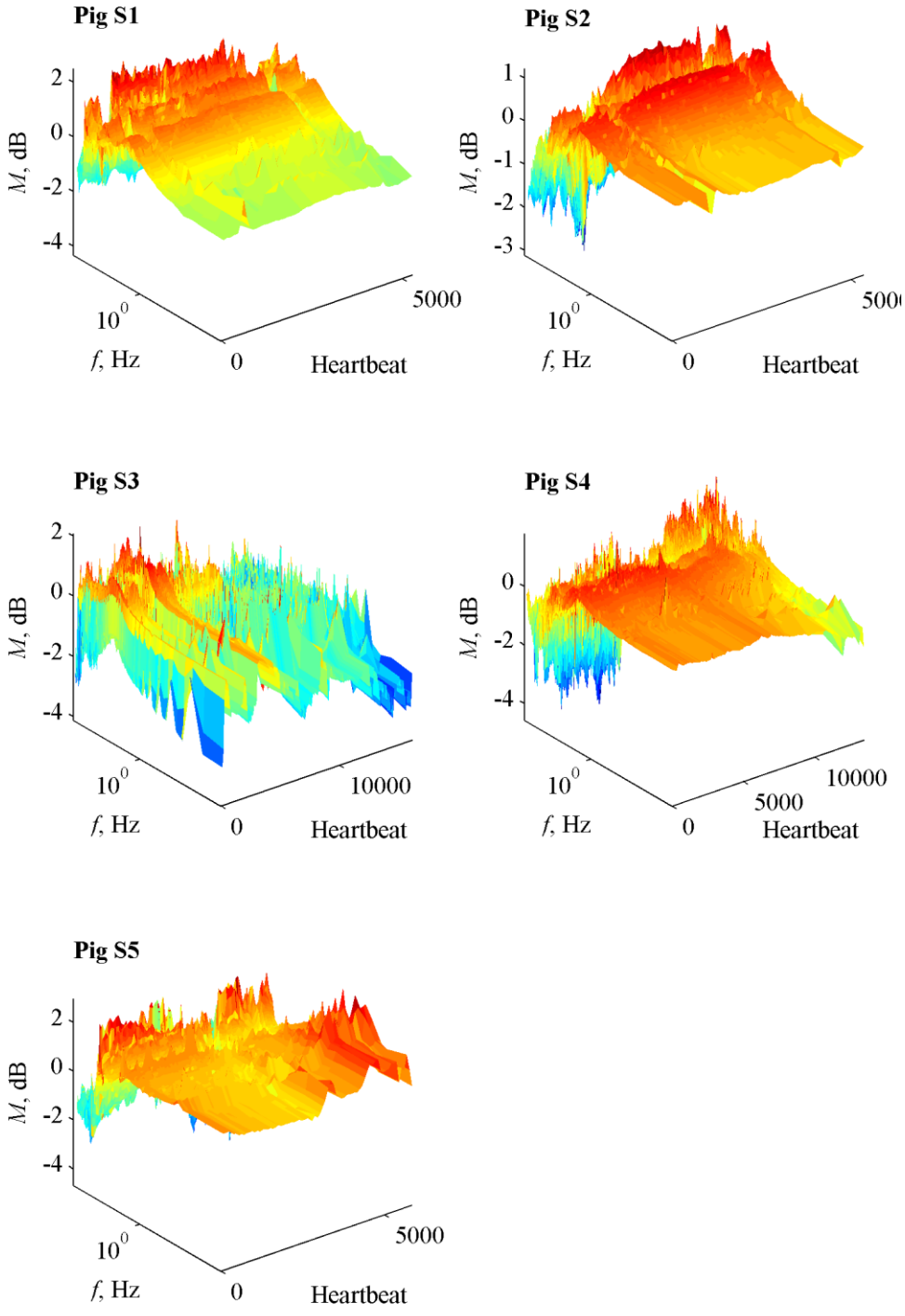

Fig. 9.4: Transfer function magnitude surface plots for Pigs S1 – S5.

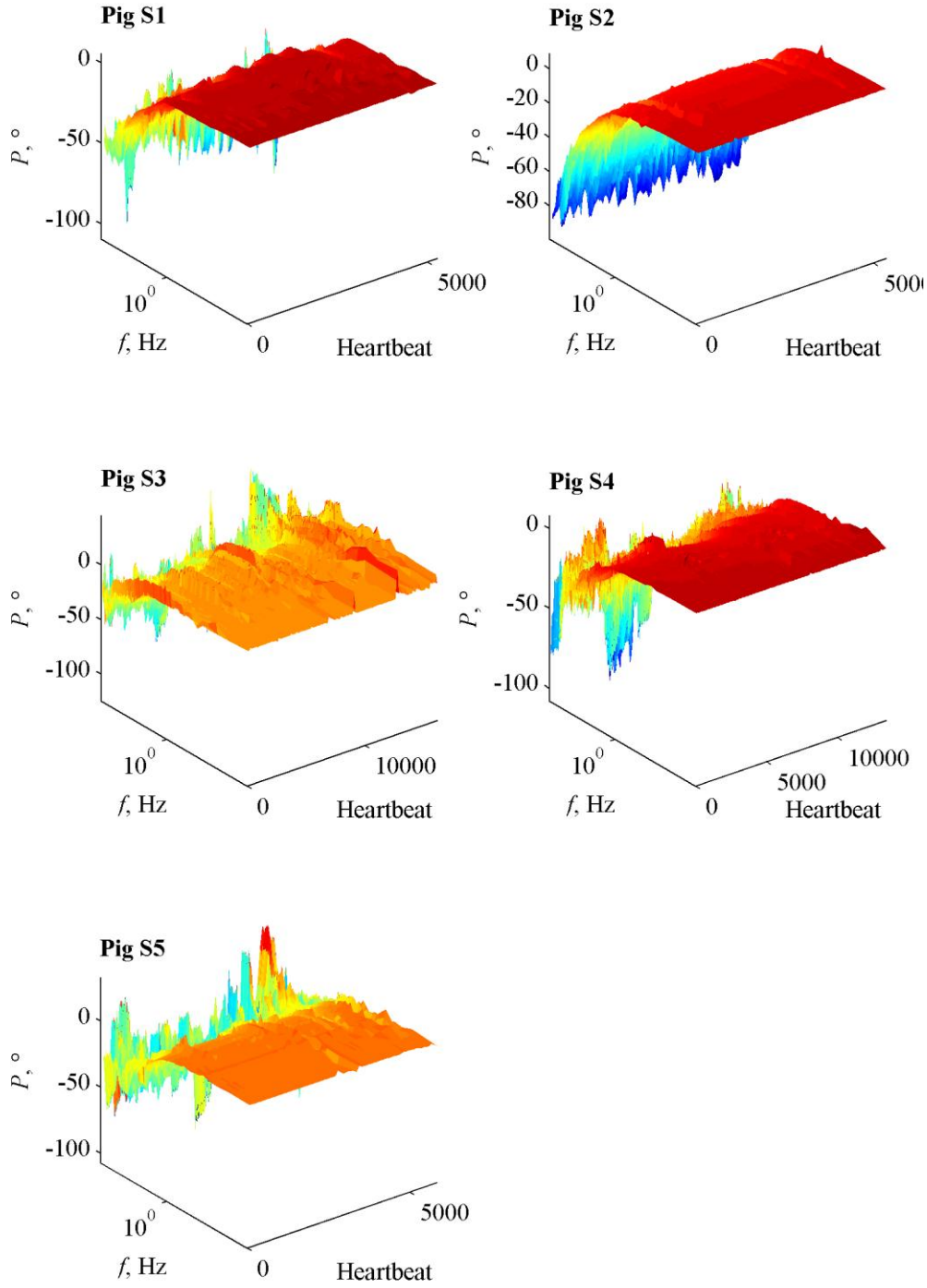

Fig. 9.5: Transfer function phase surface plots for Pigs S1 – S5.

Figs. 9.4 and 9.5 present the surface plots generated from the transfer function and phase plot, respectively, over the course of the experiment. The axes here are limited to frequencies below 10 Hz, based on the high noise levels present at higher frequencies in Figures 9.2 and 9.3. One can observe the same set of peaks and harmonics in Fig. 4 at 2 Hz, 4 Hz and 8 Hz, and phase lag in Fig. 9.5, as well as observe more clearly the evolution in these features over time.

9.4 Discussion

Fig. 2 shows the transfer function between P_{ao} and P_{fe}. Interestingly, the largest peak occurs at a frequency of approximately 2 Hz, consistently higher than the average heart rate. This peak is present at roughly the same frequency for all 5 pigs, and is followed by harmonics at 4 Hz and 8 Hz, although the size of these harmonics varies between pigs. There is also a small, intermittent peak at a frequency corresponding to the respiratory rate. Above ~8 Hz the transfer function begins to oscillate rapidly, suggesting that noise, due to discretisation errors in the catheter and mains noise amongst other issues, is dominant, and the signal is no longer interpretable. However, as this frequency is significantly higher than the heartrate at approximately 1 – 2 Hz, it is likely only higher harmonics, rather than important signal information is being lost.

Pigs that died before completion of the protocol (Pigs S1, S2 and S5) showed significantly less variation in low frequency energy transfer than pigs that survived the duration of the protocol (Pigs S3 and S4). In general, attenuation appears to occur as sepsis progresses. However, the degree of this attenuation varies, and Pig S5 is an exception.

This long term low frequency attenuation suggests a loss of pressure in the periphery, consistent with sepsis [11, 167]. The fact that it does not manifest as strongly in pigs that rapidly died is interesting. It is possible this difference is due to data being

truncated once P_{ao} and P_{fe} deteriorated to the point that features were difficult to make out. Pigs S1, S2 and S5 hit this point rapidly after endotoxin infusion.

The magnitude of the peak at breathing frequency varies significantly with time. Some of this variation is likely due to the RMs used. However, some variation is also due to P_{ao} and P_{fe} falling as sepsis progresses, resulting in a greater contribution of pressure variation due to breathing, which remains constant aside from RMs.

Fig. 9.4 shows a full surface plot of the transfer function between P_{ao} and P_{fe}. This plot reveals several interesting trends not observed in Fig. 9.2. First, sharp drops in the transfer function across all frequencies occur consistently with RM delivery, most obviously in Pigs S1 and S2. Pig S4 shows a clear, smooth, long term attenuation as sepsis progresses. Unfortunately, the other longer survivor, Pig S3, shows sharp variations in its transfer function, although clear attenuation is evident towards the end of monitoring. Pigs S4 and S5 shows a sharp peak appearing at the respiratory frequency towards the end of the monitoring period, which is also visible in Fig. 9.2.

Fig. 9.3 shows the phase plot for the transfer function between P_{ao} and P_{fe}. There is a phase lag at heartbeat frequency of about 30° – 50° which corresponds with what one would physiologically expect between P_{ao} and P_{fe}. The magnitude of this phase lag varies over the course of the protocol, and clear trends are difficult to establish across all pigs. Above the heartbeat frequency, phase lag rapidly increases, resulting in a need to restrict the scale.

There is generally a slight phase lead present at breathing frequency, which is interesting. As the aorta is in the thoracic cavity and the femoral artery is not, breathing directly effects P_{ao}, but not P_{fe}. Fig. S5 shows the surface phase plots for the transfer function between P_{ao} and P_{fe}. This plot confirms observations made from Fig. 9.3, namely that phase generally remains consistent for a given frequency regardless of

interventions, with only slight variations and no clear trends. Thus, there appears to be minimal clinical information in the phase plot and values.

Overall, a major question to be raised is whether these transfer functions provide additional information that is easier to interpret than what is directly available from observing P_{ao} and P_{fe}. Clinicians are already presented with a large volume of information in the intensive care unit (ICU), and additional diagnostic aids should seek to reduce the clinical burden of interpreting these large volumes of information. As such, due to the lack of clear and consistent trends between pigs and the relatively involved process of interpreting the figures, this process would offer more in the way of interesting insight into cardiovascular behaviour than useful direct diagnostic information or aid.

A notable limitation of this method is that both P_{ao} and P_{fe} are located upstream from the capillary beds of the systemic circulation, which are the physiological structures most effected by sepsis, as it is disease of the micro-circulation. Intuitively, one would expect the transfer function between P_{fe} and central venous pressure (P_{vc}) would provide better or further information about the state of these capillary beds. However, there are several difficulties involved with using P_{vc}, all of which stem from the low pressures present in the vena cava and venous circulation in general.

First, discretisation error becomes large due to the amplitude of P_{vc}, roughly 8 mmHg to 12 mmHg [30], which is not significantly larger than pressure catheter resolution, resulting in a series of step changes rather than smooth contours. Second, as discussed in Chapter 2, P_{vc} is significantly affected by the behaviour of the right heart, which is the source of the ‘A’ and ‘C’ peaks in the signal, which have a roughly equal magnitude to the ‘V’ peak from upstream flow [46]. As such, a large amount of post processing would be necessary to make P_{vc} usable in a transfer function, likely resulting in the loss or at least distortion of information.

9.5 Summary

A method was developed to process aortic and femoral pressure waveforms into a form appropriate for developing a transfer function between the two. This method involved grouping the waveforms into sets of 8, and adjusted the signal such that they began and ended at 0. Transfer functions were developed for 5 pigs undergoing the progression of a model of septic shock, accompanied by several clinical interventions such as recruitment manoeuvres and fluid infusions. While the transfer functions matched physiologically expected behaviour, clear, consistent trends associated with diagnostic or monitoring potential were difficult to identify. As such, the next chapter explores alternative approaches that could provide a similar input/output focused methodology as a transfer function, while incorporating more *a-priori* physiological information and providing an output that is simpler to interpret.

10

Arterial Waveform Energetics

With transfer functions failing to provide clearly interpretable information directly from circulatory waveforms, due to the assumption of linear behaviour and large amounts of output data, an alternative method was explored. This method involves using *a-priori* knowledge to identify regions of circulatory waveforms that are linearly related, and employing these regions as inputs and outputs to a simple model. This combination of *a-priori* knowledge to select regions of circulatory waveforms and simple outputs aims to address the weaknesses of the method attempted in Chapter 9.

10.1 Background

As discussed in Chapter 2, the circulatory system can be broken down into pulmonary and systemic circulations. Due to the smaller diameter of arteries and veins in the pulmonary circulation, catheters are typically placed in the systemic circulation instead [46], popularly in the aorta, femoral artery or vena cava [47-49]. The catheter measured pressure waveform passing through the systemic circulation is modulated by the systemic circuit. Thus, the evolution of the pressure waveform from the aorta to the femoral artery and to the vena cava contains information on the condition of the systemic circulation. As the systemic circulation passes through every organ in the body, the state of the systemic circulation should contain a great deal of information about patient condition. There is potential to extract this information directly from the catheter pressure waveforms, without first having to model the entire circulatory system, which could offer significant insight for relatively minimal effort.

Several existing methods compare input and output waveforms without specific modelling of the associated systems. Transfer functions, as explored in Chapter 9, are among the most common, generated using either fast Fourier transforms [168] or empirical mode decomposition [169]. While these two methods are adept at extracting information directly from waveforms, neither method is able to directly leverage the extensive *a-priori* knowledge available on the circulatory system. Further, both methods provide full spectra for every set of heartbeats analysed, an output that is not necessarily any easier to interpret than the initial waveforms, as demonstrated in Chapter 9. More specifically, and in contrast, clinical practice favours very simple, lumped approximations of the entire waveform, such as mean arterial pressure (MAP) and mean venous pressure (MVP) [46]. Hence, the metrics obtained must also be readily interpreted by clinical staff, while ensuring physiological and clinical relevance.

This chapter proposes a method for bridging this gap between the complexity of information available and the simple, lumped values favoured clinically. It focuses on comparing timing, amplitude and mean values between analogous sections of the aortic, femoral and vena cava pressure waveforms. Similar to a transfer function, it is a direct comparison of an input to an output, but operates in the time domain and provides simple, lumped outputs instead of a full spectrum. This method has the potential to provide outputs for easy, rapid interpretation in a clinical environment, while retaining more information from the underlying pressure waveforms than the lumped parameters currently popular in critical care.

10.2 Methods

The method involves two distinct input-output comparisons. The first is between the aortic pressure (P_{ao}, input) to femoral pressure (P_{fe}, output) and encompasses only the arterial system. The second is between the femoral pressure (P_{fe}, input) and vena cava pressure (P_{vc}, output) and encompasses both the arterial and venous systems.

10.2.1 From Aortic Pressure (P_{ao}) to Femoral Pressure (P_{fe})

Both P_{ao} and P_{fe} are situated in the arterial half of systemic circulation, and have very similar waveforms [46]. The primary distinction is the dicrotic notch in P_{ao}, which is a sharp dip in pressure due to the aortic valve shutting at the end of systole. Due to the elastic nature of the arterial system, this sharp dip has been smoothed out by the time the pressure wave reaches the femoral artery, and thus is not present in P_{fe}. This difference must be accounted for when comparing the two waveforms. The process used to compare P_{ao} and P_{fe} is thus defined:

1. Select P_{ao} and P_{fe} for a set of four heartbeats from beat i to beat $i+3$. A set of four heartbeats corresponds to approximately one breathing cycle as set by the mechanical ventilator (15 bpm), and thus minimises extreme fluctuations in the results.
2. Compare peak and trough timing of P_{ao} and P_{fe} to determine phase lag:

$$\delta_{ao\to fe} = \text{mean}\left(\begin{bmatrix} t_{\max(P_{fe},i)} & - & t_{\max(P_{ao},i)} \\ \vdots & & \vdots \\ t_{\max(P_{fe},i+3)} & - & t_{\max(P_{ao},i+3)} \\ t_{\min(P_{fe},i)} & - & t_{\min(P_{ao},i)} \\ \vdots & & \vdots \\ t_{\min(P_{fe},i+3)} & - & t_{\min(P_{ao},i+3)} \end{bmatrix}\right) \tag{10.1}$$

   where, for example, $t_{\max(Pfe,i)}$ represents the peak timing of the i^{th} beat of P_{fe}. $\delta_{ao\to fe}$ is thus a positive value, in ms, representing the amount of time by which P_{fe} lags P_{ao}.
3. Shift P_{ao} right by $\delta_{ao\to fe}$ such that the peaks and troughs of P_{ao} are aligned with those of P_{fe}. Henceforth, $\hat{P}_{ao}$ refers to P_{ao} that has undergone this phase shift alignment.
4. Use linear least squares on the regions of the aligned $\hat{P}_{ao}$ and P_{fe} to find relative amplitude and offset between waveforms:

$$\begin{bmatrix} \begin{pmatrix} \hat{P}_{ao}\left(t_{\min(\hat{P}_{ao},i)} - \alpha\right) \\ \vdots \\ \hat{P}_{ao}\left(t_{\max(\hat{P}_{ao},i)}\right) \end{pmatrix} & \begin{matrix} 1 \\ \vdots \\ 1 \end{matrix} \\ \begin{pmatrix} \hat{P}_{ao}\left(t_{\min(\hat{P}_{ao},i+3)} - \alpha\right) \\ \vdots \\ \hat{P}_{ao}\left(t_{\max(\hat{P}_{ao},i+3)}\right) \end{pmatrix} & \begin{matrix} 1 \\ \vdots \\ 1 \end{matrix} \end{bmatrix} \times \begin{bmatrix} A_{ao\rightarrow fe} \\ O_{ao\rightarrow fe} \end{bmatrix} = \begin{bmatrix} \begin{pmatrix} P_{fe}\left(t_{\min(\hat{P}_{ao},i)} - \alpha\right) \\ \vdots \\ P_{fe}\left(t_{\max(\hat{P}_{ao},i)}\right) \end{pmatrix} \\ \begin{pmatrix} P_{fe}\left(t_{\min(\hat{P}_{ao},i+3)} - \alpha\right) \\ \vdots \\ P_{fe}\left(t_{\max(\hat{P}_{ao},i+3)}\right) \end{pmatrix} \end{bmatrix} \quad (10.2)$$

where relative amplitude is $A_{ao\rightarrow fe}$, offset is $O_{ao\rightarrow fe}$, and α is a fixed value, typically set α = 0.2 s, of additional data prior to $t_{\min(\hat{P}_{ao})}$ that is relevant to identification. These regions are highlighted in Fig. 10.1, and minimise the influence of the dicrotic notch on the linear least squares process.

The resulting metrics characterising the relationship between the two pressure waveforms are the phase lag, $\delta_{ao\rightarrow fe}$, the relative amplitude, $A_{ao\rightarrow fe}$, and the pressure offset, $O_{ao\rightarrow fe}$.

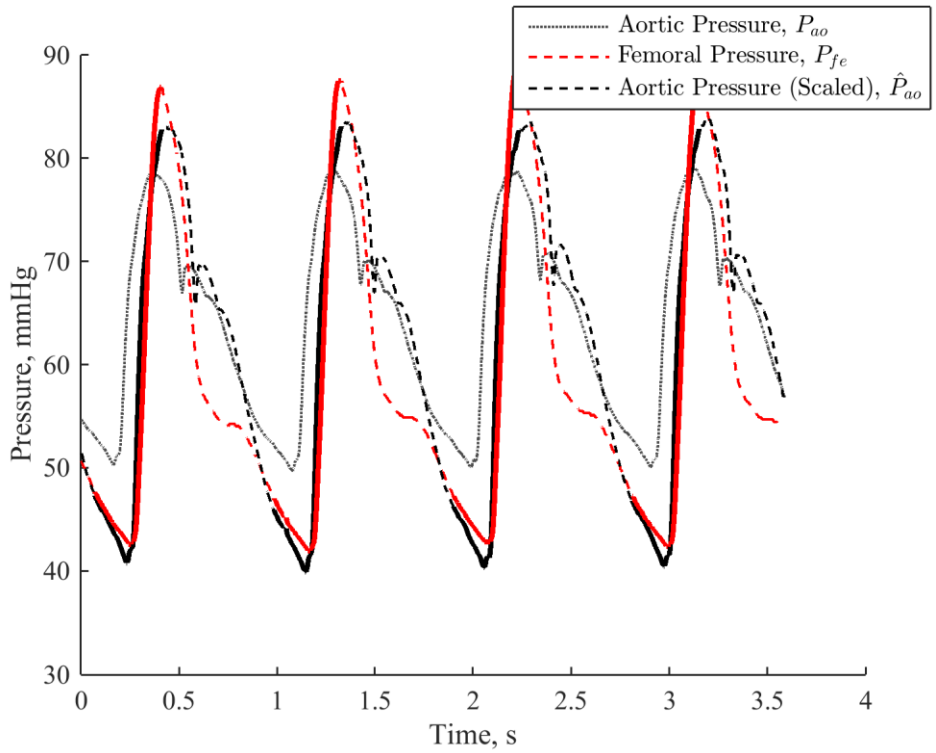

Fig. 10.1: P_{ao} scaled, offset and phase shifted to match P_{fe}. Bolded regions are those used in the linear least squares process.

10.2.2 From Femoral Pressure (P_{fe}) to Central Venous Pressure (P_{vc})

P_{fe} and P_{vc} differ significantly, in both magnitude and shape. Between the femoral artery and the vena cava sit the capillary beds of the systemic circulation, where vessel diameter and flow rate drop significantly [46]. Due to the resulting low magnitude of P_{vc}, the downstream behaviour of the right atria and ventricle exert significant effects on the waveform. The results of these downstream influences on P_{vc} must be ignored when attempting to interpret P_{vc} as a result of upstream P_{fe}. Thus, the region between the 'V' peak and the 'Y' trough of P_{vc} is used for linear least squares, as shown in Fig. 10.2, while the 'A' peak and 'C' peaks, which are the results of downstream atrial and ventricular behaviour [46], are ignored. The 'V' peak can typically be identified as the peak sitting in the latter half of the P_{vc} waveform for a given heartbeat, and the 'Y' trough as the trough directly following the 'V' peak.

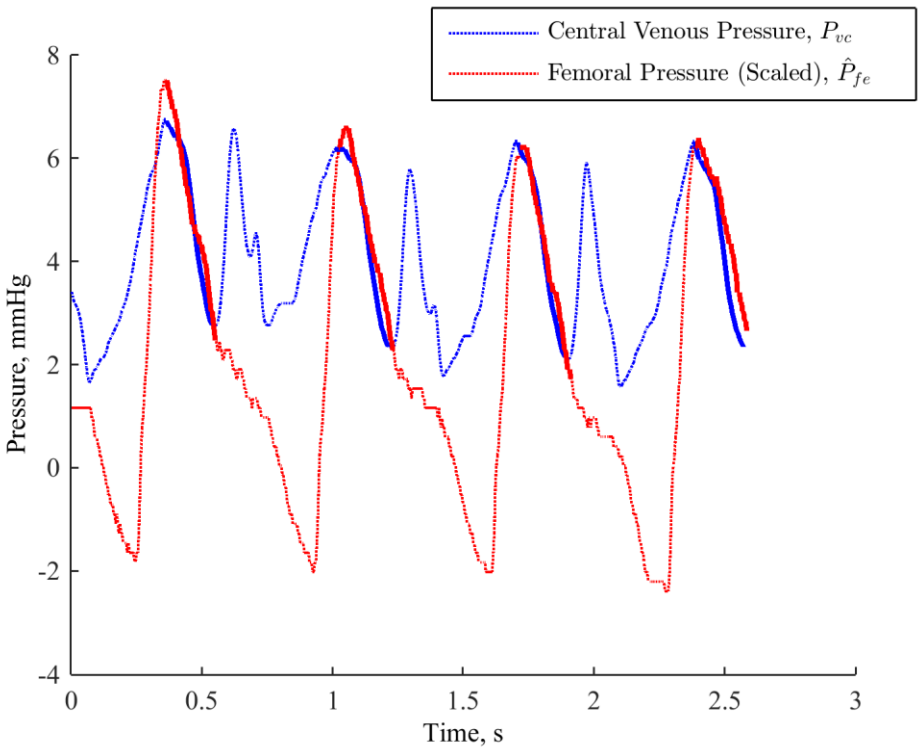

Fig. 10.2: P_{fe} scaled, offset and phase shifted to match P_{vc}. Bolded regions are those used in the linear least squares process.

Unlike P_{ao} and P_{fe}, the i^{th} beat of P_{fe} ($P_{fe,i}$) likely does not correspond to the i^{th} beat of P_{vc} ($P_{vc,i}$) as a pressure wave takes longer than a single heartbeat to pass through the systemic circulation. This point is expressed by $P_{fe,i}$ corresponding instead to $P_{vc,i+j}$, where 'j' is found on a subject specific basis by the optimisation problem:

$$j = \text{argmin}_j \left\| \max\left(\dot{P}_{vc,i+j}\right) - \max\left(\dot{P}_{fe,i}\right) \right\|_2 \tag{10.3}$$

Eq. 10.3 yields the value of *j* providing the best agreement in directional peak to peak variation between P_{vc} and P_{fe}. This process functions by aligning the inter-beat P_{fe} and P_{vc} waveforms based on their response to lower frequency influences, such as breathing. The fact that, while unbound, *j* is consistently found to be *j* = 3 supports the validity of this approach, which yields a consistent and physiologically reasonable result.

Thus, the final process used to compare P_{fe} and P_{vc} is defined:

1. Select 4 heartbeats for both P_{fe} and P_{vc}, from the beginning of beat *i* to the end of beat *i+3* for P_{fe} and from the beginning of beat *i+j* to the end of beat *i+j+3* for P_{vc}.
2. Compare peak and trough timing of P_{fe} and P_{vc} to determine phase lag:

$$\delta_{fe\rightarrow vc} = \text{mean}\left(\begin{bmatrix} t_{\max(P_{vc},i+j)} - t_{\max(P_{fe},i)} \\ \vdots \\ t_{\max(P_{vc},i+j+3)} - t_{\max(P_{fe},i+3)} \\ t_{\min(P_{vc},i+j)} - t_{\min(P_{fe},i)} \\ \vdots \\ t_{\min(P_{vc},i+j+3)} - t_{\min(P_{fe},i+3)} \end{bmatrix}\right) \tag{10.4}$$

note that $t_{\max(Pvc)}$ refers specifically to the 'V' peak of the waveform. $\delta_{fe\rightarrow vc}$ is once again a positive value, in ms, this time representing the amount of time by which P_{vc} lags P_{fe}.

3. Shift P_{fe} right by $\delta_{fe\rightarrow vc}$ such that the peaks and troughs of P_{fe} are aligned with those of P_{vc}. Henceforth, $\hat{P}_{fe}$ refers to P_{fe} that has undergone this phase shift, and is thus aligned with P_{vc}.
4. Use linear least squares on the regions of $\hat{P}_{fe}$ and P_{vc} to find:

$$\begin{bmatrix} \begin{pmatrix} \hat{P}_{fe}\left(t_{max(P_{vc},i+j)}\right) \\ \vdots \\ \hat{P}_{fe}\left(t_{min(P_{vc},i+j)}\right) \end{pmatrix} & \begin{matrix} 1 \\ \vdots \\ 1 \end{matrix} \\ \vdots & \vdots \\ \begin{pmatrix} \hat{P}_{fe}\left(t_{max(P_{vc},i+j+3)}\right) \\ \vdots \\ \hat{P}_{fe}\left(t_{min(P_{vc},i+j+3)}\right) \end{pmatrix} & \begin{matrix} 1 \\ \vdots \\ 1 \end{matrix} \end{bmatrix} \times \begin{bmatrix} A_{fe\rightarrow vc} \\ O_{fe\rightarrow vc} \end{bmatrix} = \begin{bmatrix} \begin{pmatrix} P_{vc}\left(t_{max(P_{vc},i+j)}\right) \\ \vdots \\ P_{vc}\left(t_{min(P_{vc},i+j)}\right) \end{pmatrix} \\ \vdots \\ \begin{pmatrix} P_{vc}\left(t_{max(P_{vc},i+j+3)}\right) \\ \vdots \\ P_{vc}\left(t_{min(P_{vc},i+j+3)}\right) \end{pmatrix} \end{bmatrix} \quad (10.5)$$

   where relative amplitude is $A_{fe\rightarrow vc}$, and offset is $O_{fe\rightarrow vc}$. These regions are highlighted in Fig. 10.2, and minimise the influence the upstream behaviour of the right atria and ventricle on the linear least squares process.

Once again, the parameters of interest are the phase lag, $\delta_{fe\rightarrow vc}$, the relative amplitude, $A_{fe\rightarrow vc}$, and the pressure offset, $O_{fe\rightarrow vc}$.

10.2.3 Experimental Data

This chapter makes use of the 5 Protocol S pigs not subject to exclusion. The waveforms employed are continuously sampled P_{ao}, P_{fe} and P_{vc} as method inputs and outputs for the derivation of both novel and current clinical metrics.

10.2.4 Analyses

The analysis of trends in the selected metrics will be largely qualitative, and focuses on the response of these metrics to clinical interventions. It's worth noting that all metrics employed are relative, rather than absolute. These metrics focus on the change in pressure waveforms as they pass through the systemic circulation, rather than absolute values of these waveforms, which comprise many existing clinical metrics. The best

point of comparison for these metrics in current clinical practice are MAP and MVP, as well as the difference between the two ΔMP = MAP – MVP, a surrogate for systemic resistance [46] and broadly analogous to $O_{fe \to vc}$. Thus, in comparing relative values to absolute values, it is the response to intervention or disease state that is critical in assessing diagnostic value.

Here, comparisons in this analysis focus on the relative sensitivity of the novel and established clinical metrics to clinical interventions and changes in condition, and thus their relative clinical relevance as potential diagnostic aides. Comparisons encompass direct observation of the trends present, as well as presentation of *p*-values for a Wilcoxon signed-rank test comparing pre- and post- endotoxin behaviour [170].

10.3 Results

Fig. 10.3 presents the phase lag $\delta_{ao \to fe}$, the relative amplitude $A_{ao \to fe}$, and the pressure drop $O_{ao \to fe}$, and Tables 10.1 – 10.2 the associated Wilcoxon signed-rank test *p*-values for pre- and post- endotoxin infusion.

Table 10.1: Pre- and post- endotoxin comparison of $\delta_{ao \to fe}$ and $A_{ao \to fe}$, including associated Wilcoxon signed-rank test *p*-values, for aorta to femoral artery. The notation 'up' and 'dn' denote a statistically significant increase or decrease in the respective metric post endotoxin infusion.

Pig	Phase Lag, $\delta_{ao \to fe}$ (s)	*p*	Relative Amplitude, $A_{ao \to fe}$	*p*
S1	0.07 (0.01 - 0.09) 0.04 (-0.15 - 0.09)	0.00 dn	1.47 (1.36 - 1.51) 0.78 (0.30 - 1.21)	0.00 dn
S2	0.13 (0.12 - 0.14) 0.15 (-0.01 - 0.14)	0.00 up	1.33 (1.24 - 1.37) 1.09 (0.31 - 1.29)	0.00 dn
S3	-0.07 (-0.08 - -0.01) 0.10 (-0.05 - -0.01)	0.00 up	0.88 (0.68 - 1.27) 0.37 (0.32 - 0.47)	0.00 dn
S4	0.13 (0.12 - 0.14) 0.13 (0.01 - 0.14)	0.12 –	1.49 (1.46 - 1.53) 1.15 (0.86 - 1.24)	0.00 dn
S5	0.11 (0.10 - 0.12) 0.15 (0.13 - 0.12)	0.00 up	1.69 (1.53 - 1.74) 1.55 (1.25 - 1.63)	0.00 dn

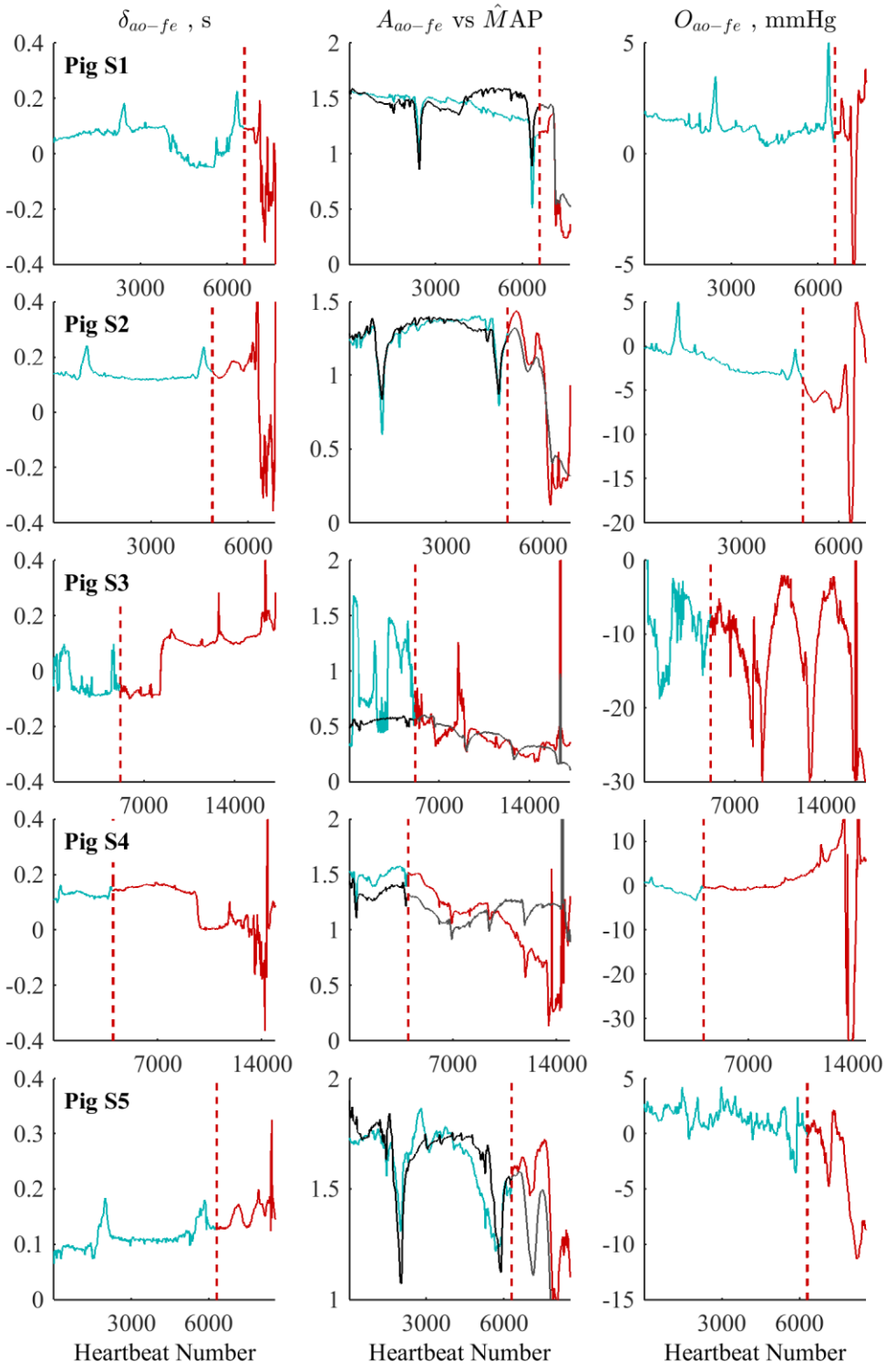

Fig. 10.3: Novel metrics for aorta to femoral artery for all 5 Protocol S pigs. Transition from cyan to red or black to grey (where present) denotes pre- and post-endotoxin infusion regions in novel and current clinical metrics respectively.

Table 10.2: Pre- and post- endotoxin comparison of $O_{ao\rightarrow fe}$ and MAP, including associated Wilcoxon signed-rank test *p*-values, for aorta to femoral artery. The notation 'up' and 'dn' denote a statistically significant increase or decrease in the respective metric post endotoxin infusion.

Pig	Pressure Offset, $O_{ao\rightarrow fe}$ (mmHg)	*p*	Mean Arterial Pressure, MAP (mmHg)	*p*
S1	1.18 (0.98 - 1.51) 0.99 (0.70 - 2.35)	0.49 –	60.1 (57.8 - 63.0) 34.8 (23.5 - 58.2)	0.00 dn
S2	-1.91 (-3.01 - -0.63) -5.57 (-6.51 - -4.15)	0.00 dn	52.4 (50.2 - 54.5 41.0 (17.7 - 45.5)	0.00 dn
S3	-8.65 (-11.68 - -5.85) -9.56 (-15.51 - -6.74)	0.00 dn	83.0 (78.6 - 85.0 60.7 (46.3 - 71.7)	0.00 dn
S4	-0.64 (-1.80 - -0.12) -0.17 (-0.55 - 3.68)	0.00 up	45.4 (44.2 - 47.6 40.6 (37.1 - 42.3)	0.00 dn
S5	1.42 (0.70 - 2.11) -1.37 (-7.85 - 0.23)	0.00 dn	49.6 (47.2 - 50.3 36.2 (16.8 - 43.1)	0.00 dn

From Tables 10.1 – 10.2 it is apparent that 2 metrics, relative amplitude and MAP, showed consistent, significant changes in a unified direction across the endotoxin infusion. From Fig. 10.3 there are a number of interesting observations to make. Phase lag shows consistent spikes during recruitment manoeuvres, but inconsistent changes post endotoxin infusion. MAP and relative amplitude show very similar profiles, though long term trends can be quite different. Pressure drop can quite frequently be negative, which is not entirely unexpected as P_{fe} regularly has a larger peak pressure than P_{ao} due to the narrower cross section of the femoral artery compared to the aorta. However, as expected, large negative spikes in pressure drop consistently occur post endotoxin infusion.

Fig. 10.4 presents the phase lag, $\delta_{fe\rightarrow vc}$, relative amplitude, $A_{fe\rightarrow vc}$, and pressure drop, $O_{fe\rightarrow vc}$, and Tables 10.3 – 10.4 the associated Wilcoxon signed-rank test *p*-values for pre- and post- endotoxin infusion. Tables 10.3 – 10.4 show all metrics change consistently and significantly between pre- and post- endotoxin infusion. This result matches expectations as the area between the femoral artery and vena cava includes the capillary beds and micro-circulation most effected by septic shock [88]. Phase lag

consistently decreases overall, though Fig. 10.4 shows this median decrease is accompanied by large variations. Relative amplitude and MVP consistently increase as well, in a broadly steady manner. Pressure drop and ΔMP consistently fall, as would be expected, corresponding to the loss in systemic resistance associated with sepsis.

Table 10.3: Pre- and post- endotoxin comparison of $\delta_{fe\rightarrow vc}$ and $A_{fe\rightarrow vc}$, including associated Wilcoxon signed-rank test *p*-values, for femoral artery to vena cava. The notation 'up' and 'dn' denote a statistically significant increase or decrease in the respective metric post endotoxin infusion.

Pig	Phase Lag, $\delta_{fe\rightarrow vc}$ (s)	*p*	Relative Amplitude, $A_{fe\rightarrow vc}$	*p*
S1	3.20 (3.19 - 3.21) 3.19 (3.18 - 3.22)	0.00 dn	0.01 (0.01 - 0.02) 0.18 (0.01 - 8.00)	0.00 up
S2	2.80 (2.76 - 2.81) 2.76 (2.72 - 2.97)	0.00 dn	0.06 (0.06 - 0.07) 0.21 (0.06 - 1.69)	0.00 up
S3	2.33 (2.32 - 2.35) 2.32 (2.32 - 2.36)	0.00 dn	0.15 (0.15 - 0.30) 0.75 (0.15 - 1.38)	0.00 up
S4	2.98 (2.96 - 2.99) 2.96 (2.97 – 3.03)	0.00 dn	0.07 (0.07 - 0.11) 0.15 (0.07 - 0.23)	0.00 up
S5	3.45 (3.44 - 3.47) 3.44 (3.40 - 3.45)	0.00 dn	0.05 (0.05 - 0.08) 0.14 (0.05 - 0.60)	0.00 up

Table 10.4: Pre- and post- endotoxin comparison of $O_{fe\rightarrow vc}$ and ΔMP, including associated Wilcoxon signed-rank test *p*-values, for femoral artery to vena cava. The notation 'up' and 'dn' denote a statistically significant increase or decrease in the respective metric post endotoxin infusion.

Pig	Pressure Offset, $O_{fe\rightarrow vc}$ (mmHg)	*p*	Pressure Delta, ΔMP (mmHg)	*p*
S1	43.4 (41.5 - 45.8) 19.6 (9.4 - 41.5)	0.00 dn	48.1 (45.9 - 50.8) 20.6 (3.1 - 45.4)	0.00 dn
S2	44.8 (42.9 - 46.4) 38.2 (19.9 - 42.9)	0.00 dn	46.1 (44.9 - 47.2) 33.4 (4.9 - 38.0)	0.00 dn
S3	81.6 (79.8 - 83.9) 59.6 (45.0 - 79.8)	0.00 dn	77.8 (73.9 - 79.2) 54.4 (35.9 - 65.1)	0.00 dn
S4	33.4 (32.9 - 34.8) 26.9 (22.1 - 32.9)	0.00 dn	34.1 (33.0 - 36.8) 27.6 (25.4 - 28.5)	0.00 dn
S5	40.8 (37.9 - 41.7) 28.0 (18.9 - 37.9)	0.00 dn	45.5 (42.0 - 46.6) 27.3 (5.9 - 35.4)	0.00 dn

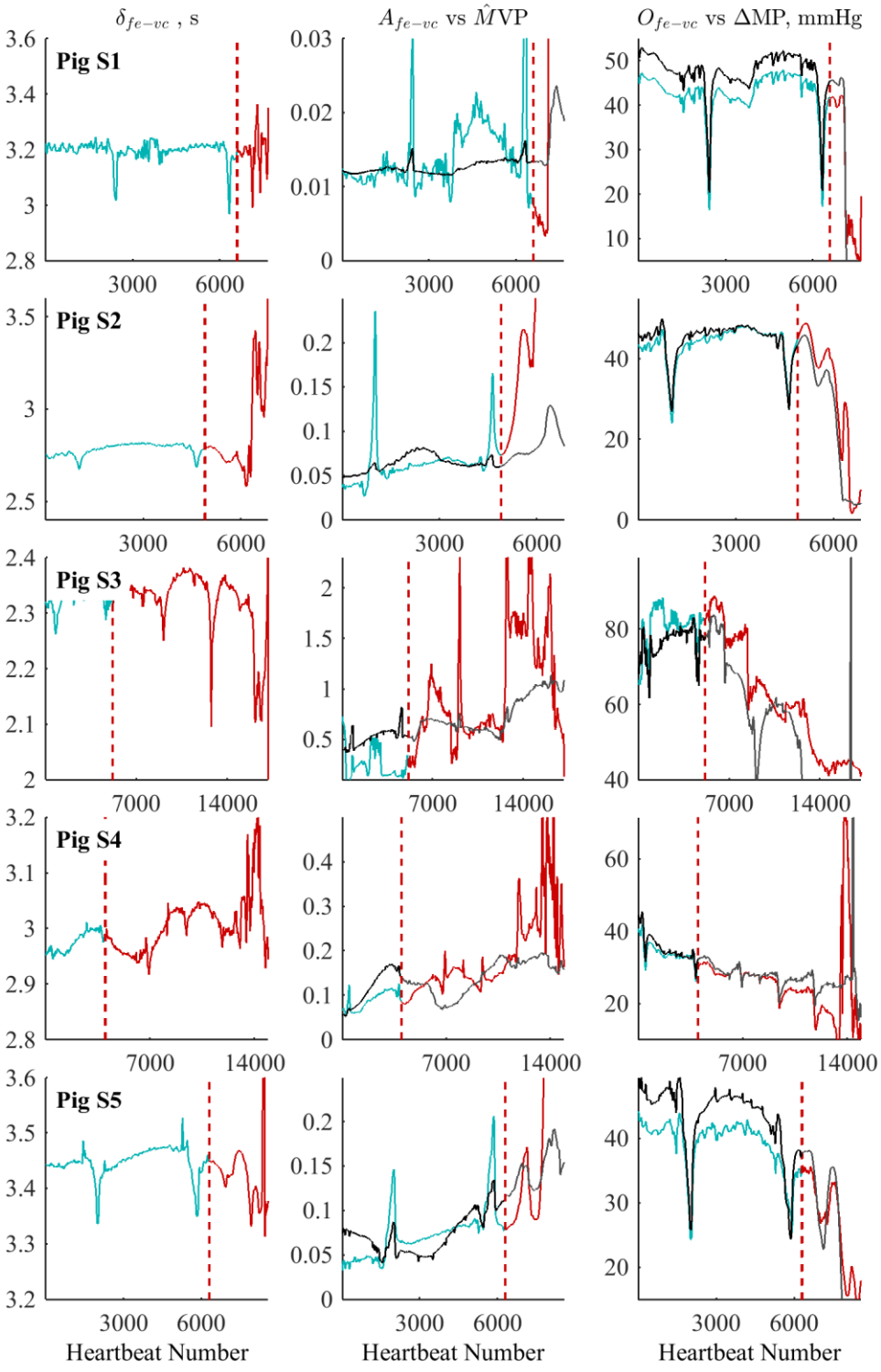

Fig. 10.4: Novel metrics for femoral artery to vena cava for all 5 Protocol S pigs. Transition from cyan to red or black to grey (where present) denotes pre- and post-endotoxin infusion regions in novel and current clinical metrics respectively.

10.4 Discussion

10.4.1 P_{ao} to P_{fe}

The phase lag between the aorta and femoral artery failed to show a consistent, statistically significant shift between pre- and post- endotoxin infusion. Consistent increases in phase lag occurred during recruitment manoeuvres, as the inflated lungs increase resistance to flow from the aorta in the thoracic cavity [171]. The presence of negative phase lag, while not physiological, can be explained by the short time taken to travel from the aorta to the femoral artery (≈0.1s) compared to the length of each heartbeat (≈0.8s). As the phase lag calculated was peak-to-peak lag, and the relative position of the peak within both the P_{ao} and P_{fe} waveforms shifts distinctly in certain regions, this negative lag could result if the peak of P_{fe} occurred roughly in line with that of P_{ao}, or even well before it in late sepsis when the waveforms become highly distorted [117]. Thus, these regions still represent a physiological change, but are difficult to interpret for clinical use with regards to pulse wave velocity.

The relative pulse amplitude between aorta and femoral artery, along with the comparable MAP, showed consistent, statistically significant, downward shifts post-endotoxin infusion. The fall in relative pulse amplitude corresponds to the loss in arterial tone experienced in sepsis [172], resulting in significant pulse energy being lost in the arterial system. Both metrics also showed consistent decreases during recruitment manoeuvres, again consistent with the increase in thoracic pressure and depression of the circulatory system associated with these manoeuvres. It is possible variations in long term trends between MAP and relative amplitude are due to MAP responding to filling and relative amplitude, being a relative metric, not responding to filling. For example, in Pig S1 at roughly beat 4000, filling causes an increase in MAP while relative amplitude remains unchanged. Additionally, at roughly beat 9000 in Pig

S4, filling causes MAP to remain roughly level, while relative amplitude shows a steady decrease as sepsis develops and arterial tone is lost.

The pressure drop between the aorta and femoral artery failed to show a consistent, clear shift between pre- and post- endotoxin infusion. However, there are several topographical features of note. First, the pressure drop tends to increase during recruitment manoeuvres, in line with the behaviour of the previous metrics. Second, post endotoxin infusion all pigs show at least one sharp, but temporary, decrease in the pressure drop, corresponding to a significant increase in P_{fe} relative to P_{ao}. It would seem likely this drop is due to P_{ao} falling significantly and P_{fe} following suit slightly later, where it is important to note that the pressure wave travels faster than the blood itself, which is the cause of this lag.

10.4.2 P_{fe} to P_{vc}

The phase lag between femoral artery and vena cava showed a statistically significant change in all cases. While the mean values fell consistently, observation of the quartiles or the visual trend lines show Pigs S2 and S4 appear to see an increase in phase lag, while Pigs S3 and S5 see a fall in phase lag. There is a consistent decrease in phase lag during recruitment manoeuvres. This decrease is interesting as the opposite might be expected due to the vena cava, which is in the thoracic cavity, being upstream of the femoral artery, which is not in the thoracic cavity.

The relative amplitude between the femoral artery and vena cava, along with MVP, consistently and significantly rose as sepsis developed. This result matches expectations, as sepsis causes a fall in systemic resistance as capillary beds, resulting in reduced attenuation of the pulse wave as well as absolute pressure [11]. In general, trends in MVP and relative amplitude match, with the main exception being Pig S3, where some disruption to the femoral catheter occurred during the experiment.

Finally, the pressure drop between the femoral artery and vena cava, along with ΔMP, both showed consistent, significant decreases as sepsis progressed. These results also agree well with the reduced systemic resistance typically observed during the progression of sepsis, as capillaries dilate and fluid is lost. Both trend lines show very close resemblance, and clear, consistent long term trends. A decease in both metrics occurs during recruitment manoeuvres, likely due to P_{vc} increasing due to being in the thoracic cavity, and P_{fe} decreasing due to upstream resistance.

10.4.3 Novel and Clinical Metrics

The novel metrics provide a set of interacting parameters designed to express the changes in a single pressure pulse as it moves through the systemic circulation. Several of these metrics were demonstrated to be consistently sensitive to changes in systemic circulation caused by sepsis. However, the analysis failed to demonstrate these metrics provide significant additional, physiologically significant information to that already available from clinical metrics such as MAP, MVP and ΔMP.

As such, further analysis should be undertaken to compare not just whether the metrics are sensitive to changes induced by sepsis, but how sensitive and on what timescale these changes can be registered. The novel metrics do not require any more instrumentation to calculate than these existing metrics, and only minimal computational effort. However, without further analysis it is difficult to provide a clear case for their clinical use from the data presented.

10.5 Summary

A method was developed to use simple, lumped parameters to express the changes to a pressure pulse as it passed through the systemic circulation, with the goal of providing easy to interpret diagnostic information in a clinical environment. This model was evaluated on an animal model of sepsis, encompassing 5 pure Piétrain pigs and

compared to common lumped clinical metrics. While several model parameters demonstrated consistent, physiologically expected changes in response to sepsis, these changes were not demonstrably clearer or more consistent than those present in existing clinical metrics. While the novel method presented requires no additional clinical instrumentation or effort over existing metrics, further analysis of the degree and timescales of sensitivity in these novel metrics are required to justify their use.

11

Conclusion

The main accomplishment of this thesis was developing a coherent, interlinked framework for the non-additionally invasive model-based and computational estimation of a number of clinically relevant cardiovascular metrics around the pressure-volume (P-V) loop, the concept of elastance, and the P-V loop itself. P-V loops and elastance are central to titrating clinical care. These metrics thus have the potential to aid in real-time clinical decision making at the patient bedside, closing the gap between the clinician's conceptual model of underlying behaviour, and the surface level measured, and summarised metrics clinically available, which typically result in care based on simplistic, population responses instead of patient-specific responses. This outcome is accomplished by using simple, physiological models and computation to extract much more information from the variety of waveforms and metrics currently measured in the intensive care unit (ICU), creating a much clearer physiological and patient-specific picture for the clinician, and decision making.

While there exist a variety of methods using similar approach to model a small part of the circulatory system, or estimate one of the various parameters estimated here, there is no comprehensive and cohesive framework for estimating the full family of physiological metrics. Similarly, there is no current framework for the non-additionally invasive estimation of the cardiac P-V loop, which is not directly available and sits at the core of this family of physiological metrics. The research in this thesis presents

non-additionally invasive methods to obtain these P-V loops within this overall methodological framework.

Chapters 3 – 8 cover the development of this framework for estimating this set of interlinked, popular, but currently clinically unavailable, physiological metrics. Specifically, Chapter 3 develops a simple model for estimation of the time varying elastance curve (TVE), which, similar to what was originally postulated in prior works, had a fixed shape with only timing subject to alteration. This approach provided a significant improvement over a fixed TVE curve as an input to larger models, but, understandably, held little additional diagnostic information in and of itself. Chapter 4 developed a method for the non-additionally invasive estimation of the unstressed or 'dead space' volume (V_d) of the left ventricle, a metric that traditionally requires highly invasive experimental procedures to measure or even estimate, and which may have direct diagnostic use. Chapter 5 looked at non-invasive estimation of the ESPVR, and thus V_{es} and V_{ed}, which, combined with existing methods, provides typically unmeasured beat-by-beat ventricular volume profile information, as well as important clinical surrogates, such as V_{ed}, a clinical surrogate for cardiac preload.

Chapter 6 drew together developments of Chapters 4 and 5 to provide a more in depth and physiological estimation of the TVE curve, using underlying estimation of left-ventricular pressure (P_{lv}), volume (V_{lv}) and V_d to avoid assuming a fixed shape for the TVE curve itself. This approach preserves the dynamic shapes and thus potential diagnostic information in the TVE curve. The approach demonstrated a statistically significant improvement in error over the more static approach presented in Chapter 3. Chapter 7 employed the method used to estimate the TVE curve for the direct estimation of the P-V loop instead. While the P-V loop uses the same inputs as the TVE curve, specifically V_{lv} and P_{lv}, the lack of normalisation and direct use of these waveforms means more clinical information is preserved, but also requires the

underlying model to be more accurate, as sources of error are not potentially attenuated by normalisation. This chapter demonstrated the method was capable of tracking trends in important clinical metrics derived from the P-V loop, such as stroke work, and in accurately locating the P-V loop itself, which are major advances over what is currently available today.

Chapter 8 compared experimentally standard, but highly invasive and clinically unavailable, estimation of ventricular volume at zero pressure (V_0) and the end-systolic pressure-volume relation (ESPVR) from a vena cava occlusion with the method presented in Chapter 4. An exponential fit helped account for the action of cardiac reflexes during the short occlusion period, providing a more accurate estimate of V_0 subject to these conditions than a linear fit, and one that broadly agreed with the estimates of V_d from Chapter 4.

Finally, Chapters 9 and 10 explored an energetics based approach to directly extracting information from arterial and venous waveforms, and the relationships between them. Chapter 9 explored using transfer functions to compare the aortic and femoral pressures. While physiologically expected results were found, the spectral outputs from the transfer function were found to be too complicated for efficient use in an ICU environment. Chapter 10 explored a simpler means of comparing the aortic, femoral and central venous pressures, characterising each waveform as subject to a phase and magnitude offset as well as a scaling factor. This approach demonstrated sensitivity to changes in condition due to sepsis, and provided simple, intuitive metrics as outputs. However, its sensitivity relative to current clinically standard metrics, such as mean arterial (MAP) and venous (MVP) pressures, and the difference between them (ΔMP), needs to be further assessed.

The methods developed in this thesis avoid the risks of parameter trade-off and identifiability inherent in larger, close looped models by combining a number of

smaller, open loop models where simultaneous parameter identification and non-linear least squares are not employed. At the same time, the methods developed in this thesis better leverage clinically available information to provide a cohesive, interlinked framework for the estimation of clinically relevant parameters. The potential to provide these parameters, which are familiar to clinicians, in a non-additionally invasive manner in real-time at the patient bedside has the potential to aid in clinical decision making concerning cardiovascular disease in the ICU.

12

Future Work

There are, as always, a variety of future avenues to extend and complement the research presented in this thesis. The following section presents several examples of such potential future work.

12.1 Further Model Validation

There are several possible paths for further validation of the work presented in this thesis. Most obviously, validation of the model on retrospective human clinical data would provide benefits in confirming the models' applicability to the target species. However, the various metrics estimated are, as aforementioned, too invasive to measure directly in a clinical environment. Thus, such a validation would rely on expected trends in these clinical metrics subject to certain interventions or changes in condition, rather than a direct comparison to a gold standard invasive measurement.

A second path for further validation is the validation of the work presented in this thesis across several other disease states that effect different parts of the cardiovascular system (CVS). For example, pulmonary embolism effects primarily the pulmonary, rather than systemic circulation, unlike sepsis. Further, method applicability to intra-ventricular conditions such as arrhythmia and valvular dysfunction should be validated, as these conditions must manifest in the aortic pressure waveform for the model to detect them. However, the model has already been validated across sepsis, which is a frequently occurring, diverse, distributive condition, as well as drugs designed to

directly alter elastance, where a number of key assumptions and the arguable focus of this thesis lie. Thus, the model framework presented in this thesis has been validated across a solid, challenging base of experimental data and cardiovascular conditions.

12.2 Clinical Sensitivity of Metrics

Several of the metrics that are clinically estimated by the modelling framework presented here have had only limited studies into their sensitivity to a variety of potential influences and conditions. In particular, the time varying elastance (TVE) curve and ventricular 'dead space' volume (V_d) and their response to various stimuli is not well documented due, in part, to the traditional difficulty in measuring or estimating these parameters under clinical conditions. An exploration of how TVE and V_d change in response to various clinical interventions and disease states, as well as a validation of the model's ability to track these changes, and potential diagnostic significance should be undertaken.

12.3 Incorporation of EDPVR

With the end-systolic pressure-volume relation (ESPVR) incorporated into the method already, and V_d available, incorporation of the end-diastolic pressure volume relation (EDPVR) into the model would allow full characterisation of the contractile state of the heart, and the boundaries of the pressure-volume (P-V) loop. Specifically, when combined with clinically estimated end-diastolic volume (V_{ed}), this would allow beat-by-beat estimation of the diastolic pressure in the ventricle (P_{dia}), which is currently set to a constant value in the model. While this would be beneficial, it is worth noting that the typical shape of the EDPVR demonstrates the relative insensitivity of P_{dia}, as compared to systolic pressure in the ventricle (P_{sys}), to changes in volume, thus justifying the current approach.

12.4 Arterial Energetics Sensitivity

Finally, further exploration of relative sensitivity of the metrics developed in Chapter 10 is needed. While these metrics demonstrated consistent sensitivity to changes in the systemic circulation induced by sepsis, whether or not these metrics provide more information than is currently available clinical estimates such as mean arterial (MAP) and venous (MVP) pressures, and the difference between them (ΔMP) needs to be further explored. Specifically, the relative temporal sensitivities of these two sets of metrics should be compared, as sepsis is a fast acting condition [11, 33, 117, 172, 173] and earlier diagnosis of oncoming septic shock could provide significant clinical benefits.

References

1. Mozaffarian D, Benjamin EJ, Go AS, Arnett DK, Blaha MJ, Cushman M, Das SR, de Ferranti S, Després J-P, Fullerton HJ: **Heart Disease and Stroke Statistics—2016 Update A Report From the American Heart Association.** *Circulation* 2015:CIR. 0000000000000350.

2. Ramsay JG: **Cardiac management in the ICU.** *CHEST Journal* 1999, **115**(suppl_2):138S-144S.

3. Mangano D: **Perioperative cardiac morbidity--epidemiology, costs, problems, and solutions.** *West J Med* 1994, **161**(1):87.

4. Dellinger RP: **Cardiovascular management of septic shock.** *Crit Care Med* 2003, **31**(3):946-955.

5. Dellinger RP, Carlet JM, Masur H, Gerlach H, Calandra T, Cohen J, Gea-Banacloche J, Keh D, Marshall JC, Parker MM: **Surviving Sepsis Campaign guidelines for management of severe sepsis and septic shock.** *Intensive Care Med* 2004, **30**(4):536-555.

6. Bahloul M, Chaari A, Kallel H, Abid L, Hamida CB, Dammak H, Rekik N, Mnif J, Chelly H, Bouaziz M: **Pulmonary embolism in intensive care unit: Predictive factors, clinical manifestations and outcome.** *Ann Thorac Med* 2010, **5**(2):97.

7. Lloyd-Jones D, Adams R, Carnethon M, De Simone G, Ferguson TB, Flegal K, Ford E, Furie K, Go A, Greenlund K: **Heart disease and stroke statistics—2009 update a report from the American Heart Association Statistics Committee and Stroke Statistics Subcommittee.** *Circulation* 2009, **119**(3):e21-e181.

8. Health Mo: **Report on New Zealand Cost-of-Illness Studies on Long-Term Conditions.** *Wellington: Ministry of Health* 2009.

9. Walsh T, McClelland D, Lee R, Garrioch M, Maciver C, McArdle F, Crofts S, Mellor I: **Prevalence of ischaemic heart disease at admission to intensive care and its influence on red cell transfusion thresholds: multicentre Scottish Study.** *Br J Anaesth* 2005, **94**(4):445-452.

10. Seferian EG, Afessa B: **Demographic and clinical variation of adult intensive care unit utilization from a geographically defined population.** *Crit Care Med* 2006, **34**(8):2113-2119.

11. Dellinger RP, Levy MM, Carlet JM, Bion J, Parker MM, Jaeschke R, Reinhart K, Angus DC, Brun-Buisson C, Beale R: **Surviving Sepsis Campaign: international guidelines for management of severe sepsis and septic shock: 2008.** *Intensive Care Med* 2008, **34**(1):17-60.

12. Turnan KJ, McCarthy RJ, March RJ, Najafi H, Ivankovich AD: **Morbidity and duration of ICU stay after cardiac surgery: a model for preoperative risk assessment.** *Chest* 1992, **102**(1):36-44.

13. Heidenreich PA, Trogdon JG, Khavjou OA, Butler J, Dracup K, Ezekowitz MD, Finkelstein EA, Hong Y, Johnston SC, Khera A: **Forecasting the future of cardiovascular disease in the United States.** *Circulation* 2011, **123**(8):933-944.

14. Boldt J: **Clinical review: Hemodynamic monitoring in the intensive care unit.** *Critical Care* 2002, **6**(1):52.

15. Pinsky MR: **Hemodynamic evaluation and monitoring in the ICU.** *CHEST Journal* 2007, **132**(6):2020-2029.

16. Tibby S, Murdoch I: **Monitoring cardiac function in intensive care.** *Arch Dis Child* 2003, **88**(1):46-52.

17. Puri N, Puri V, Dellinger RP: **History of technology in the intensive care unit.** *Crit Care Clin* 2009, **25**(1):185-200, ix.

18. Cotter G, Cotter OM, Kaluski E: **Hemodynamic monitoring in acute heart failure.** *Critical Care Medicine* 2008, **36**(1):S40-S43.

19. Frazier SK, Skinner GJ: **Pulmonary artery catheters: state of the controversy.** *J Cardiovasc Nurs* 2008, **23**(2):113-121.

20. Chatterjee K: **The swan-ganz catheters: past, present, and future a viewpoint.** *Circulation* 2009, **119**(1):147-152.

21. Pinsky MR: **Rationale for cardiovascular monitoring.** *Curr Opin Crit Care* 2003, **9**(3):222-224.

22. Thiele RH, Durieux ME: **Arterial waveform analysis for the anesthesiologist: past, present, and future concepts.** *Anesth Analg* 2011, **113**(4):766-776.

23. Mutoh T, Kazumata K, Ajiki M, Ushikoshi S, Terasaka S: **Goal-directed fluid management by bedside transpulmonary hemodynamic monitoring after subarachnoid hemorrhage.** *Stroke* 2007, **38**(12):3218-3224.

24. Halford GS, Baker R, McCredden JE, Bain JD: **How many variables can humans process?** *Psychol Sci* 2005, **16**(1):70-76.

25. Chase JG, Le Compte A, Preiser J-C, Shaw G, Penning S, Desaive T: **Physiological modeling, tight glycemic control, and the ICU clinician: what are models and how can they affect practice?** *Annals of Intensive Care* 2011, **1:11**.

26. Charlton BG: **Restoring the balance: evidence- based medicine put in its place.** *J Eval Clin Pract* 1997, **3**(2):87-98.

27. Feinstein AR, Horwitz RI: **Problems in the "evidence" of "evidence-based medicine".** *The American journal of medicine* 1997, **103**(6):529-535.

28. Sleigh J: **Logical limits of randomized controlled trials.** *J Eval Clin Pract* 1997, **3**(2):145-148.

29. Tonelli MR: **The philosophical limits of evidence-based medicine.** *Acad Med* 1998, **73**(12):1234-1240.

30. Boyd JH, Forbes J, Nakada T-a, Walley KR, Russell JA: **Fluid resuscitation in septic shock: a positive fluid balance and elevated central venous pressure are associated with increased mortality.** *Crit Care Med* 2011, **39**(2):259-265.

31. Dickstein K: **Diagnosis and assessment of the heart failure patient: the cornerstone of effective management.** *European journal of heart failure* 2005, **7**(3):303-308.

32. Perkins GD, McAuley DF, Davies S, Gao F: **Discrepancies between clinical and postmortem diagnoses in critically ill patients: an observational study.** *Critical care* 2003, **7**(6):R129.

33. Angus DC, Linde-Zwirble WT, Lidicker J, Clermont G, Carcillo J, Pinsky MR: **Epidemiology of severe sepsis in the United States: analysis of incidence, outcome, and associated costs of care.** *Crit Care Med* 2001, **29**(7):1303-1310.

34. Pineda LA, Hathwar VS, Grant BJ: **Clinical suspicion of fatal pulmonary embolism.** *CHEST Journal* 2001, **120**(3):791-795.

35. Chase JG, Shaw G, Le Compte A, Lonergan T, Willacy M, Wong X-W, Lin J, Lotz T, Lee D, Hann C: **Implementation and evaluation of the SPRINT protocol for tight glycaemic control in critically ill patients: a clinical practice change.** *Critical Care* 2008, **12**(2):R49.

36. Compte AL, Chase JG, Lynn A, Hann C, Shaw G, Wong X-W, Lin J: **Blood glucose controller for neonatal intensive care: virtual trials development and first clinical trials.** In: SAGE Publications; 2009.

37. Lonergan T, Compte AL, Willacy M, Chase JG, Shaw GM, Hann CE, Lotz T, Lin J, Wong X-W: **A pilot study of the SPRINT protocol for tight glycemic control in critically Ill patients.** *Diabetes Technol Ther* 2006, **8**(4):449-462.

38. Wong X-W, Chase JG, Hann CE, Lotz TF, Lin J, Le Compte AJ, Shaw GM: **Development of a clinical type 1 diabetes metabolic system model and in silico simulation tool.** In: SAGE Publications; 2008.

39. Evans A, Shaw GM, Le Compte A, Tan C-S, Ward L, Steel J, Pretty CG, Pfeifer L, Penning S, Suhaimi F: **Pilot proof of concept clinical trials of Stochastic Targeted (STAR) glycemic control.** *Annals of intensive care* 2011, **1**(1):38.

40. Marik PE, Baram M: **Noninvasive hemodynamic monitoring in the intensive care unit.** *Crit Care Clin* 2007, **23**(3):383-400.

41. Chiari L, Cappello A, Tartarini R, Paolini F, Calzavara P: **Model-based dialysis adequacy prediction by continuous dialysate urea monitoring.** *The International journal of artificial organs* 1998, **21**(9):526-534.

42. Pasterkamp E, Kruithof C, Van der Meer F, Rosendaal F, Vanderschoot J: **A model- based algorithm for the monitoring of long- term anticoagulation therapy.** *J Thromb Haemost* 2005, **3**(5):915-921.

43. Uckun S, Dawant BM, Lindstrom DP: **Model-based diagnosis in intensive care monitoring: the YAQ approach.** *Artif Intell Med* 1993, **5**(1):31-48.

44. Starfinger C, Hann CE, Chase JG, Desaive T, Ghuysen A, Shaw GM: **Model-based cardiac diagnosis of pulmonary embolism.** *Computer Methods and Programs in Biomedicine* 2007, **87**(1):46-60.

45. Revie JAM: **Model-based cardiovascular monitoring in critical care for improved diagnosis of cardiac dysfunction.** 2013.

46. Hall JE: *Guyton and Hall textbook of medical physiology*. Elsevier Health Sciences; 2010.

47. Gershengorn HB, Wunsch H, Scales DC, Zarychanski R, Rubenfeld G, Garland A: **Association between arterial catheter use and hospital mortality in intensive care units.** *JAMA Internal Medicine* 2014, **174**(11):1746-1754.

48. Gershengorn HB, Garland A, Kramer A, Scales DC, Rubenfeld G, Wunsch H: **Variation of arterial and central venous catheter use in United States intensive care units.** *The Journal of the American Society of Anesthesiologists* 2014, **120**(3):650-664.

49. Harvey S, Harrison DA, Singer M, Ashcroft J, Jones CM, Elbourne D, Brampton W, Williams D, Young D, Rowan K: **Assessment of the clinical effectiveness of pulmonary artery catheters in management of patients in intensive care (PAC-Man): a randomised controlled trial.** *Lancet* 2005, **366**(9484):472-477.

50. Paeme S: **Mathematical Modeling of the Mitral Valve: From Local to Global Haemodynamics.** *GIGA-Cardiovascular Sciences, University of Liege* 2013.

51. Iaizzo PA: *Handbook of cardiac anatomy, physiology, and devices*. Springer; 2009.

52. Pan J, Tompkins WJ: **A real-time QRS detection algorithm.** *Biomedical Engineering, IEEE Transactions on* 1985(3):230-236.

53. Suga H: **Ventricular energetics.** *Physiol Rev* 1990, **70**(2):247-277.

54. Burkhoff D, Sagawa K: **Ventricular efficiency predicted by an analytical model.** *American Journal of Physiology-Regulatory, Integrative and Comparative Physiology* 1986, **250**(6):R1021-R1027.

55. Suga H, Sagawa K, Shoukas AA: **Load independence of the instantaneous pressure-volume ratio of the canine left ventricle and effects of epinephrine and heart rate on the ratio.** *Circ Res* 1973, **32**(3):314-322.

56. Broscheit J-A, Weidemann F, Strotmann J, Steendijk P, Karle H, Roewer N, Greim C-A: **Time-varying elastance concept applied to the relation of**

carotid arterial flow velocity and ventricular area. *J Cardiothorac Vasc Anesth* 2006, **20**(3):340-346.

57. Sagawa K: **Editorial: the end-systolic pressure-volume relation of the ventricle: definition, modifications and clinical use.** *Circulation* 1981, **63**(6).

58. Grossman W, Braunwald E, Mann T, McLaurin L, Green L: **Contractile state of the left ventricle in man as evaluated from end-systolic pressure-volume relations.** *Circulation* 1977, **56**(5):845-852.

59. Davidson S, Pretty C, Pironet A, Desaive T, Janssen N, Lambermont B, Morimont P, Chase JG: **Minimally invasive estimation of ventricular dead space volume through use of Frank-Starling curves.** *PLoS One* 2017, **12**(4):e0176302.

60. Paolocci N, Katori T, Champion HC, John MES, Miranda KM, Fukuto JM, Wink DA, Kass DA: **Positive inotropic and lusitropic effects of HNO/NO− in failing hearts: independence from β-adrenergic signaling.** *Proceedings of the National Academy of Sciences* 2003, **100**(9):5537-5542.

61. Suga H, Hisano R, Goto Y, Yamada O, Igarashi Y: **Effect of positive inotropic agents on the relation between oxygen consumption and systolic pressure volume area in canine left ventricle.** *Circ Res* 1983, **53**(3):306-318.

62. Michard F, Alaya S, Zarka V, Bahloul M, Richard C, Teboul J-L: **Global end-diastolic volume as an indicator of cardiac preload in patients with septic shock.** *CHEST Journal* 2003, **124**(5):1900-1908.

63. Vincent J-L, Gerlach H: **Fluid resuscitation in severe sepsis and septic shock: an evidence-based review.** *Crit Care Med* 2004, **32**(11):S451-S454.

64. Schierhout G, Roberts I: **Fluid resuscitation with colloid or crystalloid solutions in critically ill patients: a systematic review of randomised trials.** *BMJ* 1998, **316**(7136):961-964.

65. Stewart RM, Park PK, Hunt JP, McIntyre Jr RC, McCarthy J, Zarzabal LA, Michalek JE: **Less Is More: Improved Outcomes in Surgical Patients with Conservative Fluid Administration and Central Venous Catheter Monitoring.** *Journal of the American College of Surgeons* 2009, **208**(5):725-735.

66. Kastrup M, Markewitz A, Spies C, Carl M, Erb J, Grosse J, Schirmer U: **Current practice of hemodynamic monitoring and vasopressor and inotropic therapy in post- operative cardiac surgery patients in Germany: results from a postal survey.** *Acta Anaesthesiol Scand* 2007, **51**(3):347-358.

67. O'Neill D, Perrin D: **Fluid resuscitation in critical care.** *Nurs Times* 2002, **98**(37):39-40.

68. Kelly R, Gibs H, O'ROURKE M, Daley J, Mang K, Morgen J, Avolid A: **Nitroglycerin has more favourable effects on left ventricular afterload than apparent from measurement of pressure in a peripheral artery.** *Eur Heart J* 1990, **11**(2):138-144.

69. Petersen JW, Felker GM: **Inotropes in the management of acute heart failure.** *Critical care medicine* 2008, **36**(1):S106-S111.

70. Bangash MN, Kong ML, Pearse RM: **Use of inotropes and vasopressor agents in critically ill patients.** *Brit J Pharmacol* 2012, **165**(7):2015-2033.

71. Beale RJ, Hollenberg SM, Vincent J-L, Parrillo JE: **Vasopressor and inotropic support in septic shock: an evidence-based review.** *Critical care medicine* 2004, **32**(11):S455-S465.

72. Stevenson LW: **Clinical use of inotropic therapy for heart failure: looking backward or forward? Part I: inotropic infusions during hospitalization.** *Circulation* 2003, **108**(3):367-372.

73. Cousins TR, O'Donnell JM: **Arterial cannulation: a critical review.** *AANA J* 2004, **72**(4).

74. Marik PE, Baram M, Vahid B: **Does central venous pressure predict fluid responsiveness?: a systematic review of the literature and the tale of seven mares.** *CHEST Journal* 2008, **134**(1):172-178.

75. Kumar A, Anel R, Bunnell E, Habet K, Zanotti S, Marshall S, Neumann A, Ali A, Cheang M, Kavinsky C: **Pulmonary artery occlusion pressure and central venous pressure fail to predict ventricular filling volume, cardiac performance, or the response to volume infusion in normal subjects.** *Crit Care Med* 2004, **32**(3):691-699.

76. Klabunde R: *Cardiovascular physiology concepts.* Lippincott Williams & Wilkins; 2011.

77. Frank O: **Zur dynamik des herzmuskels.** *Z Biol* 1895, **32**:370-447.

78. Otto F: **Die grundform des arteriellen pulses.** *Zischr F Biol* 1899, **37**:483-526.

79. Starling E, Visscher M: **The regulation of the energy output of the heart.** *The Journal of physiology* 1927, **62**(3):243-261.

80. Pinsky MR: **Cardiovascular issues in respiratory care.** *CHEST Journal* 2005, **128**(5_suppl_2):592S-597S.

81. Soni N, Williams P: **Positive pressure ventilation: what is the real cost?** *Br J Anaesth* 2008, **101**(4):446-457.

82. Shekerdemian L, Bohn D: **Cardiovascular effects of mechanical ventilation.** *Arch Dis Child* 1999, **80**(5):475-480.

83. Pironet A, Dauby PC, Chase JG, Kamoi S, Janssen N, Morimont P, Lambermont B, Desaive T: **Model-Based Stressed Blood Volume is an Index of Fluid Responsiveness⁎⁎ This work was supported by the French Community of Belgium, the Belgian Funds for Scienti_c Research (FRS-FNRS) and EU Marie Curie Actions (FP7-PEOPLE-2012-IRSES).** *IFAC-PapersOnLine* 2015, **48**(20):291-296.

84. Porterfield JE, Kottam AT, Raghavan K, Escobedo D, Jenkins JT, Larson ER, Treviño RJ, Valvano JW, Pearce JA, Feldman MD: **Dynamic correction for parallel conductance, GP, and gain factor, α, in invasive murine left ventricular volume measurements.** *J Appl Physiol* 2009, **107**(6):1693-1703.

85. Fujiwara H, Ashraf M, Sato S, Millard RW: **Transmural cellular damage and blood flow distribution in early ischemia in pig hearts.** *Circ Res* 1982, **51**(6):683-693.

86. Jardin F, Farcot J-C, Boisante L, Curien N, Margairaz A, Bourdarias J-P: **Influence of positive end-expiratory pressure on left ventricular performance.** *N Engl J Med* 1981, **304**(7):387-392.

87. Courtois M, Vered Z, Barzilai B, Ricciotti NA, Pérez JE, Ludbrook PA: **The transmitral pressure-flow velocity relation. Effect of abrupt preload reduction.** *Circulation* 1988, **78**(6):1459-1468.

88. Nguyen HB, Rivers EP, Abrahamian FM, Moran GJ, Abraham E, Trzeciak S, Huang DT, Osborn T, Stevens D, Talan DA: **Severe sepsis and septic shock: review of the literature and emergency department management guidelines.** *Ann Emerg Med* 2006, **48**(1):54. e51.

89. Stevenson D, Revie J, Chase JG, Hann CE, Shaw GM, Lambermont B, Ghuysen A, Kolh P, Desaive T: **Beat-to-beat estimation of the continuous left and right cardiac elastance from metrics commonly available in clinical settings.** *Biomed Eng Online* 2012, **11**:73.

90. Stevenson D, Revie J, Chase JG, Hann CE, Shaw GM, Lambermont B, Ghuysen A, Kolh P, Desaive T: **Algorithmic processing of pressure waveforms to facilitate estimation of cardiac elastance.** *Biomed Eng Online* 2012, **11**(1):1-16.

91. Senzaki H, Chen C-H, Kass DA: **Single-beat estimation of end-systolic pressure-volume relation in humans a new method with the potential for noninvasive application.** *Circulation* 1996, **94**(10):2497-2506.

92. Sunagawa K, Sagawa K, Maughan WL: **Ventricular interaction with the loading system.** *Ann Biomed Eng* 1984, **12**(2):163-189.

93. Revie JA, Stevenson D, Chase JG, Pretty CJ, Lambermont BC, Ghuysen A, Kolh P, Shaw GM, Desaive T: **Evaluation of a model-based hemodynamic monitoring method in a porcine study of septic shock.** *Comput Math Methods Med* 2013, **2013**:505417.

94. Revie JA, Stevenson DJ, Chase JG, Hann CE, Lambermont BC, Ghuysen A, Kolh P, Shaw GM, Heldmann S, Desaive T: **Validation of subject-specific cardiovascular system models from porcine measurements.** *Comput Methods Programs Biomed* 2013, **109**(2):197-210.

95. Chung D, Niranjan S, Clark J, Bidani A, Johnston W, Zwischenberger J, Traber D: **A dynamic model of ventricular interaction and pericardial influence.** *Am J Physiol Heart Circ Physiol* 1997, **272**(6):H2942-H2962.

96. Starfinger C, Chase J, Hann C, Shaw G, Lambermont B, Ghuysen A, Kolh P, Dauby P, Desaive T: **Model-based identification and diagnosis of a porcine**

model of induced endotoxic shock with hemofiltration. *Math Biosci* 2008, **216**(2):132-139.

97. Smith BW, Chase JG, Nokes RI, Shaw GM, Wake G: **Minimal haemodynamic system model including ventricular interaction and valve dynamics.** *Med Eng Phys* 2004, **26**(2):131-139.

98. Suga H, Sagawa K: **Instantaneous pressure-volume relationships and their ratio in the excised, supported canine left ventricle.** *Circ Res* 1974, **35**(1):117-126.

99. Zhong L, Ghista DN, Ng EY, Lim ST: **Passive and active ventricular elastances of the left ventricle.** *Biomed Eng Online* 2005, **4**(1):10.

100. Swamy G, Kuiper J, Gudur MS, Olivier NB, Mukkamala R: **Continuous left ventricular ejection fraction monitoring by aortic pressure waveform analysis.** *Ann Biomed Eng* 2009, **37**(6):1055-1068.

101. Ten Brinke E, Klautz R, Verwey H, Van Der Wall E, Dion R, Steendijk P: **Single- beat estimation of the left ventricular end- systolic pressure–volume relationship in patients with heart failure.** *Acta physiologica* 2010, **198**(1):37-46.

102. Shishido T, Hayashi K, Shigemi K, Sato T, Sugimachi M, Sunagawa K: **Single-beat estimation of end-systolic elastance using bilinearly approximated time-varying elastance curve.** *Circulation* 2000, **102**(16):1983-1989.

103. Dawber TR, Thomas HE, McNamara PM: **Characteristics of the dicrotic notch of the arterial pulse wave in coronary heart disease.** *Angiology* 1973, **24**(4):244-255.

104. Tuttle RR, Mills J: **Dobutamine: development of a new catecholamine to selectively increase cardiac contractility.** *Circ Res* 1975, **36**(1):185-196.

105. Borow KM, Neumann A, Wynne J: **Sensitivity of end-systolic pressure-dimension and pressure-volume relations to the inotropic state in humans.** *Circulation* 1982, **65**(5):988-997.

106. Sunagawa K, Maughan W, Friesinger G, Chang M, Sagawa K: **Coronary Perfusion-Pressure and Left-Ventricular Endsystolic Pressure-Volume Relation.** In *Circulation*. American Heart Association; 1980:203-203.

107. Pironet AD, T.; Chase, J. G.; Morimont, P.; Dauby, P. C.: **Model-Based Computation of Total Stressed Blood Volume from a Preload Reduction Experiment.** 2013.

108. Kamoi S, Pretty C, Docherty P, Squire D, Revie J, Chiew YS, Desaive T, Shaw GM, Chase JG: **Continuous stroke volume estimation from aortic pressure using zero dimensional cardiovascular model: proof of concept study from porcine experiments.** *PLoS One* 2014, **9**(7):e102476.

109. Kass D, Maughan W, Guo ZM, Kono A, Sunagawa K, Sagawa K: **Comparative influence of load versus inotropic states on indexes of**

ventricular contractility: experimental and theoretical analysis based on pressure-volume relationships. *Circulation* 1987, **76**(6):1422-1436.

110. Paulus WJ, Tschöpe C, Sanderson JE, Rusconi C, Flachskampf FA, Rademakers FE, Marino P, Smiseth OA, De Keulenaer G, Leite-Moreira AF: **How to diagnose diastolic heart failure: a consensus statement on the diagnosis of heart failure with normal left ventricular ejection fraction by the Heart Failure and Echocardiography Associations of the European Society of Cardiology.** *Eur Heart J* 2007.

111. Mehmel H, Stockins B, Ruffmann K, Von Olshausen K, Schuler G, Kübler W: **The linearity of the end-systolic pressure-volume relationship in man and its sensitivity for assessment of left ventricular function.** *Circulation* 1981, **63**(6):1216-1222.

112. Van der Velde E, Burkhoff D, Steendijk P, Karsdon J, Sagawa K, Baan J: **Nonlinearity and load sensitivity of end-systolic pressure-volume relation of canine left ventricle in vivo.** *Circulation* 1991, **83**(1):315-327.

113. Sato T, Shishido T, Kawada T, Miyano H, Miyashita H, Inagaki M, Sugimachi M, Sunagawa K: **ESPVR of in situ rat left ventricle shows contractility-dependent curvilinearity.** *Am J Physiol Heart Circ Physiol* 1998, **274**(5):H1429-H1434.

114. Kirkpatrick E, Shillingford AJ, Cohen MS: **Echocardiography in the ICU.** In *Pediatric and Congenital Cardiology, Cardiac Surgery and Intensive Care*. Springer; 2014: 879-899.

115. Golub GH, Van Loan C: **Total least squares.** In *Smoothing Techniques for Curve Estimation.* Springer; 1979: 69-76.

116. Randles RH: **Wilcoxon signed rank test.** *Encyclopedia of statistical sciences* 1988.

117. Hunter J, Doddi M: **Sepsis and the Heart.** *Br J Anaesth* 2010, **104**(1):3-11.

118. Sarnoff SJ, Berglund E: **Ventricular function I. Starling's law of the heart studied by means of simultaneous right and left ventricular function curves in the dog.** *Circulation* 1954, **9**(5):706-718.

119. Lee Rodgers J, Nicewander WA: **Thirteen ways to look at the correlation coefficient.** *Am Stat* 1988, **42**(1):59-66.

120. Faes TJ, Kerkhof PL: **The Volume Regulation Graph versus the Ejection Fraction as Metrics of Left Ventricular Performance in Heart Failure with and without a Preserved Ejection Fraction: A Mathematical Model Study.** *Clin Med Insights Cardiol* 2015, **9**(Suppl 1):73.

121. Glower DD, Spratt JA, Snow ND, Kabas J, Davis J, Olsen C, Tyson G, Sabiston D, Rankin J: **Linearity of the Frank-Starling relationship in the intact heart: the concept of preload recruitable stroke work.** *Circulation* 1985, **71**(5):994-1009.

122. Davidson S, Kannangara, DO, Pretty, CG, Kamoi, S, Pironet, A, Desaive, T, Chase, JG: **Modelling of the Nonlinear End-Systolic Pressure-Volume**

Relation and Volume-at-Zero-Pressure in Porcine Experiments. In *Conf Proc IEEE Eng Med Biol Soc*; *August 25-29, 2015; Milan, Italy*. 2015:4.

123. Fernandes Jr CJ, de Assuncao MSC: **Myocardial dysfunction in sepsis: a large, unsolved puzzle.** *Crit Care Res Pract* 2012, **2012**.

124. Kamoi S, Pretty C, Balmer J, Davidson S, Pironet A, Desaive T, Shaw GM, Chase JG: **Improved pressure contour analysis for estimating cardiac stroke volume using pulse wave velocity measurement.** *Biomed Eng Online* 2017, **16**(1):51.

125. Crottogini AJ, Willshaw P, Barra JG, Breitbart GJ, Pichel RH: **End-systolic pressure-volume relationships in dogs during ventilation with PEEP.** *Am J Physiol Heart Circ Physiol* 1988, **254**(4):H664-H670.

126. Lang RM, Badano LP, Mor-Avi V, Afilalo J, Armstrong A, Ernande L, Flachskampf FA, Foster E, Goldstein SA, Kuznetsova T: **Recommendations for cardiac chamber quantification by echocardiography in adults: an update from the American Society of Echocardiography and the European Association of Cardiovascular Imaging.** *J Am Soc Echocardiogr* 2015, **28**(1):1-39. e14.

127. Vieillard-Baron A, Slama M, Cholley B, Janvier G, Vignon P: **Echocardiography in the intensive care unit: from evolution to revolution?** *Intensive Care Med* 2008, **34**(2):243-249.

128. Malm S, Frigstad S, Sagberg E, Larsson H, Skjaerpe T: **Accurate and reproducible measurement of left ventricular volume and ejection fraction by contrast echocardiography.** *J Am Coll Cardiol* 2004, **44**(5):1030-1035.

129. Schiller NB, Acquatella H, Ports TA, Drew D, Goerke J, Ringertz H, Silverman NH, Brundage B, Botvinick EH, Boswell R: **Left ventricular volume from paired biplane two-dimensional echocardiography.** *Circulation* 1979, **60**(3):547-555.

130. van Hout GP, Jansen SJ, Gho JM, Doevendans PA, van Solinge WW, Pasterkamp G, Chamuleau SA, Hoefer IE: **Admittance- based pressure–volume loops versus gold standard cardiac magnetic resonance imaging in a porcine model of myocardial infarction.** *Physiological reports* 2014, **2**(4):e00287.

131. Burkhoff D, De Tombe PP, Hunter WC: **Impact of ejection on magnitude and time course of ventricular pressure-generating capacity.** *American Journal of Physiology-Heart and Circulatory Physiology* 1993, **265**(3):H899-H909.

132. Baan J, Van Der Velde ET: **Sensitivity of left ventricular end-systolic pressure-volume relation to type of loading intervention in dogs.** *Circulation research* 1988, **62**(6):1247-1258.

133. De Ferrari GM, Crijns HJ, Borggrefe M, Milasinovic G, Smid J, Zabel M, Gavazzi A, Sanzo A, Dennert R, Kuschyk J: **Chronic vagus nerve stimulation: a new and promising therapeutic approach for chronic heart failure.** *Eur Heart J* 2011, **32**(7):847-855.

134. Bouvier E, Logeart D, Sablayrolles J-L, Feignoux J, Scheublé C, Touche T, Thabut G, Cohen-Solal A: **Diagnosis of aortic valvular stenosis by multislice cardiac computed tomography.** *Eur Heart J* 2006, **27**(24):3033-3038.

135. Davidson S, Pretty C, Pironet A, Kamoi S, Balmer J, Desaive T, Chase JG: **Minimally invasive, patient specific, beat-by-beat estimation of left ventricular time varying elastance.** *Biomed Eng Online* 2017, **16**(1):42.

136. Tuchschmidt J, Fried J, Astiz M, Rackow E: **Elevation of cardiac output and oxygen delivery improves outcome in septic shock.** *Chest* 1992, **102**(1):216-220.

137. Weaver ME, Pantely GA, Bristow JD, D LADLEY H: **A quantitative study of the anatomy and distribution of coronary arteries in swine in comparison with other animals and man.** *Cardiovasc Res* 1986, **20**(12):907-917.

138. Hasenfuss G: **Animal models of human cardiovascular disease, heart failure and hypertrophy.** *Cardiovasc Res* 1998, **39**(1):60-76.

139. Chen C-H, Fetics B, Nevo E, Rochitte CE, Chiou K-R, Ding P-A, Kawaguchi M, Kass DA: **Noninvasive single-beat determination of left ventricular end-systolic elastance in humans.** *J Am Coll Cardiol* 2001, **38**(7):2028-2034.

140. Klotz S, Hay I, Dickstein ML, Yi G-H, Wang J, Maurer MS, Kass DA, Burkhoff D: **Single-beat estimation of end-diastolic pressure-volume relationship: a novel method with potential for noninvasive application.** *Am J Physiol Heart Circ Physiol* 2006, **291**(1):H403-H412.

141. Karunanithi MK, Feneley MP: **Single-beat determination of preload recruitable stroke work relationship: derivation and evaluation in conscious dogs.** *J Am Coll Cardiol* 2000, **35**(2):502-513.

142. Lee W-S, Huang W-P, Yu W-C, Chiou K-R, Ding PY-A, Chen C-H: **Estimation of preload recruitable stroke work relationship by a single-beat technique in humans.** *Am J Physiol Heart Circ Physiol* 2003, **284**(2):H744-H750.

143. Ferrandis M-J, Ryden I, Lindahl TL, Larsson A: **Ruling out cardiac failure: Cost-benefit analysis of a sequential testing strategy with NT-proBNP before echocardiography.** *Ups J Med Sci* 2013, **118**(2):75-79.

144. Berry MF, Pirolli TJ, Jayasankar V, Burdick J, Morine KJ, Gardner TJ, Woo YJ: **Apelin has in vivo inotropic effects on normal and failing hearts.** *Circulation* 2004, **110**(11 suppl 1):II-187-II-193.

145. Lips DJ, vd Nagel T, Steendijk P, Palmen M, Janssen BJ, Dantzig J-Mv, de Windt LJ, Doevendans PA: **Left ventricular pressure–volume measurements in mice: Comparison of closed–chest versus open–chest approach.** *Basic Res Cardiol* 2004, **99**(5):351-359.

146. Signal M, Gottlieb R, Le Compte A, Chase JG: **Continuous glucose monitoring and trend accuracy: NEWS about a Trend Compass.** *J Diabetes Sci Technol* 2014, **8**(5):986-997.

147. Bland JM, Altman DG: **Statistical methods for assessing agreement between two methods of clinical measurement.** *Lancet* 1986, **1**:307 - 310.

148. Kass DA, Beyar R, Lankford E, Heard M, Maughan WL, Sagawa K: **Influence of contractile state on curvilinearity of in situ end-systolic pressure-volume relations.** *Circulation* 1989, **79**(1):167-178.

149. Kolh P, Ghuysen A, Tchana-Sato V, D'Orio V, Gerard P, Morimont P, Limet R, Lambermont B: **Effects of increased afterload on left ventricular performance and mechanical efficiency are not baroreflex-mediated.** *Eur J Cardiothorac Surg* 2003, **24**(6):912-919.

150. Lankhaar J-W, Rövekamp F, Steendijk P, Faes TC, Westerhof B, Kind T, Vonk-Noordegraaf A, Westerhof N: **Modeling the Instantaneous Pressure–Volume Relation of the Left Ventricle: A Comparison of Six Models.** *Ann Biomed Eng* 2009, **37**(9):1710-1726.

151. Douglas WR: **Of pigs and men and research.** *Space Life Sci* 1972, **3**(3):226-234.

152. Tofallis C: **Model fitting for multiple variables by minimising the geometric mean deviation.** In *Total Least Squares and Errors-in-Variables Modeling.* Springer; 2002: 261-267.

153. Yamaoka K, Nakagawa T, Uno T: **Application of Akaike's information criterion (AIC) in the evaluation of linear pharmacokinetic equations.** *J Pharmacokinet Biopharm* 1978, **6**(2):165-175.

154. MONROE RG, FRENCH GN: **Left ventricular pressure-volume relationships and myocardial oxygen consumption in the isolated heart.** *Circ Res* 1961, **9**(2):362-373.

155. Weber KT, Janicki JS, Hefner LL: **Left ventricular force-length relations of isovolumic and ejecting contractions.** *American Journal of Physiology--Legacy Content* 1976, **231**(2):337-343.

156. Shimizu J, Todaka K, Burkhoff D: **Load dependence of ventricular performance explained by model of calcium-myofilament interactions.** *Am J Physiol Heart Circ Physiol* 2002, **282**(3):H1081-H1091.

157. Luecke T, Pelosi P: **Clinical review: positive end-expiratory pressure and cardiac output.** *Critical Care* 2005, **9**(6):607.

158. Johnston WE, Vinten-Johansen J, Santamore WP, Case LD, Little WC: **Mechanism of Reduced Cardiac Output during Positive End-Expiratory Pressure in the Dog.** *Am Rev Respir Dis* 1989, **140**:1257-1264.

159. Wei WW-S: *Time series analysis.* Addison-Wesley publ Reading; 1994.

160. Takewaki I: **Optimal damper placement for minimum transfer functions.** *Earthquake Eng Struct Dyn* 1997, **26**(11):1113-1124.

161. Chase JG, Breneman SE, Smith HA: **Robust H∞ static output feedback control with actuator saturation.** *J Eng Mech* 1999, **125**(2):225-233.

162. Horowitz I, Shaked U: **Superiority of transfer function over state-variable methods in linear time-invariant feedback system design.** *IEEE Transactions on Automatic Control* 1975, **20**(1):84-97.

163. Bracewell RN, Bracewell RN: *The Fourier transform and its applications.* McGraw-Hill New York; 1986.

164. Saul JP, Berger RD, Albrecht P, Stein S, Chen MH, Cohen R: **Transfer function analysis of the circulation: unique insights into cardiovascular regulation.** *Am J Physiol Heart Circ Physiol* 1991, **261**(4):H1231-H1245.

165. Berger RD, Saul JP, Cohen RJ: **Transfer function analysis of autonomic regulation. I. Canine atrial rate response.** *Am J Physiol Heart Circ Physiol* 1989, **256**(1):H142-H152.

166. Karamanoglu M, O'rourke M, Avolio A, Kelly R: **An analysis of the relationship between central aortic and peripheral upper limb pressure waves in man.** *Eur Heart J* 1993, **14**(2):160-167.

167. Dombrovskiy VY, Martin AA, Sunderram J: **Facing the challenge: Decreasing case fatality rates in severe sepsis despite increasing hospitalization.** *Crit Care Med* 2005, **33**:2555 - 2562.

168. Welch P: **The use of fast Fourier transform for the estimation of power spectra: a method based on time averaging over short, modified periodograms.** *IEEE Transactions on audio and electroacoustics* 1967, **15**(2):70-73.

169. Huang NE, Shen Z, Long SR, Wu MC, Shih HH, Zheng Q, Yen N-C, Tung CC, Liu HH: **The empirical mode decomposition and the Hilbert spectrum for nonlinear and non-stationary time series analysis.** In *Proceedings of the Royal Society of London A: mathematical, physical and engineering sciences*. The Royal Society; 1998:903-995.

170. Wilcoxon F, Katti S, Wilcox RA: **Critical values and probability levels for the Wilcoxon rank sum test and the Wilcoxon signed rank test.** *Selected tables in mathematical statistics* 1970, **1**:171-259.

171. Nielsen J, Østergaard M, Kjaergaard J, Tingleff J, Berthelsen PG, Nygård E, Larsson A: **Lung recruitment maneuver depresses central hemodynamics in patients following cardiac surgery.** *Intensive Care Med* 2005, **31**(9):1189-1194.

172. Bogle R, Vallance P: **Regulation of vascular smooth muscle tone in sepsis.** *Pharmacology of vascular smooth muscle* 1996:369-386.

173. Esper AM, Moss M, Lewis CA, Nisbet R, Mannino DM, Martin GS: **The role of infection and comorbidity: Factors that influence disparities in sepsis.** *Crit Care Med* 2006, **34**:2576 - 2582.